HEINRICH HEINE
UNIVERSITÄT
DÜSSELDORF

Mechanisms and Consequences of Particle Uptake in Alveolar Macrophages

Inaugural-Dissertation

zur Erlangung des Doktorgrades
der Mathematisch-Naturwissenschaftlichen Fakultät
der Heinrich-Heine-Universität Düsseldorf

vorgelegt von

Agnes Martha Scherbart

aus Düren

Düsseldorf, Oktober 2010

aus dem Institut für Umweltmedizinische Forschung (IUF)
an der Heinrich-Heine Universität Düsseldorf gGmbH

Gedruckt mit der Genehmigung der
Mathematisch-Naturwissenschaftlichen Fakultät der
Heinrich-Heine-Universität Düsseldorf

Referentin: Prof. Dr. Christine R. Rose

Koreferentin: Prof. Dr. Charlotte Esser

Tag der mündlichen Prüfung: 01. Dezember 2010

Die Neugier steht immer an erster Stelle eines Problems, das gelöst werden will.

Galileo Galilei

15.02.1564 - 08.01.1642
italienischer Physiker und Astronom

To my parents Renata and Diethard Scherbart and

To my sister Eva-Maria Scherbart

CHAPTER I

GENERAL INTRODUCTION

1.1 THE BACKGROUND - WHERE IT ALL BEGAN

Humans have been exposed to air pollutants including particles throughout their evolutionary stages by natural combustion processes like forest fires or volcanic eruptions and biogenic sources like pollen or mould fungus. The exposure to particulate air pollutants raised dramatically by beginning of industrial revolution during the 19th century due to increased anthropogenic sources such as the growing traffic by combustion engines, running of power plants and other sources of thermodegradation in industrial processes [Oberdörster et al 2005b].

Particle research and particle toxicology have been historically closely connected to industrial activities or materials and have focussed on high occupational exposures at the work place, like in coal mines. Awareness of the health risk in dusty trades became triggered initially by observations on high disease or death rates associated with extreme exposure situations. A historical example is the Hawk's Nest Tunnel Disaster where a large proportion of workers involved in the construction of a railway tunnel rapidly developed lung diseases and died as a result of extreme exposure to crystalline silica dusts [Thomas & Kelley 2010].

The severity dimensions of air pollution in non-occupational exposure settings became obvious for the first time by the London smog in December of 1952 which has been estimated to cause over 12,000 deaths. This event has resulted in a fundamental change in terms of governmental regulation, public awareness towards air pollution and in science. In the UK, the pollution was effectively reduced by the Clean Air Acts and research became funded by Government [Seaton et al 2010]. On the 15th of July in 1980 the council of the European communities legislative introduced the first political regulation with a directive on air quality limit values and guide values for sulphur dioxide and suspended particulates (80/779/EEC). Among others it was found, that more than half of the particles in the London's smog were less than 0.1 µm in diameter [Lawther et al 1968]. The significance of this observation was initially recognized in the beginning of the 1990s, when two lines of research converged: epidemiology and toxicology. Epidemiological studies demonstrated an association between daily mortality and exposure to particulate matter < 10 µm (PM_{10}). Increased exposure to PM_{10} was found to be associated specifically with an increase in respiratory diseases and cardiovascular deaths [Pope et al 1992; Schwartz 1994]. A new age of interaction with other disciplines and clinical specialities was started.

Meanwhile, toxicological investigations with PM_{10} collected from different locations [e.g. Ghio & Devlin 2001] provided support for the epidemiological observations. Further toxicological investigations *in vivo* showed that particles in the nanosize range are being retained in the lungs or translocated to the interstitial tissues [Ferin et al 1992]. Ambient particles suddenly

became responsible for extra-pulmonary effects. Recently it could be shown that translocation of nanoparticles (NP) across the air-blood-barrier from lung and the subsequent distribution to other secondary target organs is determined by material and size of the NP [Kreyling et al 2009]. As such, inhalation of these particles has been implicated in adverse health effects that reach beyond the respiratory tract. Indeed, epidemiological studies as well as experimental toxicological studies have linked particulate pollution to increased rates of cardiopulmonary and cardiovascular diseases, and more recently to neurodegenerative diseases [Pope et al 2002; Peters et al 2006; Crüts et al 2008; Ranft et al 2009].

Particle research has currently reached an impact it has never seen before. Nowadays various types of NP are being generated from highly skilled research labs and produced for wide applications and in many countries. In the near future up-scaling of production is expected and worker exposure and consumer contact are expected to increase dramatically [Borm 2008; Chaudhry et al 2008; Seaton et al 2010]. This rapid development of different engineered NP as well as nanomaterials presents a dilemma to regulators regarding hazard identification and risk assessment. A screening strategy consisting of a combination of non-cellular NP characterization and conventional *in vitro* investigations on cellular toxicity and on intracellular mechanisms as well as the determination of hallmark responses would account to a unique evaluation of specific NP [Oberdörster et al 2005a; Unfried et al 2007].

In the following section, this chapter goes into detail in terms of particle characteristics and physiological conditions of the lung as the main target organ for airborne particles. The focus of this thesis is on alveolar macrophages (AMΦ) being key cells in particle clearance within the alveoli, and on the mediating of cellular responses after getting in contact with inhaled particles, e.g. generation of inflammatory mediators and reactive oxygen species (ROS), respectively.

1.2 NANOPARTICLES - BENEFITS AND RISKS

A number of definitions of NPs have evolved over time. In a commonly used definition introduced recently by the British Standards Institution (BSI), a NP is a nano-object with a diameter < 100 nm in all three dimensions. Within this definition a nano-object is a "discrete piece of material with one or more external dimensions in the nanoscale", while nanoscale refers to a "size range from approximately 1 nm to 100 nm" [Stone et al 2009]. This definition does not include other nano-objects such as long nanotubes.
Aggregates/agglomerates of NP can be much larger in diameter than 100 nm but they are still included since they may break down. The term "nano-" or "ultrafine" particle respectively, includes all engineered and ambient particles smaller than 0.1 µm. In toxicology, "fine" particles are selected for particles between 0.1 and 1.0 µm. Particles bigger than 1.0 µm are per toxicological definition "coarse" particles. Due to their small size NP demonstrate new physical or chemical properties different to bigger particles of the same material, implying benefit and risk at the same time [Borm & Müller-Schulte 2006].

The use of engineered nanomaterials and primarily NP has become an emerging field during the past decades and will probably develop to a key position in future technology, science and medicine due to their outstanding properties in terms of saving energy and resources. Their possible applications encompasses diverse branches of industries ranging from automotive, aircraft and space industry, to chemical and environmental engineering, to optics, electronics and communication technologies, to pharmacology and medicine, but also to day to day consumer products, like food, cosmetics and healthcare, thus making the human exposure to NP inevitable. Consequently, NP may find their way into organisms by different uptake or translocation routes upon inhalation, ingestion, dermal exposure or application and injection, as is depicted in Figure 1.1. The underlying mechanisms of the subsequent distribution of NP in the body like translocation rates, accumulation and retention in critical target sites are largely unknown [Geiser & Kreyling 2010].
A crucial basis for current concerns for the implications of NP on possible adverse health effects was provided by Oberdörster et al [2005b]. His research in the field of inhalation toxicology lead among others to the observation that nano-sized particles show considerably stronger pulmonary toxicity compared to equal mass dose of larger sized particles with the same chemical composition. This indicates that inflammation may be initiated at lower mass exposure concentrations as a result of the higher surface area of NP compared to larger sized materials of the same chemical composition [Brown et al 2004; Unfried et al 2007].

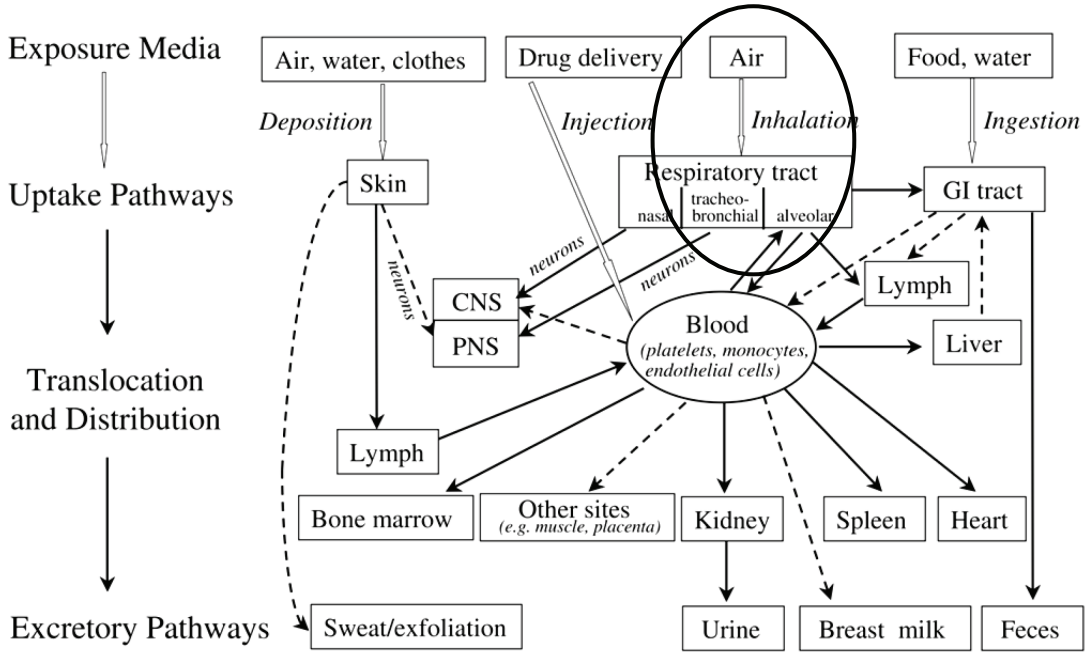

Figure 1.1 Biokinetics of nanoparticles.
Many uptake and translocation routes for NP have been already demonstrated (solid lines), while others are still hypothetical (dashed lines). The circle represents the area of interest of this thesis [Oberdörster et al 2005a]

Specifically for fine and ultrafine TiO_2, it could be shown that dose-response curves for both materials overlapped, when dose became expressed as surface area, rather than mass. However, several studies also indicate that specific NP, because of their unique physico-chemical properties, do not only show such quantitative differences, but also qualitative differences in cellular and molecular mechanisms of toxicity, as will be discussed at a later stage of this chapter.

While the use of NP types and applications continues to increase, studies to characterize their effects after exposure and to address their potential toxicity are few in comparison [Lewinski et al 2008]. By this rapid development of engineered NP, risk assessment and suitable but unique testing strategies are urgently required especially since adverse health effects of some nano-sized particles are already known. It has been shown that the number of internalized NP may correlate for instance to cytotoxicity [Chang et al 2006]. Various types of engineered NP, especially those that are poorly soluble, cannot be destroyed by the defence mechanisms of a cell. Such NP are persistent within cells and tissues, which can lead to the induction of persistent inflammatory and/or oxidative responses. In turn, this may result in alterations of gene-expression and cell-cycle regulation. At present the main concern about nano-related products refers to "free" engineered nanomaterials and their effects on human health, on the environment and along their entire life cycle [Mantovani et al 2009].

Unfried et al [2007] reviewed the assumed mechanisms whereby NP may be taken up and processed by cells.

1.2.1 THE PARTICLE SURFACE PROPERTIES - REACTIVE OR NOT

Apart from the size of NP, their surface properties are considered to be extremely relevant with regard to their toxicity. Herein, the generation of ROS has been proposed as a central mechanism. The high specific surface area (SSA) of particles and/or contamination of the surface with organics and metals (e.g. as impurities or on combustion-derived NP), are considered to be responsible in radical generation and induction of oxidative stress in cell systems as well as the activation of pro-inflammatory mediators [Borm & Müller-Schulte 2006; Unfried et al 2007] [Figure 1.2, right panel].

Organic matter bound to the surfaces of combustion generated (nano)particles, including quinones, are considered to be a major source of ROS from ambient particulate matter (PM). Upon their release from the particle surfaces into biological environments they may undergo redox cycling or phase I biotransformation reactions resulting in the formation of redox-active compounds [Knaapen et al 2004; Xia et al 2004; Unfried et al 2007]. Transition metal ions released from the particle surfaces are also implicated in ROS formation via Fenton-like reactions [Equation 1]:

$$(1) \quad Fe^{2+} + H_2O_2 \rightarrow Fe^{3+} + OH^- + HO^{\cdot}$$

Apart from iron, other transition metals such as nickel, copper and vanadium that are abundant in PM may also catalyse a Fenton-like reaction [Knaapen et al 2004; Schins & Knaapen 2007]. Fenton-like reactions have also been implicated in the ROS generating properties of quartz dusts. A further important mechanism whereby quartz particles are considered to cause oxidative stress is via the action of surface associated free radicals, e.g. $SiO^{\cdot}$ and $SiO^{\cdot}_2$ [Fubini & Hubbard 2003].

The amount of surface molecules increases exponentially when particle size decreases < 100 nm, reflecting the importance of surface area in terms of increased chemical and biologic activity of NP [Figure 1.2, left panel]. This increased biologic activity can be positive (e.g. antioxidant activity, carrier capacity for therapeutics, penetration of cellular barriers), negative (e.g. toxicity, induction of oxidative stress or of cellular dysfunction), or a mix of both for further reactions or an impact on human health [Oberdörster et al 2005b; Xia et al 2004].

These aspects of particle size and surface area are discussed further in detail in paragraph 1.2.3.

The surface charge of particles is another important issue in the toxicity of (nano)particles, since cell membranes are hydrophobic and negatively charged. NP with a cationic surface are hydrophobic as well, thus simplifying the translocation of particles into cells. This transcellular trafficking across a cell membrane is an active process and due to the hydrophobicity, which is responsible for different binding capacity and uptake mechanisms of fine particles into epithelial cells. In contrast, anionic surfaces and neutral surfaces express a lower translocation rate of particles, thus being more biocompatible. This indicates that toxicity may be partly due to the affinity of cationic particles to the negatively charged cell membrane together with other physico-chemical characteristics [Goodman et al 2004; des Rieux et al 2005; Yacobi et al 2008].

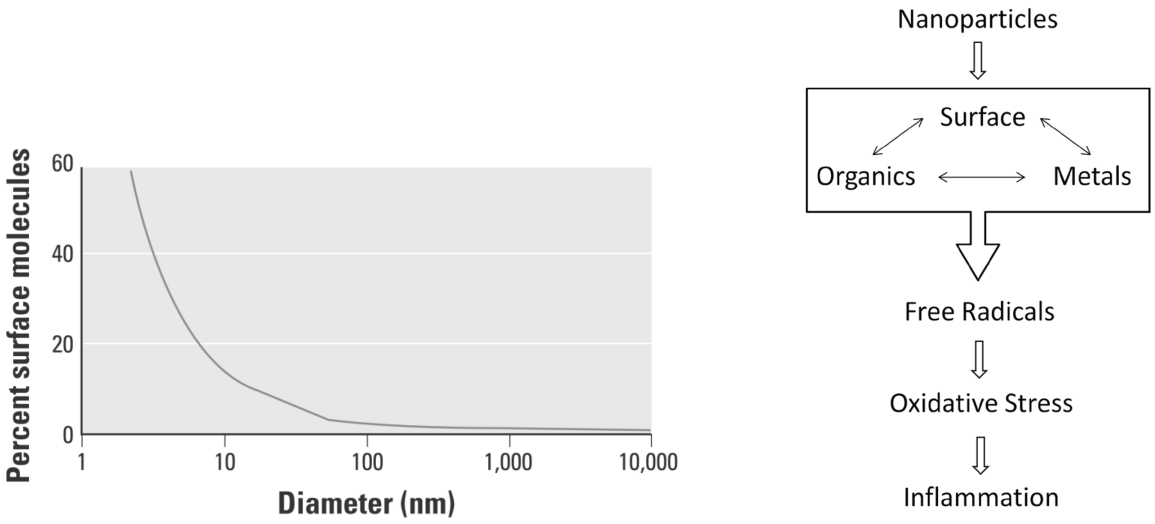

Figure 1.2 The relationship of surface molecules and particles size.
left: Surface molecules as a function of particle size [taken from Oberdörster et al 2005b]
right: Scheme of the likely relationship between the three main characteristics of combustion derived NP and their ability to cause inflammation [Borm & Müller-Schulte 2006]

The addition of surface coatings confounds the bioactivity and potential toxicity of the functional groups on the NP surface with the core NP. For many NP that are used in biological or medical applications several types of surface coating are required depending on the purpose of application like making a particle more water soluble by addition of hydrophilic molecules [Lewinski et al 2008].

1.2.2 THE PARTICLE SIZE DISTRIBUTION

Ambient PM is a complex mixture of inhalable particles and liquid droplets suspended in the air. Particle pollution is made up of a number of components, including acids (such as nitrates and sulphates), organic chemicals, metals, and soil or dust particles. They originate from a variety of sources, such as power plants, industrial processes, and diesel trucks, and they are formed in the atmosphere by transformation of gaseous emissions. Their chemical and physical compositions depend on location, time of year, and weather [Becker et al 2005]. For standard classification of PM the American Environmental Protection Agency (EPA) introduced a "national air quality standard for particulate matter" and defined for ambient PM different size-fractions according to the aerodynamic diameter [US Environmental Protection Agency 1997], which have been taken over by the EU [1999] and WHO [2000] [Table 1.1].
PM can be split up in several size fractions, based on the aerodynamic diameter, that is defined as the diameter of a spherical particle having a unit density of 1 g/cm^3 that has the same inertial properties and settling speed as the particle of interest of whatever shape and density [Holgate et al 1999].

Table 1.1 Particulate matter standards of the Environmental Protection Agency

Particle classification		Aerodynamic diameter	Inhalable fraction
coarse	PM_{10}	< 10 µm	thoratic
fine	$PM_{2.5}$	< 2.5 µm	alveolar
ultrafine/NP	$PM_{0.1}$	< 0.1 µm	alveolar

The fraction of PM_{10} includes all lower size fractions. These particles are small enough to reach the thoratic region of the lung. $PM_{2.5}$ includes the fine and ultrafine fraction, thus $PM_{0.1}$ as well, whose particles are able to reach the deepest region of the lung, the alveoli [Donaldson & Stone 2003; WHO 2006].

1.2.3 THE ULTRAFINE HYPOTHESIS - A QUESTION OF SIZE

It is generally considered that the mass of PM_{10} is not the most dominant dose metric explaining for the adverse health effects of particulate air pollution. NP are the dominant particle type in PM_{10} by number, exhibiting a large surface area per unit mass compared to bigger particles. Since the effects of PM_{10} are often dominated by the effect of the NP fraction, particle number or surface area are considered as better dose metrics [Oberdörster et al 2005b]. The largest database on the toxicity of NP is based on PM_{10} literature, where the ultrafine hypothesis has proved to be a powerful force for research [Borm & Müller-Schulte 2006]. One example is the reinterpretation of the exposure data on the London smog by Maynard and Maynard [2002], since much of the London smog particulate in historic lungs can be seen to be nano-sized particles [Hunt et al 2003]. They recalculated exposure as surface area, a method that takes particle size into account and emphasises the role of NP surfaces and particle number. They revealed that surface area was a better indicator of health effects associated with exposure to PM. The majority of deaths associated with air pollution in epidemiological studies have been shown to result from cardiac rather than respiratory disease [Borm & Müller-Schulte 2006]. The ultrafine hypothesis proposes that observed effects are not a consequence of the mass of particles but of their number. This explains that toxicological tiny doses of PM, e.g. carbon, to the lungs could cause death from failure of another organ [Seaton et al 2010]. Figure 1.1 shows possible routes for NP to translocate and distribute from the lung into secondary organs.

1.2.4 THE WAY OF EXPOSURE TO ENGINEERED NANOPARTICLES

Nowadays, most humans are in daily contact with engineered NP during occupational, environmental and consumer exposure [Royal Society and Royal Academy of Engineering 2004]. More than 1,000 consumer products already containing NP are currently on the market [http://www.nanotechproject.org/inventories/consumer/], like sunscreen and skin lotions, personal care products, food additives, cleaning products and paints. There are multiple potential exposure scenarios for a single material depending on the details of its manufacture, use and disposal. For many products deliberate exposure is intended, mainly by ingestion or dermal application. Different types of NP as zinc oxide (ZnO), titanium dioxide (TiO_2) or nanosilver are used in these products often at mass concentrations greater than 10 % in the case of sunscreens.

Up to recently, there has been no official regulation for labelling consumer products in terms of contained NP. However, in 2009 the European Parliament adopted a regulation for product

labelling applicable to cosmetic products on the EU internal market that will enter into force in 2012. Another regulation concerning food labelling is subject of current discussions.
Apart from the deliberate exposure, incidental exposure to humans is possible and cannot be excluded, e.g. by spraying paint containing NP or simply by air [Seaton et al 2010]. In urban air for instance, particles are derived mostly from combustion, e.g. diesel exhaust. But air pollution is not only an issue of urban areas. Particles greater than $PM_{2.5}$ are removed by settling and rain within hours, whereas ultrafine particles remain suspended in the air for weeks. Therefore, clouds of particles are able to drift over long distances, thus influencing rural areas as well [Seaton et al 1995]. A comparison of indoor personal monitoring to outdoor fixed-point sampling resulted in the same composition of PM showing that most indoor environments are unlikely to provide substantial protection from the risk of inhaling those [Brauer et al 1991].

1.3 THE LUNG - FROM PARTICLE INHALATION TO PATHOGENESIS

The adult human lung has an enormous surface area of 100 - 200 m^2 that is exposed to about 10,000 - 15,000 litres of inhaled air every day, depending on sex and physical condition. Thus, our lung is exposed to a wide range of pathogens like microorganisms, toxicants and infectious agents like cigarette smoke, automobile exhaust, ozone (O_3), sulphur dioxide (SO_2) or nitrogen dioxide (NO_2) as well as PM in fine and nanosize range [Azad et al 2008]. Inhalation of these pathogens may result in lung injury and generation of reactive oxygen/nitrogen species (ROS/RNS), triggering signalling cascades and thus the production of pro-inflammatory cytokines and chemokines [Emmendoerffer et al 2000].

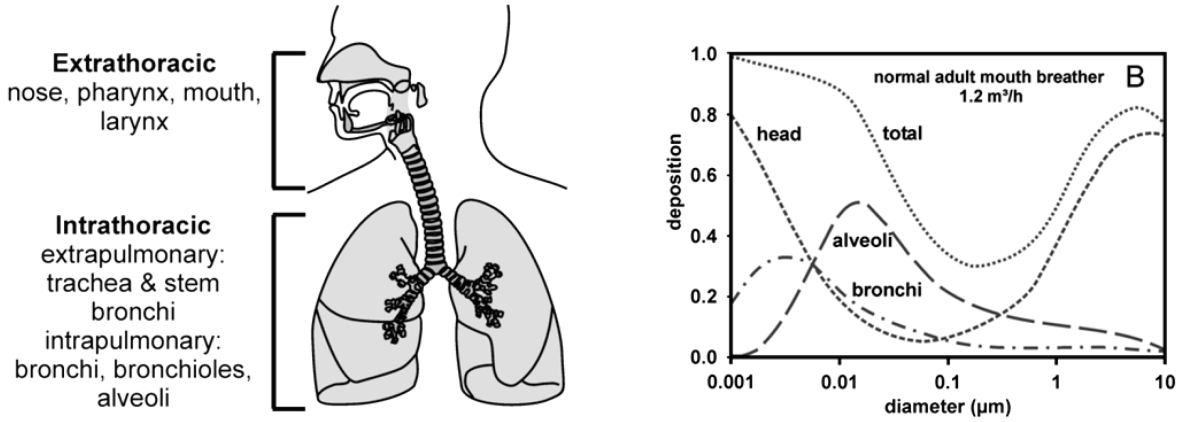

Figure 1.3 The human respiratory tract.
left: Anatomic structure of the respiratory tract, i.e. conducting region of the lung
right: Particle deposition as a function of particle size in an adult mouth breathing male human [Geiser & Kreyling 2010]

For inhaled particles the deposition is important for subsequent reactions within the lung. The rate of particle deposition is dependent on particle size and mass, thus varying between the distinct regions of the lung [Lastbom & Camner 2000] [see paragraph 1.2.2]. The specific pattern of deposition of particles in the lung is a determinant in the development of pulmonary diseases since this pattern determines the local doses within the lung and the subsequent redistribution of the deposited particles [Darquenne 2006].

1.3.1 PARTICLE DEPOSITION IN THE LUNG

Apart from particle size additional factors affect particle deposition within the lung including physiological and environmental factors, lung anatomy, temperature and humidity, respectively, or breathing patterns [ICRP Publication 66 1994].

Five mechanisms influence particle deposition within the respiratory tract: (1) inertial impaction, (2) gravitational sedimentation, (3) Brownian diffusion, (4) interception and (5) electrostatic precipitation [Figure 1.4].

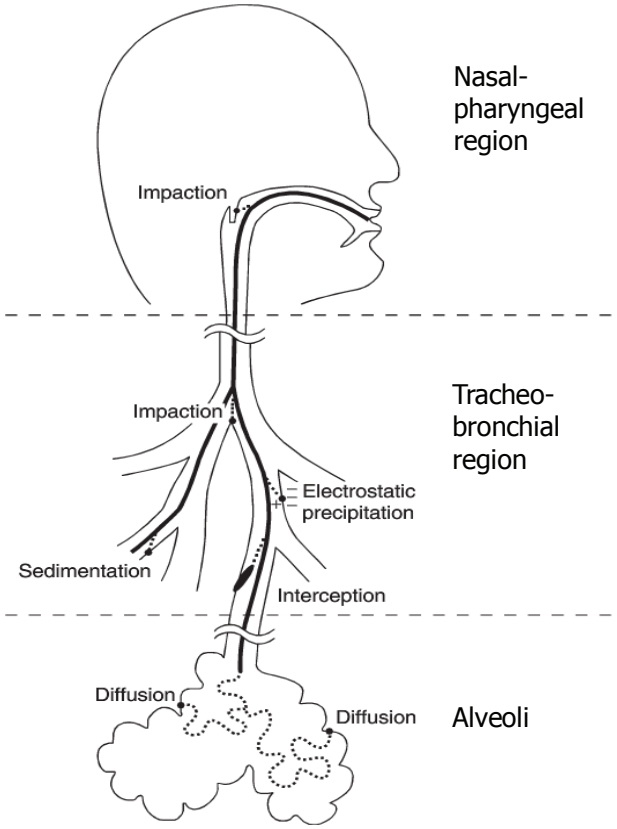

Figure 1.4 Mechanisms of deposition of inhaled particles in the respiratory tract.
These mechanisms are not restricted to the zone of the lung as shown in the figure e.g. deposition by sedimentation can also occur in the alveoli [modified from Darquenne 2006].

Inertial impaction is an important deposition mechanism for inhalable particles that takes place in the upper respiratory tract, nasal-pharyngeal region and or tracheo-bronchial region. Gravitational sedimentation is most important in the small airways and alveoli; schematically depicted in Figure 1.5. It is the dominant mechanism of deposition for particles with a diameter ranging between 0.5 and 5 µm. The sedimentation probability increases with particle size and density as well as residence time in the airways.

Deposition by Brownian diffusion results from the random motions of the particles caused by collisions with gas molecules. Unlike impaction and sedimentation, deposition by Brownian

diffusion increases with decreasing particle size and becomes the dominant mechanism of deposition for particles < 0.5 µm in diameter. This mechanism occurs mainly in the alveolar region of the lung. For particles < 0.01 µm, deposition by diffusion is also significant in the nose, mouth and pharyngeal airways.

Electrostatic precipitation results from charged particles inducing image charges of opposite sign onto the surfaces of the airways that are electrically conducting while normally uncharged. Charged particles become electrostatically attracted to the airway walls, thus deposition of charged particles may be greater than that of neutral particles. The contribution of electrostatic precipitation is less than 10 % of overall deposition.

Deposition by interception is usually for particles with a large ratio between length and diameter, such as fibers (e.g. asbestos). In detail, the centre of gravity of an elongated particle is in the gas phase while one of its ends touches an airway or alveolar wall. Interception is more likely to occur if the dimensions of the particle are comparable to those of the airspaces [Darquenne 2006].

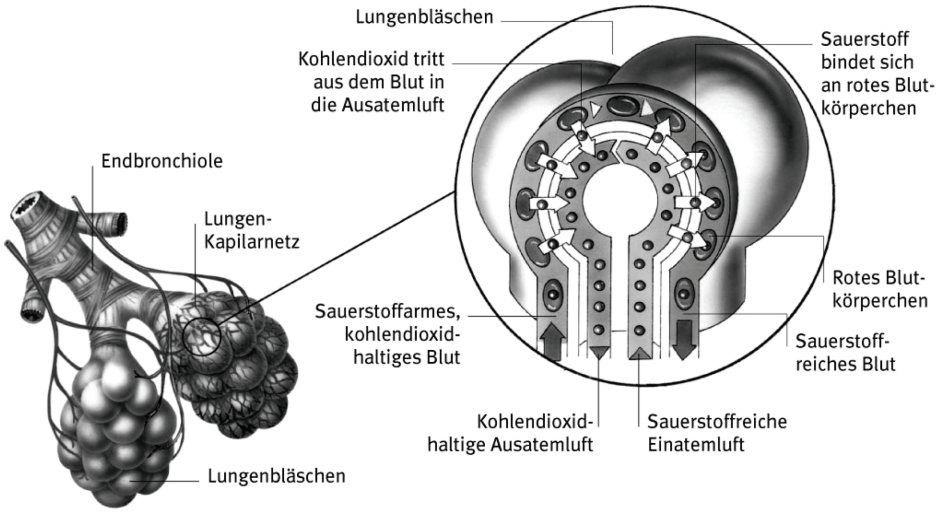

Figure 1.5 Schematic presentation of alveoli.
Magnification shows a cartoon of the constitution of the blood-air barrier [www.bertelsmann-bkk.de]

1.3.2 THE CLEARANCE OF PARTICLES

In the uppermost part of the respiratory tract, the nasal-pharyngeal region, deposited particles are easily cleared by coughing and sneezing. The lung possesses two major clearance mechanisms: the mucociliary and the phagocytic system.

The mucociliary system takes place in the trachea-bronchial airway that is lined by a ciliated epithelium covered by mucous and serous secretions produced by cells and glands of the

epithelium. Respireable particles (approximately < 5 µm in humans) are trapped by this secretion. Beating of the cilia tends to drive the secretions toward the mouth in order to be removed by expectorating or swallowing, thus making the gastrointestinal tract to a second target organ for particles [Witschi & Last 1996].

Particles of a small fine or ultrafine size < 0.1 µm mainly deposit in the non-ciliated terminal bronchioles or alveoli. In this region of the lung particles are removed by resident alveolar macrophages (AMΦ). Depending on the type and amount of particles to which the AMΦ is exposed to, this cell can become activated and release various pro-inflammatory mediators as will be discussed in detail in paragraph 1.7. During inflammation polymorphonuclear leukocytes (PMN) and monocytes are recruited to the alveoli via chemotaxis in order to assist in pathogen defence [Nicod 1999].

AMΦ cells reside on the luminar side of the lung, where they are constantly exposed to the environment via inhaled air, thus being the first cells within the lungs that get into contact with inhaled particles. AMΦ take up the particles and migrate into the lung interstitium, the lymphatic system or they move up the airways to be caught and removed by the mucociliary escalator [Lippmann & Schlesinger 1984]. The processes of uptake of particles by AMΦ are discussed in further detail in paragraph 1.4.

Depending on the concentration of inhaled particles AMΦ may also remain in the alveoli due to the so-called mechanism of overload which impairs migration of these cells. Apart from this overload situation, clearance may also be impaired if the inhaled particles are highly toxic and thereby cause direct damage to the AMΦ. In both cases, the alveolar epithelial cells will become increasingly exposed to particles. These epithelial cells have also been shown to take up particles and become activated like MΦ, e.g. by the production of cytokines, and thus contribute to the pulmonary inflammation [Churg 1996; Ohtoshi et al 1998].

1.4 MACROPHAGES - THEIR ORIGIN, DEVELOPMENT, DIFFERENTIATION & FUNCTION

MΦ serve as immunological sentinels of the body. MΦ are highly distributed throughout the body being on standby in all tissues for the response to invaded pathogens, thus playing a critical role in host defence. They are the linking cell type between the innate and adaptive immune systems and function as accessory cells in the recognition and activation phases of adaptive immune responses and as major effector cells. Therefore, MΦ are found in abundance at sites that interact with the environment, e.g. in the lung being exposed substantially to pathogens and environmental pollutants as discussed in the previous paragraphs. MΦ are increasingly evident by their trophic roles for other cell types in development and homeostasis [Abbas & Lichtman 2003; Gwinn & Vallyathan 2006].

MΦ are derived from hematopoietic stem cells in the bone marrow [Figure 1.6]. The direct precursor cells of MΦ are circulating blood monocytes, which enter various tissues and differentiate into tissue-specific MΦ populations under the influence of the microenvironment [Kennedy & Abkowitz 1998]. Additionally, MΦ are designated to that tissue by certain names e.g. AMΦ in pulmonary airways, microglia in the CNS, Kupffer cells in the liver, or osteoclasts for multinucleate phagocytes in the bone [Abbas & Lichtman 2003].

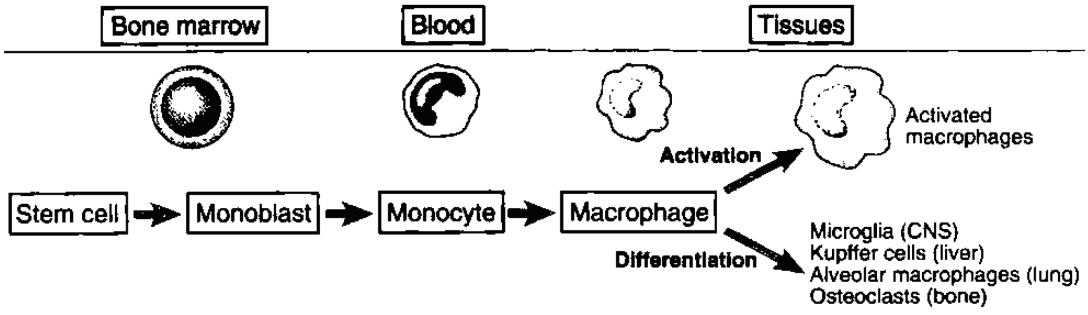

Figure 1.6 Maturation of macrophages. [Abbas & Lichtman 2003]

Together with dentritic cells (DC), PMN and MΦ has been defined as the mononuclear phagocyte system (MPS), representing the cell types with a common bone marrow lineage whose primary function is phagocytosis [Hume 2006]. These cell types are important effector cells in both innate and adaptive immunity. The part of innate immunity includes phagocytosis of pathogens, resulting in cytokine production that recruit and activate other inflammatory cells. In adaptive immune responses they have numerous roles in cell-mediated and humoral immunity [Abbas & Lichtman 2003].

MΦ are equipped with an array of various functions besides their characteristic phagocytosis, like bactericidal activity, antigen presentation, tumour cytotoxicity, removal of aged and apoptotic cells or cell debris, repair of injured tissue and bone resorption. Most of these functions are dependent on calcium-mediated signalling [Hoyal et al., 1998]. In general, MΦ develop their specialized functions depending on the needs of the tissue. In the case of the lung, AMΦ acquire the capacity to release large amounts of high cytotoxic oxidants [Laskin 2009].

1.5 PHAGOCYTOSIS & PINOCYTOSIS - PORTALS OF ENTRY INTO THE CELL

Internalization of macromolecules, particles and even cells is designated as endocytosis. This process encompasses several mechanisms. Basically, the attached macromolecule is progressively enclosed by the plasma membrane forming an intracellular vesicle by detaching from the membrane. Endocytosis is categorized by the size of the formed vesicles. Phagocytosis is the uptake of large particles, and pinocytosis, is known as the uptake of fluids and solutes [Figure 1.7; Conner & Schmid 2003].

Phagocytosis is restricted to cells of the MPS, specialized phagocytes that are characterized by a receptor-mediated and actin-based uptake process. This is the main mechanism for the clearance of insoluble 1 - 3 µm particles from the alveoli [Geiser 2010; Geiser & Kreyling 2010].

Pinocytosis is used by many cell types to take up material, mostly fluids or solutes from the surrounding. Pinocytosis can be classified according to at least four basic mechanisms of endocytosis, namely: macropinocytosis, clathrin-mediated, caveolae-mediated, and clathrin- and caveolae-independent endocytosis [Geiser 2010].

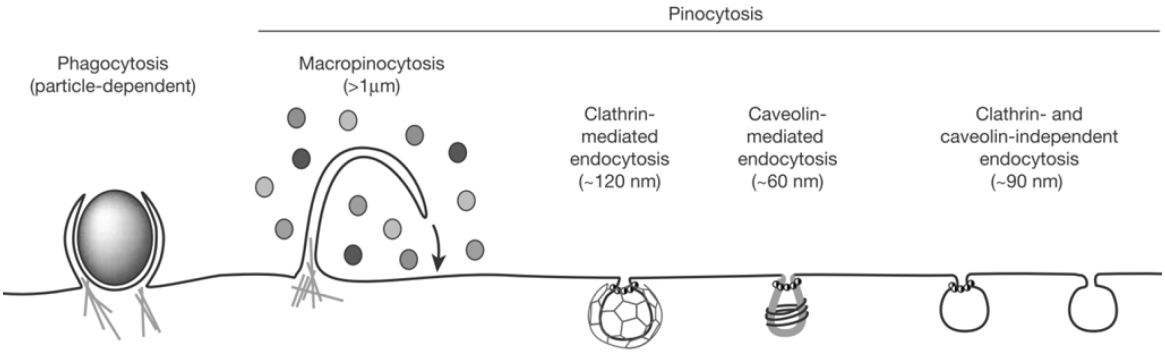

Figure 1.7 The mechanism of vesicle formation determines the subsequent endocytotic transport. [Conner & Schmid 2003]

1.5.1 ACTIN-DEPENDENT ENDOCYTOSIS

1.5.1.1 PHAGOCYTOSIS

Phagocytosis and macropinocytosis are the responsible uptake mechanisms for larger particles in the range of 1 - 5 µm. Both these mechanisms are actin-driven, thus active processes; however their primary trigger is different.

Phagocytosis is initiated by receptor binding on the cellular surface leading to intracellular signalling for actin polymerization, coordinated cytoskeletal movements, extension of membranes, followed by the initiation of phagocytosis. Within the cell the formed phagosome fuses with a lysosome to a phagolysosome, in which the ingested material is degraded by lysosomal enzymes, if possible [Geiser 2010].

Phagocytotic processes can be distinguished by the way phagocytotic receptors are activated due to distinct recognition motives on the pathogens' surface. By this means receptors are firstly subdivided in their opsonin dependency. Opsonin-independent receptors recognize directly specific structures on the particle surface like bacterial proteins (e.g. LPS) or sugar residues (e.g. α-mannan). Prior to opsonin-dependent phagocytosis, pathogens have to be targeted for phagocytosis by macromolecules, like immunoglobulins (e.g IgG antibody) or complement fragments, thus secondly, characterising these receptors by their opsonin-specificity (Fc-receptor (FcR), complement-receptor (CR), mannose-receptor (MR), scavenger-receptor (SR)) [Abbas & Lichtman 2003]. Depending on the activated receptor distinct signalling pathways and subsequent cellular responses are induced. Phagocytosis via FcR or MR induces pro-inflammatory responses, while activation of CR or SR leads to anti-inflammatory action [Aderem & Underhill 1999].

1.5.1.2 THE FCγ RECEPTOR-MEDIATED PHAGOCYTOSIS

FcR are important in linking the humoral and cellular arms of the immune response [Dai et al 2009]. These receptors are specialized for the Ig fragment crystallisable region, characterized by the specificity for one Ig subtype, i.e. FcαR (IgA), FcγR (IgG) and FcεR (IgE). The main class of FcR is represented by FcγR, that is mainly expressed on the surface of immune cells of the MPS and as such the most prominent FcR involved in phagocytosis [Ravetch & Kinet 1991; Hogarth 2002].

Functionally, there are two different classes of FcR: the activation and inhibitory receptors. They transmit their signals via phosphorylation of the immunoreceptor tyrosine-based activation (ITAM) or inhibitory motifs (ITIM), respectively, that are located on the cytoplasmatic domain of the FcR. The paired expression of activating and inhibitory

molecules on the same cell is the key for the generation of a balanced immune response [Ravetch & Lanier 2000].

FcγR is expressed in 3 classes: FcγRI (CD 64), FcγRII (CD32), FcγRIII (CD16) each of them has a variety of isoforms with differing affinities for IgG, tissue distribution, and level of expression. The high-affinity IgG receptor FcγRI is constitutively expressed on monocyte and macrophage lineage cells, mainly binding to monomeric IgG1 and IgG3. FcγRI is a member of the multichain immune recognition receptor family, comprising hetero-oligomeric complexes of a ligand-binding α-chain and a signalling γ-chain usually found in association with other immune receptors [Ravetch & Kinet 1991; Hogarth 2002]. The low-affinity receptors FcγRII and FcγRIII are mainly expressed on neutrophils and mononuclear phagocytes and natural killer cells, respectively. Binding of IgG molecules mainly takes place when presented on immune complexes or on opsonized pathogens, displaying an array of Fc regions [Abbas & Lichtman 2003].

FcγRII is the most broadly distributed FcR, existing in 3 isoforms (A, B, C), all equipped with similar intracellular domains and ligand specificities, but differing in cytoplasmatic tail structure, cell distribution, and functions. The carboxyl termini of FcγRIIA and FcγRIIC contain ITAM and can deliver an activation signal to phagocytes. FcγRIIA is the only FcR that does not need to oligomerize with a γ-chain in order to signal [Graziano & Fanger 1987].

FcγRIIB is exclusively expressed by lymphocytes, especially B cells, containing ITIM, thus counteracting activating signals delivered to B cells, which may shut off B cell activation. Among all these FcγR presented above, phagocytosis is mainly induced by FcγRI and FcγRIIA and negatively regulated by FcγRIIB [Aderem & Underhill 1999; Abbas & Lichtman 2003].

1.5.1.3 MACROPINOCYTOSIS

Macropinocytosis is pathogen-indepenent and unspecific. Macropinosomes are formed spontaneously or upon stimulation by e.g. growth factors. The induced signalling cascade triggers the actin-driven formation of membrane protrusions, the lamellopodia. Unlike phagocytosis, these lamellopodia do not "zipper up" along an antibody-coated pathogen, instead they collapse onto and fuse with the plasma membrane on the other side by forming a large vesicle, the macropinosome. This accidentally enclosed material may serve the phagocyte to sample the extracellular milieu for immune-relevant factors, thus fulfilling their immune competent tasks [Conner & Schmid 2003].

1.5.2 ACTIN-INDEPENDENT ENDOCYTOSIS

1.5.2.1 CLATHRIN-MEDIATED ENDOCYTOSIS

Clathrin-coated pits are formed by cell membrane invagination; their subsequent closure with material leads to the formation of clathrin-coated vesicles of about 100 - 120 nm in diameter. In the case of particle uptake, clathrin-coated pits expand, thus being able to enclose particles of around 200 nm [Rejman et al 2004]. The coat is shed in seconds and vesicles fuse with endosomes. At this stage, if receptors are involved, e.g. for the ligands transferrin or LDL, they dissociate and are recycled. The vesicles constantly fuse with larger vesicles and the endocytosed material ends up in degradative lysosomes. This may be important for the drug delivery field [Geiser 2010].

1.5.2.2 CAVEOLAE-MEDIATED ENDOCYTOSIS

Caveolae are flask-shaped invaginated plasma membrane domains, which are especially enriched in cholesterol and sphingolipids. They are characterized by the presence of the integral membrane protein caveolin. The vesicles, which have heterogenous morphology, range from 50 to 100 nm in diameter. Although primary caveolae vesicles are smaller than clathrin-coated pits, uptake of larger particles with a diameter of 500 nm are preferred [Rejman et al 2004]. Caveolae vesicles have been proposed to mediate the extensive transcellular shuttling of extracellular material. Caveolin-mediated endocytosis may be also important for drug delivery, as nanocarriers, tailored to enter this pathway, escape lysosomal degradation and hence sustained functionality [Conner & Schmid 2003].

1.5.2.3 CLATHRIN- & CAVEOLIN - INDEPENDENT ENDOCYTOSIS

These alternative endocytic carrier vesicles are small structures of 40 - 50 nm in diameter. They evolved from lipid microdomains and present a unique lipid composition. These small rafts can presumably be captured by any endocytotic vesicle, followed by internalisation. For instance, this kind of endocytosis also occurs in neurons and neuroendocrine cells, and function in the rapid recovery of membrane proteins after stimulated secretion. Additionally, other uncharacterized procedures for pinocytic uptake were observed in other cell types. It is likely that each of these pathways fulfils unique functions in the cell and varies mechanistically not only in how the vesicles are formed, but in terms of which cargo molecules they transport, to what intracellular destination their cargo is delivered, and how their entry is regulated. Nevertheless, triggers or mechanisms that govern caveolae- and clathrin-independent endocytosis remain poorly understood [Conner & Schmid 2003].

1.6 OXIDATIVE STRESS - A CELL FIGHTS BACK

The steady-state formation of prooxidants in cells and organs is balanced by a similar rate of their consumption by antioxidants that are enzymatic and/or non-enzymatic. When increased amounts of ROS are formed, a resulting imbalance of the prooxidant-antioxidant equilibrium may occur, in favour of the prooxidants. This is defined as oxidative stress [Sies 1991].
ROS include oxygen centred free radicals which are highly reactive molecules due to the presence of an unpaired valence shell electron. ROS molecules are derived from molecular oxygen O_2 being a reactive species itself or they are easily converted in such [Table 1.2]. Persistent oxidative stress is considered to be involved in respiratory illness like asthma or chronic obstructive pulmonary disease (COPD), but it is also supposed to be a cause of other diseases including neurodegenerative disorders (Alzheimer's Disease, Parkinson's Disease, Huntington's Disease) and aging processes [Valko et al 2005]. Environmental sources of ROS comprise already reactive molecules being ready for further reaction for instance constituents of air pollution particles, ozone, UV-light, cigarette smoke, and various drugs and pesticides [reviewed in Oberdanner 2003]. Additionally, various pathogens, including inhaled toxic particles, are also able to activate immune cells, like AMΦ or PMN in the lung, leading to an acute oxidative stress situation resulting in a rapid increase of ROS, the oxidative burst [DeCoursey & Ligeti 2005].

1.6.1 CELLULAR GENERATION OF REACTIVE OXYGEN / NITROGEN SPECIES

Various types of particles are able to generate ROS from their intrinsic physico-chemical properties, e.g. via their large and reactive surface areas, or their contamination with organics and/or transition metals [see paragraph 1.2.1]. In addition, ROS/RNS may be produced indirectly by the particles itself upon their interaction with cells, as will be discussed below. ROS/RNS produced by the particles and/or during different cellular reactions may be either beneficial or harmful to the cells, thus acting as a "double-edged sword" in cellular reactions. ROS/RNS are very important in cell metabolism, since they may act as secondary messengers involved in many signalling pathways, especially in AMΦ. This ROS-dependent signal transduction is termed redox signalling [Azad et al 2008]. In this paragraph ROS and RNS will be discussed separately, but in the following both reactive species will be termed just as ROS, since RNS are also oxygen-derived.
The production of ROS by cells is not only restricted to situations of hazard or defence. Under normal conditions ROS are synthesized in mitochondria as a by-product during oxidative phosphorylation in cellular respiration. In contrast, during environmental stress ROS

production may increase dramatically resulting in a broad damage of cell structures. However, ROS are not only implicated in a detrimental cellular response, like apoptosis. They have also positive effects, such as inducing host defence genes and mobilizing ion transport systems in order to destroy pathogens like bacteria or fungi [Dröge 2002].

Chronic ROS generation by either exogenous factors, like particles, or from cellular sources are implicated in various cellular responses including induction of DNA-damage (i.e. genotoxicity), cell proliferation, inflammation and apoptosis which have impact in various diseases e.g. cancer [Figure 1.8]. Therefore, the balance between oxygen utilization, ROS/RNS formation, and antioxidant activity is essential for normal functions of the body.

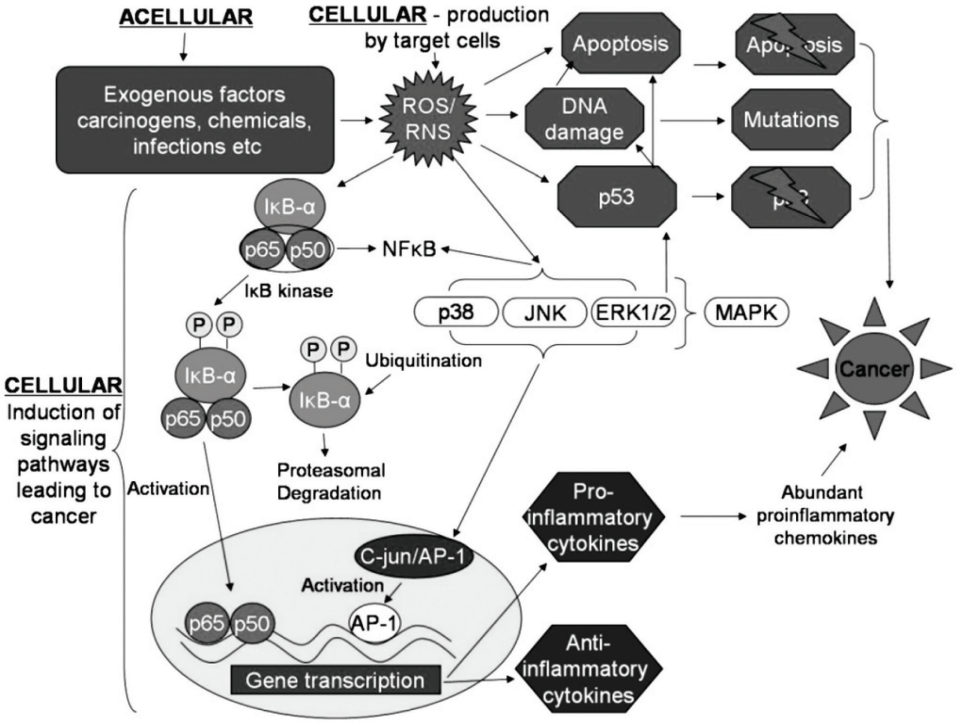

Figure 1.8 Scheme of key molecular events and signalling pathways induced by ROS/RNS. Various cytotoxic and genotoxic insults trigger chronic inflammation either directly or indirectly [Azad et al 2008]

Activated AMΦ or PMN are capable to generate an array of various ROS and RNS including superoxide ($O_2^{\bullet-}$), hydroxyl radicals ($HO^{\bullet}$), nitric oxide radical ($NO^{\bullet}$), peroxynitrite ($ONOO^-$) (through combination of $O_2^{\bullet-}$ and $NO^{\bullet}$) as well as hydrogen peroxide (H_2O_2) and hydrochlorous acid (HOCl) as metabolites [Figure 1.9]. These ROS/RNS are produced by different enzymes, like NADPH-oxidase (NOX) enzymes, xanthine-oxidase (XO) and cytochromes P450 in order to kill invaded pathogens [Emmendoerffer et al 2000; Valko et al 2005].

The NOX enzyme family contains 7 members: NOX1 - NOX5, DUOX1 and DUOX2 [Bedard & Krause 2007]. Especially NOX2 of activated professional phagocytes leads to the production of enormous quantities of $O_2^{\cdot -}$, and secondary to a number of additional ROS, like $HO^{\cdot}$, H_2O_2 and HOCl. This enzyme transfers electrons from NADPH into the cytoplasm, across the cell membrane of the phagocytic vacuole and catalyzes the production of $O_2^{\cdot -}$ from O_2 and NADPH, thus playing essential roles in killing bacteria and other invaders [Cross & Segal 2004].

MΦ express lower amounts of the phagocyte NADPH-oxidase and releases less $O_2^{\cdot -}$ than PMN into the phagosome where the myeloperoxidase (MPO) catalyzes predominantly the formation of HOCl from chloride and H_2O_2 during the respiratory burst. MPO is an important heme containing lysosomal protein with microbicidal properies, which is most abundantly present in the primary granules of PMN or in lysosomes of MΦ. Upon phagocytosis NADPH-oxidase is translocated to phagosomal membranes, where granules/lysosomes fuse with the pathogen-containing phagosome, and MPO is released into the phagosomal lumen. In the case of uncontrolled PMN or MΦ function this reaction can contribute to the damage of healthy tissues [Rada & Leto 2008].

Table 1.2 Examples of free and non-free radical reactive oxygen and nitrogen species. [according to Dröge 2002; Oberdanner 2003]

Free Radicals		Non-free Radicals	
Superoxide	$O_2^{\cdot -}$	Singlet Oxygen	$^1O_2$
Hydroxylradical	$HO^{\cdot}$	Ozone	O_3
Alkoxylradical	$RO^{\cdot}$	Dinitrogen trioxide	N_2O_3
Perhydroxylradical	$HOO^{\cdot}$	Hypochlorous acid	HOCl
Peroxylradical	$ROO^{\cdot}$	Nitrous acid	HNO_2
Nitrogen dioxide	$NO^{\cdot}_2$	Hydroperoxide	ROOH
Peroxynitrite	$ONOO^-$		
Nitric Oxide	$NO^{\cdot}$		

RNS are a family of antimicrobial molecules derived from $NO^{\cdot}$ mainly synthesized by the NO synthases (NOS) as a by-product of the catalysis from L-arginine to L-citrulline. In phagocytes $NO^{\cdot}$ is primarily generated via the inducible and calcium-independent isoform (iNOS), and to lesser extent also by the constitutively and calcium-dependent isoforms, the neuronal (nNOS) and epithelial NOS (eNOS). $NO^{\cdot}$ is a nitrogen-centred free radical and oxidizes in tissues to nitrate (NO_3^-) and nitrite (NO_2^-) [Alderton et al 2001; Brüne 2003]. It is less reactive than ROS but nevertheless, NOs toxicity depends on increased $NO^{\cdot}$ synthesis and the simultaneous synthesis of $O_2^{\cdot -}$, which react very fast to the formation of $ONOO^-$

[Beckman & Koppenol 1996]. As such RNS act together with ROS causing cell damage; therefore these two species are often collectively referred as ROS/RNS [Squadrito & Pryor 1998]. Table 1.2 lists important free and non-free radicals.

Apart from phagocytic cells which generate ROS and RNS in large amounts, ROS can also be generated in other cells, including lung epithelial cells, although at lower amounts. Important sources of such ROS, which have been implicated mainly in activation of cell signalling cascades, are mitochondria and dual oxidases (DUOX) [Geiszt et al 2003; Rada & Leto 2008]. Both NADPH-oxidase and iNOS are assembled or up-regulated respectively, in activated MΦ following induction by cytokines and microbial products, notably interferon-gamma (IFN-γ) and lipopolysaccharides (LPS) [Iovine et al 2008].

1.6.2 CELLULAR ANTIOXIDANT DEFENCE MECHANISMS - TAKING CARE OF ONESELF

The term "antioxidant" refers to any molecule capable of quenching or deactivating free radicals before they impair cellular compounds. Cellular antioxidant mechanisms have evolved highly complex enzymatic and non-enzymatic antioxidant systems, which work synergistically to protect the cells and organ systems of the body against free radical damage. The balance of oxidants and antioxidant system is an important factor for cellular homeostasis; otherwise it leads to several detrimental events, starting with oxidizing of cellular compounds like proteins or DNA. Antioxidants can have endogenous origin or obtained exogenously as a part of a diet or as dietary supplements [Rahman 2007].

The lung has a well-developed biological defence system comprising efficient antioxidant mechanisms against oxidative and nitrosative damage. Several antioxidants are present in the lung epithelial lining fluids like reduced glutathione, ascorbic acid, taurine, uric acid, α-tocopherol as well as antioxidant enzymes [Khan 2002]. These enzymes include glutathione peroxidases, catalases, thioredoxins and superoxide dismutases (SOD) [Figure 1.9]. They catalyse decomposition of reactive species into compounds that are harmless to the cellular system. For instance, SOD converts $O_2^{\cdot-}$ into H_2O_2, which in turn can be converted into H_2O and O_2 by catalase. Also glutathione peroxidase can reduce H_2O_2 by oxidizing glutathione from GSH to GSSG [Halliwell & Gutteridge 2001].

Reduced glutathione (GSH) is the major antioxidant in mammalian cells. The mitochondrial amount of GSH is indeed relevant for protecting against ONOO- mediated cellular damages. In contrast, the antioxidant ability of the extracellular space is less, whereby the most important plasma antioxidant in humans seems to be uric acid [Halliwell & Gutteridge 2001]. In the lumen of the alveolar region glutathione is considered as most important antioxidant

[Kelly 1999]. The total level of GSH or the ratio of GSH and GSSH, respectively, are used as indicators for the redox balance in cellular extracts, tissues or body fluids, thus providing information of oxidative stress and cellular toxicity [Pastore et al 2001].

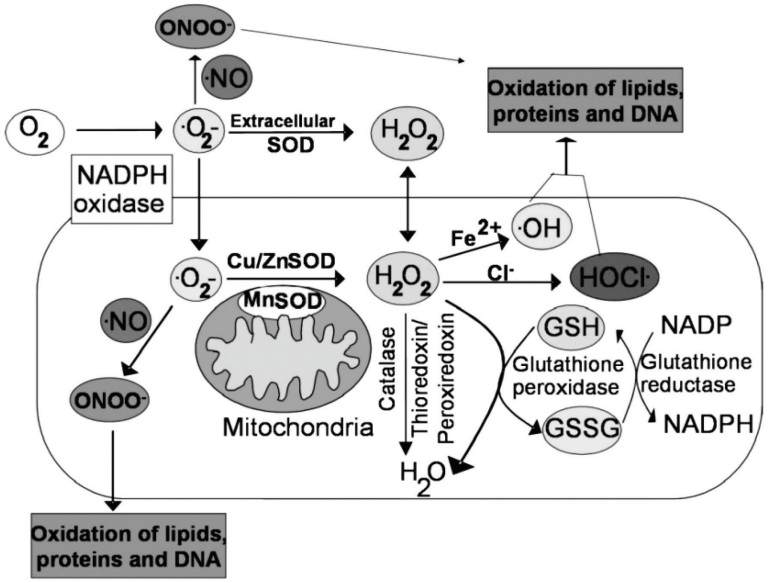

Figure 1.9 Major pathways involved in the production and elimination of ROS.
[Azad et al 2008]

Non-enzymatic defences include compounds primarily derived from diet, such as carotenoids, flavonoids, and the vitamins E and C [Khan 2002]. Some antioxidants can interact with other antioxidants, thereby regenerating their original properties, a mechanism that is often referred to as the "antioxidant network" [Sies et al 2005].

1.7 INFLAMMATION & OXIDATIVE STRESS - CELLULAR RESPONSES

Inflammation and oxidative stress are considered as the driving mechanisms responsible for the pulmonary toxicity as observed with specific types of particles after inhalation. Therefore, these two mechanisms are in the focus of investigations to gain more knowledge of systemic diseases associated with particle exposure in the lung. The concentration on the regulation of gene expression related to inflammation or oxidative stress is one of the basis for diseases and thus subject of investigations.

The pro-inflammatory and redox sensitive transcription factor nuclear factor kappa-light-chain-enhancer of activated B cells (NF-κB) is crucial in the gene regulation in a broad range of biological processes including innate and adaptive immunity, inflammation and stress responses [Nichols et al 2001]. Dimeric NF-κB/Rel protein complexes reside in the cytosol inhibited by being bound to the inhibitor of NF-κB (IκB) proteins, mostly IκBα. Pro-inflammatory cytokines, LPS, growth factors and antigen receptors activate the transcription factor by inducing the cascade of phosphorylation, ubiquitination and proteasomal degradation of IκB, thus freeing NF-κB/Rel complexes. Various types of particles are also known to activate the NF-κB pathway [Schins & Donaldson 2000]. Active NF-κB/Rel complexes are in turn activated by phosphorylation, followed by translocation into the nucleus where, either alone or in combination with other transcription factor families as for instance activator protein 1 (AP-1), induces target gene transcription [Schins & Donaldson 2000; Castranova 2004; Hess et al 2004].

The acute inflammatory cytokines tumour necrosis factor alpha (TNF-α) and interleukin-1 beta (IL-1β) are the prominent examples for NF-κB-regulated genes [Piguet et al 1990; Kida et al 2005], that are also involved in particle-induced diseases, like silicosis [Dubois et al 1989; Davis et al 1998; Albrecht et al 2004]. ROS are known as well to be capable of activating NF-κB [Schreck et al 1991; Janssen-Heininger et al 1999] being generated as acute stress responses to pathogens, e.g. during silica exposure [Porter et al 2002; Zeidler et al 2004]. NF-κB has been shown *in vivo* and *in vitro* upon exposure to quartz, mainly in AMΦ and pulmonary epithelial cells, and thus this transcription factor is strongly implicated in the development of quartz-induced pulmonary diseases [Hubbard et al 2002; Albrecht et al 2004; van Berlo et al 2010].

Oxidative stress has emerged as the dominant paradigm for how particles initiate inflammation and genotoxicity that is further augmented by inflammatory cells releasing their own arsenal of oxidants [Schins & Borm 1999; Borm 2008]. Especially AMΦ, which modulate much of the physiological and immunological function of the lung, are susceptible targets for environmental oxidants, like H_2O_2 producing agents for instance, which are also capable in

causing elevation of free intracellular calcium concentration $[Ca^{2+}]_i$ in some cells [Hoyal et al 1998].

In situations of oxidative stress, intracellular Ca^{2+} pools, like the endoplasmic reticulum, mitochondria and the extracellular space, phospholipid- and Ca^{2+}-binding proteins as well as annexins, release Ca^{2+}, a crucial second messenger, into the cytoplasm. Many of the essential enzymes in cellular signalling cascades are Ca^{2+}-dependent, as are numerous proteins that participate in the regulated function. This emphasises the importance of regulation of the $[Ca^{2+}]_i$ in physiological signal transduction [Hoyal et al 1998].

Direct contact with pathogens and subsequent endocytosis may lead to MΦ activation resulting in the production of distinct mediators listed in Table 1.3. These secretory products mediate among others the initiation of inflammation by recruitment of further immune cells, like PMN or B-cells, to the site of need. Furthermore, MΦ may influence physiological properties by their released factors, like vascular permeability at the inflammatory site, controlling the cell growth, cell differentiation, tissue repair and function of surrounding cells [Akagawa 2002].

Table 1.3 Key macrophage-secretory products. [modified from Nicod 1999]

Cytokines	**Chemokines**	**Defensins**
IL-1β / IL-1 ra TNF-α / TNFsRs IL-6, -10, -12	IL-8 MIP-1 α/β RANTES MCP-1/-3	ROS RNS
Enzymes	**Bioactive Lipids**	**Complement Proteins**
MMP-1,-9 / TIMPs MΦ-metalloelectase urokinase acid hydrolases	cyclooxygenase products	most complement proteins inhibitor C1q

Abbreviations: MIP-1α/β - MΦ inflammatory protein-1α/β
RANTES - regulated on activation normal T-cell expressed and secreted
MCP-1/3 - monocyte chemoattractant protein-1/3

In detail, initiation of inflammation by release of the early pro-inflammatory cytokines IL-1β or TNF-α will induce a cascade of events in the alveolar milieu such as the release of chemokines or growth factors (granulocyte-/MΦ-colony stimulating factor) or the appearance of adhesion molecules on endothelial or epithelial cells [see Table 1.3]. Inflammatory cytokines will favour the activation of neighbouring cells and attract several inflammatory

elements from the blood. In addition, bioactive lipids mostly derived from cyclooxygenase products of arachidonate (thromboxane A2, leukotriene B4, prostaglandin E_2 and D_2) will influence vasoactive mechanisms, the function of T- and B-lymphocytes as well as the MΦ in an autocrine manner.

MΦ are able to control inflammation by the release of an inhibitor of IL-1 or TNF-α in the form of IL-1 receptor antagonist or TNF-soluble receptors, respectively [Galve-de Rochemonteix et al 1996]. They have the capacity to block IL-1 or TNF production by their own release of IL-10 [Nicod et al 1995]. Defensins are cationic proteins capable of killing a wide variety of gram-positive and gram negative bacteria and fungi. ROS and/or RNS are also involved in killing microorganisms and eventually tumour cells [see paragraph 1.6.1]. MΦ are also known to be involved in lung remodelling and repair. Indeed, they produce MΦ-metalloelastases, collagenase, matrix metalloproteinases (MMP1, MMP9) and the tissue inhibitors of metalloproteinases (TIMP) under the tight regulation of cytokines [Lacraz et al 1992]. MΦ thus remodel matrix constituents by their own production of urokinase to remove fibrin deposition. They can also release fibroblast growth factors such as transforming growth factor or platelet-derived growth factor. By their production of several components of complement as well as of the C1q inhibitor, they are likely to facilitate the opsonisation of bacteria, while they are able to inhibit undue inflammation by controlling the effect of the activation of the complement cascades [Hamacher et al 1998].

1.7.1 ALVEOLAR MACROPHAGES - A BALANCE OF PRO- & ANTI-INFLAMMATORY ACTIONS

Accumulating evidence suggests that the diverse biological activities of MΦ are mediated by functionally distinct subpopulations that are phenotypically polarized by their microenvironment and by exposure to inflammatory mediators [Figure 1.10].

These divergent polarized MΦ subpopulations are broadly classified on the basis of Th1/Th2 nomenclature, into two major groups: classically activated M1 cells expressing pro-inflammatory function, and alternatively activated M2 cells - subdivided in M2a, M2b and M2c - exhibiting anti-inflammatory function. Correspondingly, M1 and the various forms of M2 cells express distinct repertoires for cytokine and chemokine receptors [Mantovani et al 2005]. The outcome of the responses to tissue injury is determined on the balance of the produced mediators by these two subpopulations of MΦ, as summarised and illustrated in Figure 1.10, allegorized by nomenclature of star wars - the movie.

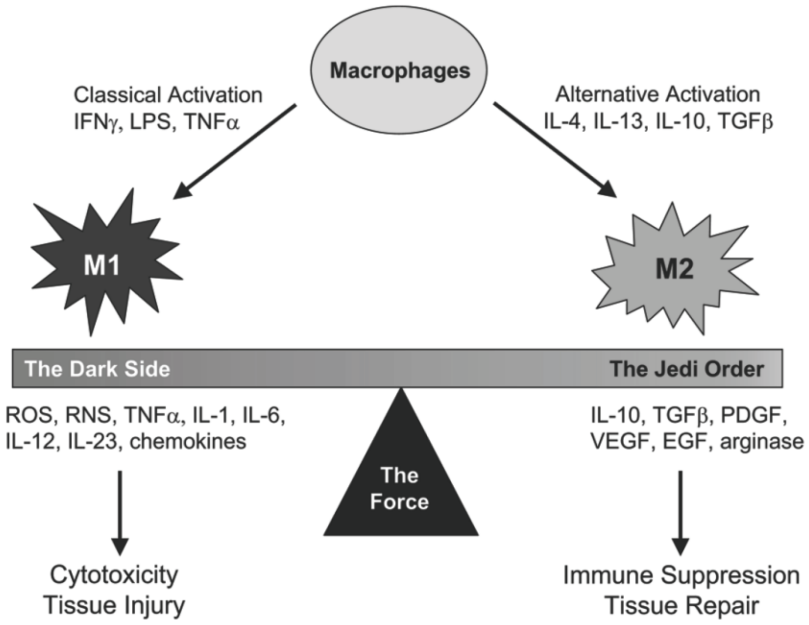

Figure 1.10 Macrophages develop into classically activated M1 cells or alternatively activated M2 cells.
The type of the developing cell depends on the inflammatory signals encountered at sites of injury or infection [Laskin 2009].

1.8 THE AIM OF THE THESIS

The focus of this thesis was concentrated on the mechanisms and consequences of interactions between AMΦ and particles. Experimental inhalation studies in rodents as well as occupational toxicology data have demonstrated marked contrasts with regard to the hazards of different types of particles. Therefore, in the present study a set of different particles were evaluated for their ability to induce oxidative stress and activate markers of inflammation in MΦ, in relation to their various specific physico-chemical properties. Table 1.4 lists the evaluated particles in relation to their characteristics and applications.

Table 1.4 Particulate materials that were investigated in this thesis.

Titanium dioxide	• Highly insoluble metal oxide particle occurring as anatase, rutile, brookite or as mixed forms [Mo & Ching 1995] • $fTiO_2$ is considered inert and therefore widely used in several industries, for instance used as food additive with the E-number 171 [Chaudhry et al 2008]. • $ufTiO_2$ and $fTiO_2$ have been used together as model compounds to test the "ultrafine hypothesis" of particles [Oberdörster et al 2005b; Johnston et al 2010]. • Occupational exposure exists, environmental rather unknown, but considered to increase in near future because of applications in the nanotechnology field.
Quartz	• A form of crystalline silica which is known to lead to severe lung diseases including silicosis and COPD [Schins & Borm 1999; Hnizdo & Vallyathan 2003] • Crystalline silica is classified by the IARC as human carcinogen [IARC 1997]. • The quartz sample DQ12 represents a well-defined respirable sample of high-purity, crystallinity and minimal contamination with metal impurities. It has been used for many decades as positive control in particle toxicity studies [Hill & Hobbs 1982; Huaux et al 1995; Creutzenberg et al 2008]. • Impurities of crystalline silica are considered to impact on the toxic and inflammatory potency of this material [Donaldson & Borm 1998]. Exemplary, contamination of natural occurring quartz with aluminium compounds has been considered to reduce the surface reactivity and hence the toxic potential of this material [Duffin et al 2001; Schins et al 2002; Albrecht et al 2004].
Hydroxyapatite	• Occurs mainly as hydroxyapatite-protein-composite in biomedical applications [Tampieri et al 2005; Wahl & Czernuszka 2006] • Used as active biomaterial in toothpaste, for bone grafts or as coating to promote bone ingrowth into prosthetic implants [Huber et al 2008; Palmer et al 2008]

The chosen cellular endpoints of oxidative stress and pro-inflammatory response were determined on various cellular levels. As a model throughout this thesis, the well-established rat AMΦ cell line NR8383 was used [Helmke et al 1989]. Moreover, in one specific study, primary AMΦ from Wistar rats were used for comparison with the effects in the NR8383 cell line. The well-known high toxic crystalline silica sample DQ12 was used as a reference material [Table 1.4]. In the framework of this thesis three independent studies have been performed. The specific objectives of these respective studies and the particulate materials that were used are listed in Table 1.5.

Table 1.5 Study overview of this thesis with focused objectives.

Study	Particles	Objectives
1	**TiO_2** fine vs ultrafine	One material, different size distributions and specific surface areas: • What are the uptake mechanisms for these different materials? • How do the effects of the fTiO_2, which is considered as inert, compare to those with TiO_2 in the nanosize? • How do the effects compare to that of the DQ12 reference material?
2	**Quartz** different amount of iron loading	Used as a highly toxic particle, well-known for its ability to induce fibrosis and lung cancer. Moreover, surface modification of quartz particles by iron ions leads to generation of hydroxyl and carbon centred free radicals in an acellular system: • How does this modification of the quartz surface and associated chemical reactivity impact on oxidative stress and pro-inflammatory responses in AMΦ? • How does the effect of the model quartzes used, compare to that of the DQ12 quartz?
3	**Hydroxyapatite** fine vs ultrafine differently-shaped surface modified	Investigation of the biocompatibility of hydroxyapatite particulates of different size, as well as of a particle-protein-composite: • Which influence do the nanosize and protein coating have on the reactivity of hydroxyapatite? • How do the effects compare to that of the DQ12 reference sample?

1.9 REFERENCES

Abbas AK, Lichtman AH. Cellular and Molecular Immunology. Elsevier Science (Saunders) 2003.

Aderem A, Underhill DM. Mechanisms of phagocytosis in macrophages. Annu Rev Immunol 1999, 17:593-623.

Akagawa KS. Functional heterogeneity of colony-stimulating factor-induced human monocyte-derived macrophages. Int J Hematol 2002, 76(1):27-34.

Albrecht C, Schins RP, Höhr D, Becker A, Shi T, Knaapen AM, Borm PJ. Inflammatory time course after quartz instillation: role of tumor necrosis factor-alpha and particle surface. Am J Respir Cell Mol Biol 2004, 31(3):292-301.

Alderton WK, Cooper CE, Knowles RG. Nitric oxide synthases: structure, function and inhibition. Biochem J 2001, 357(Pt 3):593-615.

Azad N, Rojanasakul Y, Vallyathan V. Inflammation and lung cancer: roles of reactive oxygen/nitrogen species. J Toxicol Environ Health B Crit Rev 2008, 11(1):1-15.

Becker S, Dailey LA, Soukup JM, Grambow SC, Devlin RB, Huang YC. Seasonal variations in air pollution particle-induced inflammatory mediator release and oxidative stress. Environ Health Perspect 2005, 113(8):1032-8.

Beckman JS, Koppenol WH. Nitric oxide, superoxide, and peroxynitrite: the good, the bad, and ugly. Am J Physiol 1996, 271(5 Pt 1):C1424-37.

Bedard K, Krause KH. The NOX family of ROS-generating NADPH oxidases: physiology and pathophysiology. Physiol Rev 2007, 87(1):245-313.

Borm PJ. Future interactions in Particle Toxicology: the role of PFT. Part Fibre Toxicol 2008, 5:5.

Borm PJ, Müller-Schulte D. Nanoparticles in drug delivery and environmental exposure: same size, same risks? Nanomedicine (Lond) 2006, 1(2):235-49.

Brauer M, Koutrakis P, Keeler GJ, Spengler JD. Indoor and outdoor concentrations of inorganic acidic aerosols and gases. J Air Waste Manage Assoc 1991, 41(2):171-81.

Brown DM, Donaldson K, Borm PJ, Schins RP, Dehnhardt M, Gilmour P, Jimenez LA, Stone V. Calcium and ROS-mediated activation of transcription factors and TNF-alpha cytokine gene expression in macrophages exposed to ultrafine particles. Am J Physiol Lung Cell Mol Physiol 2004, 286(2):L344-53.

Brüne B. Nitric oxide: NO apoptosis or turning it ON? Cell Death Differ 2003, 10(8):864-9.

Castranova V. Signaling pathways controlling the production of inflammatory mediators in response to crystalline silica exposure: role of reactive oxygen/nitrogen species. Free Radic Biol Med 2004, 37(7):916-25.

Chang E, Thekkek N, Yu WW, Colvin VL, Drezek R. Evaluation of quantum dot cytotoxicity based on intracellular uptake. Small 2006, 2(12):1412-7.

Chaudhry Q, Scotter M, Blackburn J, Ross B, Boxall A, Castle L, Aitken R, Watkins R. Applications and implications of nanotechnologies for the food sector. Food Addit Contam Part A Chem Anal Control Expo Risk Assess 2008, 25(3):241-58.

Churg A. The uptake of mineral particles by pulmonary epithelial cells. Am J Respir Crit Care Med 1996, 154(4 Pt 1):1124-40.

Conner SD, Schmid SL. Regulated portals of entry into the cell. Nature 2003, 422(6927):37-44.

Creutzenberg O, Hansen T, Ernst H, Muhle H, Oberdorster G, Hamilton R. Toxicity of a quartz with occluded surfaces in a 90-day intratracheal instillation study in rats. Inhal Toxicol 2008, 20(11):995-1008.

Cross AR, Segal AW. The NADPH oxidase of professional phagocytes--prototype of the NOX electron transport chain systems. Biochim Biophys Acta 2004, 1657(1):1-22.

Crüts B, van Etten L, Tornqvist H, Blomberg A, Sandstrom T, Mills NL, Borm PJ. Exposure to diesel exhaust induces changes in EEG in human volunteers. Part Fibre Toxicol 2008, 5:4.

Dai X, Jayapal M, Tay HK, Reghunathan R, Lin G, Too CT, Lim YT, Chan SH, Kemeny DM, Floto RA, Smith KG, Melendez AJ, MacAry PA. Differential signal transduction, membrane trafficking, and immune effector functions mediated by FcgammaRI versus FcgammaRIIa. Blood 2009, 114(2):318-27.

Darquenne C. Particle Deposition in the lung. www.scribd.com/doc/28978774/Particle-Deposition-in-the-Lung#stats 2006.

Davis GS, Pfeiffer LM, Hemenway DR. Persistent overexpression of interleukin-1beta and tumor necrosis factor-alpha in murine silicosis. J Environ Pathol Toxicol Oncol 1998, 17(2):99-114.

DeCoursey TE, Ligeti E. Regulation and termination of NADPH oxidase activity. Cell Mol Life Sci 2005, 62(19-20):2173-93.

des Rieux A, Ragnarsson EG, Gullberg E, Preat V, Schneider YJ, Artursson P. Transport of nanoparticles across an in vitro model of the human intestinal follicle associated epithelium. Eur J Pharm Sci 2005, 25(4-5):455-65.

Donaldson K, Borm PJ. The quartz hazard: a variable entity. Ann Occup Hyg 1998, 42(5):287-94.

Donaldson K, Stone V. Current hypotheses on the mechanisms of toxicity of ultrafine particles. Ann Ist Super Sanita 2003, 39(3):405-10.

Dröge W. Free radicals in the physiological control of cell function. Physiol Rev 2002, 82(1):47-95.

Dubois CM, Bissonnette E, Rola-Pleszczynski M. Asbestos fibers and silica particles stimulate rat alveolar macrophages to release tumor necrosis factor. Autoregulatory role of leukotriene B4. Am Rev Respir Dis 1989, 139(5):1257-64.

Duffin R, Gilmour PS, Schins RP, Clouter A, Guy K, Brown DM, MacNee W, Borm PJ, Donaldson K, Stone V. Aluminium lactate treatment of DQ12 quartz inhibits its ability to cause inflammation, chemokine expression, and nuclear factor-kappaB activation. Toxicol Appl Pharmacol 2001, 176(1):10-7.

Emmendoerffer A, Hecht M, Boeker T, Mueller M, Heinrich U. Role of inflammation in chemical-induced lung cancer. Toxicol Lett 2000, 112-113:185-91.

Ferin J, Oberdorster G, Penney DP. Pulmonary retention of ultrafine and fine particles in rats. Am J Respir Cell Mol Biol 1992, 6(5):535-42.

Fubini B, Hubbard A. Reactive oxygen species (ROS) and reactive nitrogen species (RNS) generation by silica in inflammation and fibrosis. Free Radic Biol Med 2003, 34(12):1507-16.

Galve-de Rochemonteix B, Nicod LP, Dayer JM. Tumor necrosis factor soluble receptor 75: the principal receptor form released by human alveolar macrophages and monocytes in the presence of interferon gamma. Am J Respir Cell Mol Biol 1996, 14(3):279-87.

Geiser M. Update on macrophage clearance of inhaled micro- and nanoparticles. J Aerosol Med Pulm Drug Deliv 2010, 23(4):207-17.

Geiser M, Kreyling WG. Deposition and biokinetics of inhaled nanoparticles. Part Fibre Toxicol 2010, 7:2.

Geiszt M, Witta J, Baffi J, Lekstrom K, Leto TL. Dual oxidases represent novel hydrogen peroxide sources supporting mucosal surface host defense. Faseb J 2003, 17(11):1502-4.

Ghio AJ, Devlin RB. Inflammatory lung injury after bronchial instillation of air pollution particles. Am J Respir Crit Care Med 2001, 164(4):704-8.

Goodman CM, McCusker CD, Yilmaz T, Rotello VM. Toxicity of gold nanoparticles functionalized with cationic and anionic side chains. Bioconjug Chem 2004, 15(4):897-900.

Graziano RF, Fanger MW. Fc gamma RI and Fc gamma RII on monocytes and granulocytes are cytotoxic trigger molecules for tumor cells. J Immunol 1987, 139(10):3536-41.

Gwinn MR, Vallyathan V. Respiratory burst: role in signal transduction in alveolar macrophages. J Toxicol Environ Health B Crit Rev 2006, 9(1):27-39.

Halliwell B, Gutteridge JMC. Free Radicals in Biology and Medicine. Oxford University Press 2001.

Hamacher J, Sadallah S, Schifferli JA, Villard J, Nicod LP. Soluble complement receptor type 1 (CD35) in bronchoalveolar lavage of inflammatory lung diseases. Eur Respir J 1998, 11(1):112-9.

Helmke RJ, German VF, Mangos JA. A continuous alveolar macrophage cell line: comparisons with freshly derived alveolar macrophages. In Vitro Cell Dev Biol 1989, 25(1):44-8.

Hess J, Angel P, Schorpp-Kistner M. AP-1 subunits: quarrel and harmony among siblings. J Cell Sci 2004, 117(Pt 25):5965-73.

Hill JO, Hobbs CH. Comparative cytotoxicity of DQ12-quartz and fly ash particles from coal combustion. Toxicol Lett 1982, 10(4):399-403.

Hnizdo E, Vallyathan V. Chronic obstructive pulmonary disease due to occupational exposure to silica dust: a review of epidemiological and pathological evidence. Occup Environ Med 2003, 60(4):237-43.

Hogarth PM. Fc receptors are major mediators of antibody based inflammation in autoimmunity. Curr Opin Immunol 2002, 14(6):798-802.

Holgate ST, Koren HS, Samet JM, Maynard RL. Air pollution and health. *In:* Air pollution and lung cancer - Samet JM & Cohen AJ, Academic Press 1999, San Diego (CA).

Hoyal CR, Giron-Calle J, Forman HJ. The alveolar macrophage as a model of calcium signaling in oxidative stress. J Toxicol Environ Health B Crit Rev 1998, 1(2):117-34.

Huaux F, Lasfargues G, Lauwerys R, Lison D. Lung toxicity of hard metal particles and production of interleukin-1, tumor necrosis factor-alpha, fibronectin, and cystatin-c by lung phagocytes. Toxicol Appl Pharmacol 1995, 132(1):53-62.

Hubbard AK, Timblin CR, Shukla A, Rincon M, Mossman BT. Activation of NF-kappaB-dependent gene expression by silica in lungs of luciferase reporter mice. Am J Physiol Lung Cell Mol Physiol 2002, 282(5):L968-75.

Huber FX, Berger I, McArthur N, Huber C, Kock HP, Hillmeier J, Meeder PJ. Evaluation of a novel nanocrystalline hydroxyapatite paste and a solid hydroxyapatite ceramic for the treatment of critical size bone defects (CSD) in rabbits. J Mater Sci Mater Med 2008, 19(1):33-8.

Hume DA. The mononuclear phagocyte system. Curr Opin Immunol 2006, 18(1):49-53.

Hunt A, Abraham JL, Judson B, Berry CL. Toxicologic and epidemiologic clues from the characterization of the 1952 London smog fine particulate matter in archival autopsy lung tissues. Environ Health Perspect 2003, 111(9):1209-14.

IARC. Silica, Some Silicates, Coal Dust and Para-Aramid Fibrils. IARC Monogr Eval Carcinog Risks Hum 1997, 68:1-475.

ICRP Publication 66. Human respiratory tract model for radiological protection. A report of a Task Group of the International Commission on Radiological Protection. Ann ICRP 1994, 24(1-3):1-482.

Iovine NM, Pursnani S, Voldman A, Wasserman G, Blaser MJ, Weinrauch Y. Reactive nitrogen species contribute to innate host defense against Campylobacter jejuni. Infect Immun 2008, 76(3):986-93.

Janssen-Heininger YM, Macara I, Mossman BT. Cooperativity between oxidants and tumor necrosis factor in the activation of nuclear factor (NF)-kappaB: requirement of Ras/mitogen-activated protein kinases in the activation of NF-kappaB by oxidants. Am J Respir Cell Mol Biol 1999, 20(5):942-52.

Johnston H, Hutchison GR, Christensen FM, Peters S, Hankin S, Stone V. Identification of the mechanisms that drive the toxicity of TiO_2 particulates: the contribution of physicochemical characteristic. Part Fib Tox 2010, 6:33.

Kelly FJ. Gluthathione: in defence of the lung. Food Chem Toxicol 1999, 37(9-10):963-6.

Kennedy DW, Abkowitz JL. Mature monocytic cells enter tissues and engraft. Proc Natl Acad Sci U S A 1998, 95(25):14944-9.

Khan NA. Antioxidants and cancer. Sciences 2002, 2 38-43.

Kida Y, Kobayashi M, Suzuki T, Takeshita A, Okamatsu Y, Hanazawa S, Yasui T, Hasegawa K. Interleukin-1 stimulates cytokines, prostaglandin E2 and matrix metalloproteinase-1 production via activation of MAPK/AP-1 and NF-kappaB in human gingival fibroblasts. Cytokine 2005, 29(4):159-68.

Knaapen AM, Borm PJ, Albrecht C, Schins RP. Inhaled particles and lung cancer. Part A: Mechanisms. Int J Cancer 2004, 109(6):799-809.

Kreyling WG, Semmler-Behnke M, Seitz J, Scymczak W, Wenk A, Mayer P, Takenaka S, Oberdorster G. Size dependence of the translocation of inhaled iridium and carbon nanoparticle aggregates from the lung of rats to the blood and secondary target organs. Inhal Toxicol 2009, 21 Suppl 1:55-60.

Lacraz S, Nicod L, Galve-de Rochemonteix B, Baumberger C, Dayer JM, Welgus HG. Suppression of metalloproteinase biosynthesis in human alveolar macrophages by interleukin-4. J Clin Invest 1992, 90(2):382-8.

Laskin DL. Macrophages and inflammatory mediators in chemical toxicity: a battle of forces. Chem Res Toxicol 2009, 22(8):1376-85.

Lastbom BL, Camner P. Deposition and clearance of particles in the human lung. Scand J Work Environ Health 2000, 26 Suppl 1:23-7.

Lawther PJ, Ellison JMK, Waller RE. Some medical aspects of aerosol research. Proc Roy Soc A 1968, 307:223-34.

Lewinski N, Colvin V, Drezek R. Cytotoxicity of nanoparticles. Small 2008, 4(1):26-49.

Lippmann M, Schlesinger RB. Interspecies comparisons of particle deposition and mucociliary clearance in tracheobronchial airways. J Toxicol Environ Health 1984, 13(2-3):441-69.

Mantovani A, Sica A, Locati M. Macrophage polarization comes of age. Immunity 2005, 23(4):344-6.

Mantovani E, Porcari A, Morrison MJ, Geertsma RE. Developments in Nanotechnologies Regulation and Standards. Report of the Observatory Nano 2009.

Maynard AD, Maynard RL. Ambient aerosol exposure-response as a function of particulate surface area: a re-interpretation of historic data using numerical modelling. Ann Occup Hyg 2002, Suppl 1:444-49.

Mo SD, Ching WY. Electronic and optical properties of three phases of titanium dioxide: Rutile, anatase, and brookite. Phys Rev B Condens Matter 1995, 51(19):13023-32.

Nichols TC, Fischer TH, Deliargyris EN, Baldwin AS, Jr. Role of nuclear factor-kappa B (NF-kappa B) in inflammation, periodontitis, and atherogenesis. Ann Periodontol 2001, 6(1):20-9.

Nicod LP. Pulmonary defence mechanisms. Respiration 1999, 66(1):2-11.

Nicod LP, el Habre F, Dayer JM, Boehringer N. Interleukin-10 decreases tumor necrosis factor alpha and beta in alloreactions induced by human lung dendritic cells and macrophages. Am J Respir Cell Mol Biol 1995, 13(1):83-90.

Oberdanner CB. Reactive Oxygen Species (ROS) in biologischen Systemen und ihre Rolle in Apoptose [german]. Department of Physics and Biophysics, University Salzburg, Austria 2003.

Oberdörster G, Maynard A, Donaldson K, Castranova V, Fitzpatrick J, Ausman K, Carter J, Karn B, Kreyling W, Lai D, Olin S, Monteiro-Riviere N, Warheit D, Yang H. Principles for characterizing the potential human health effects from exposure to nanomaterials: elements of a screening strategy. Part Fibre Toxicol 2005a, 2:8.

Oberdörster G, Oberdörster E, Oberdörster J. Nanotoxicology: an emerging discipline evolving from studies of ultrafine particles. Environ Health Perspect 2005b, 113(7):823-39.

Ohtoshi T, Takizawa H, Okazaki H, Kawasaki S, Takeuchi N, Ohta K, Ito K. Diesel exhaust particles stimulate human airway epithelial cells to produce cytokines relevant to airway inflammation in vitro. J Allergy Clin Immunol 1998, 101(6 Pt 1):778-85.

Palmer LC, Newcomb CJ, Kaltz SR, Spoerke ED, Stupp SI. Biomimetic systems for hydroxyapatite mineralization inspired by bone and enamel. Chem Rev 2008, 108(11):4754-83.

Pastore A, Piemonte F, Locatelli M, Lo Russo A, Gaeta LM, Tozzi G, Federici G. Determination of blood total, reduced, and oxidized glutathione in pediatric subjects. Clin Chem 2001, 47(8):1467-9.

Peters A, Veronesi B, Calderon-Garciduenas L, Gehr P, Chen LC, Geiser M, Reed W, Rothen-Rutishauser B, Schurch S, Schulz H. Translocation and potential neurological effects of fine and ultrafine particles a critical update. Part Fibre Toxicol 2006, 3:13.

Piguet PF, Collart MA, Grau GE, Sappino AP, Vassalli P. Requirement of tumour necrosis factor for development of silica-induced pulmonary fibrosis. Nature 1990, 344(6263):245-7.

Pope CA, 3rd, Burnett RT, Thun MJ, Calle EE, Krewski D, Ito K, Thurston GD. Lung cancer, cardiopulmonary mortality, and long-term exposure to fine particulate air pollution. Jama 2002, 287(9):1132-41.

Pope CA, 3rd, Schwartz J, Ransom MR. Daily mortality and PM10 pollution in Utah Valley. Arch Environ Health 1992, 47(3):211-7.

Porter DW, Millecchia L, Robinson VA, Hubbs A, Willard P, Pack D, Ramsey D, McLaurin J, Khan A, Landsittel D, Teass A, Castranova V. Enhanced nitric oxide and reactive oxygen species production and damage after inhalation of silica. Am J Physiol Lung Cell Mol Physiol 2002, 283(2):L485-93.

Rada B, Leto TL. Oxidative innate immune defenses by Nox/Duox family NADPH oxidases. Contrib Microbiol 2008, 15:164-87.

Rahman K. Studies on free radicals, antioxidants, and co-factors. Clin Interv Aging 2007, 2(2):219-36.

Ranft U, Schikowski T, Sugiri D, Krutmann J, Kramer U. Long-term exposure to traffic-related particulate matter impairs cognitive function in the elderly. Environ Res 2009, 109(8):1004-11.

Ravetch JV, Kinet JP. Fc receptors. Annu Rev Immunol 1991, 9:457-92.

Ravetch JV, Lanier LL. Immune inhibitory receptors. Science 2000, 290(5489):84-9.

Rejman J, Oberle V, Zuhorn IS, Hoekstra D. Size-dependent internalization of particles via the pathways of clathrin- and caveolae-mediated endocytosis. Biochem J 2004, 377(Pt 1):159-69.

Royal Society and Royal Academy of Engineering. Nanoscience and nanotechnologies: opportunities and uncertainties. The Royal Society, London, UK 2004.

Schins RP, Borm PJ. Mechanisms and mediators in coal dust induced toxicity: a review. Ann Occup Hyg 1999, 43(1):7-33.

Schins RP, Duffin R, Höhr D, Knaapen AM, Shi T, Weishaupt C, Stone V, Donaldson K, Borm PJ. Surface modification of quartz inhibits toxicity, particle uptake, and oxidative DNA damage in human lung epithelial cells. Chem Res Toxicol 2002, 15(9):1166-73.

Schins RP, Knaapen AM. Genotoxicity of poorly soluble particles. Inhal Toxicol 2007, 19 Suppl 1:189-98.

Schins RPF, Donaldson K. Nuclear factor kappa B activation by particles and fibres. Inhal Toxicol 2000, (12):317-26.

Schreck R, Rieber P, Baeuerle PA. Reactive oxygen intermediates as apparently widely used messengers in the activation of the NF-kappa B transcription factor and HIV-1. Embo J 1991, 10(8):2247-58.

Schwartz J. Air pollution and daily mortality: a review and meta analysis. Environ Res 1994, 64(1):36-52.

Seaton A, MacNee W, Donaldson K, Godden D. Particulate air pollution and acute health effects. Lancet 1995, 345(8943):176-8.

Seaton A, Tran L, Aitken R, Donaldson K. Nanoparticles, human health hazard and regulation. J R Soc Interface 2010, 7 Suppl 1:S119-29.

Sies H. Role of reactive oxygen species in biological processes. Klin Wochenschr 1991, 69(21-23):965-8.

Sies H, Stahl W, Sevanian A. Nutritional, dietary and postprandial oxidative stress. J Nutr 2005, 135(5):969-72.

Squadrito GL, Pryor WA. Oxidative chemistry of nitric oxide: the roles of superoxide, peroxynitrite, and carbon dioxide. Free Radic Biol Med 1998, 25(4-5):392-403.

Stone V, Johnston H, Schins RP. Development of in vitro systems for nanotoxicology: methodological considerations. Crit Rev Toxicol 2009, 39(7):613-26.

Tampieri A, Celotti G, Landi E. From biomimetic apatites to biologically inspired composites. Anal Bioanal Chem 2005, 381(3):568-76.

Thomas CR, Kelley TR. A brief review of silicosis in the United States. Environ Health Insights 2010, 4:21-6.

Unfried K, Albrecht C, Klotz L-O, von Mikecz A, Grether-Beck S, Schins RPF. Cellular responses to nanoparticles: target structures and mechanisms. Nanotoxicology 2007:1-20.

US Environmental Protection Agency. Exposure Factors Handbook (Final Report) EPA/600/P-95/002Fa-c 1997, Washington, DC.

Valko M, Morris H, Cronin MT. Metals, toxicity and oxidative stress. Curr Med Chem 2005, 12(10):1161-208.

van Berlo D, Knaapen AM, van Schooten FJ, Schins RP, Albrecht C. NF-kappaB dependent and independent mechanisms of quartz-induced proinflammatory activation of lung epithelial cells. Part Fibre Toxicol 2010, 7:13.

Wahl DA, Czernuszka JT. Collagen-hydroxyapatite composites for hard tissue repair. Eur Cell Mater 2006, 11:43-56.

WHO. WHO's global air-quality guidelines. Lancet 2006, 368(9544):1302.

Witschi H, Last JA. Toxic Responses of the Respiratory System. *In:* Casarett & Doull's Toxicology - The Basic Science of Poisons - Klaassen CD, McGraw-Hill Professional 1996.

Xia T, Korge P, Weiss JN, Li N, Venkatesen MI, Sioutas C, Nel A. Quinones and aromatic chemical compounds in particulate matter induce mitochondrial dysfunction: implications for ultrafine particle toxicity. Environ Health Perspect 2004, 112(14):1347-58.

Yacobi NR, Demaio L, Xie J, Hamm-Alvarez SF, Borok Z, Kim KJ, Crandall ED. Polystyrene nanoparticle trafficking across alveolar epithelium. Nanomedicine 2008, 4(2):139-45.

Zeidler P, Hubbs A, Battelli L, Castranova V. Role of inducible nitric oxide synthase-derived nitric oxide in silica-induced pulmonary inflammation and fibrosis. J Toxicol Environ Health A 2004, 67(13):1001-26.

CHAPTER II

CONTRASTING MACROPHAGE ACTIVATION BY FINE AND ULTRAFINE TITANIUM DIOXIDE PARTICLES IS ASSOCIATED WITH DIFFERENT UPTAKE MECHANISMS

Agnes M. Scherbart, Julia Langer, Alexey Bushmelev, Damiën van Berlo, Petra Haberzettl, Frederik-Jan van Schooten, Annette M. Schmidt, Christine R. Rose, Roel P.F. Schins, Catrin Albrecht

Particle and Fibre Toxicology
submitted for publication

DECLARATION - STUDY 1

Uptake, inflammatory and oxidative stress responses of titanium dioxide in alveolar macrophages: A question of size?

Declaration:
The manuscript is submitted to a peer-review journal.
Most experimental work presented, was done by Agnes M. Scherbart.
The impact on authoring this paper can be estimated to 90 %.

ABSTRACT

Inhalation of (nano)particles may lead to pulmonary inflammation. However, the precise mechanisms of particle uptake and generation of inflammatory mediators by alveolar macrophages (AMΦ) are still poorly understood. The aim of this study was to investigate the interactions between particles and AMΦ and their associated pro-inflammatory effects in relation to particle size and physico-chemical properties.

NR8383 rat lung AMΦ were treated with ultrafine (uf), fine (f) TiO_2 or fine crystalline silica (DQ12 quartz). Physico-chemical particle properties were investigated by transmission electron microscopy, elemental analysis and thermogravimetry. Aggregation and agglomeration tendency of the particles were determined in assay-specific suspensions by means of dynamic light scattering.

All three particle types were rapidly taken up by AMΦ. DQ12 and ufTiO_2, but not fTiO_2, increased extracellular reactive oxygen species (ROS), heme oxygenase 1 mRNA expression and TNF-α release. Only ufTiO_2 enhanced inducible nitric oxide synthase mRNA expression, while DQ12 exclusively triggered interleukin 1β release. Our findings suggest that the contrasting AMΦ responses to fTiO_2, ufTiO_2 and DQ12 relate to differences in the involvement of specific uptake mechanisms, i.e. actin cytoskeleton, clathrin-coated pit formation and Fcγ receptor II internalization. However, oscillations of intracellular calcium concentration and increased intracellular ROS were observed with all samples, and therefore could not explain for their differential uptake mechanisms and pro-inflammatory responses. In conclusion, marked contrasts exist concerning their toxicity and ability to activate AMΦ which might relate to particle type-specific differences in their uptake mechanisms.

2.1 INTRODUCTION

The introduction and application of novel types of nanomaterials and nanodevices is rapidly increasing in recent years. Risks of exposure to nanoparticles (NP, which can be defined as nano-objects with at all three external dimensions in the nanoscale, i.e. < 100 nm; [Stone et al 2009]) often cannot be reliably estimated at this time. Due to their novel physico-chemical properties, concerns have been raised about their potential to cause adverse effects in biological systems and their impact on human health. Testing strategies to investigate possible health risks caused by NP are therefore urgently needed [Oberdörster et al 2005].

Hints for a potential toxicity of NP arose predominantly from the field of inhalation toxicology, where it has been shown that (aggregates of) specific NP, like carbon black (CB) or titanium dioxide (TiO_2), exhibit a markedly higher biological activity at cellular and subcellular levels [Shvedova et al 2003; Oberdörster et al 2005; Nel et al 2006] when compared to equal mass dose of their larger sized counterparts [Oberdörster 2001; Stoeger et al 2006; Singh et al 2007]. Currently, TiO_2 particles are used widely and in large quantities in many industrial applications like cosmetics, pharmaceuticals, paints and in food industry, as well as in medical and dental prosthesis in either fine (> 100 nm) or ultrafine sizes [Lindenschmidt et al 1990; Johnston et al 2010].

Animal studies have shown that $fTiO_2$ particles predominantly deposit within the deeper regions of the lung and can subsequently induce inflammatory responses [Bermudez et al 2004]. However, this typically does not result in marked lung fibrosis [Lindenschmidt et al 1990; Lardot et al 1998], unlike other inorganic particles, e.g. crystalline silica [Donaldson & Tran 2002; Kuempel et al 2003; Rimal et al 2005]. Such contrasting outcomes pointed to the existence of fundamental differences between different types of inorganic particles concerning their toxic potential. Investigations of the acute inflammatory effects of an ultrafine and a fine sample of TiO_2 in rats and mice have shown that the smaller particles are more potent on a mass dose basis, but that the responses do not differ when the samples are adjusted to an equal surface area dose [Oberdörster et al 2005]. This suggests that the specific surface area (SSA) of NP *per se* may define their pro-inflammatory effects. However, on the cellular level biological effects of NP are considered to be driven by their specific physico-chemical interactions with cells and subcellular constituents, including initial recognition and/or interference with specific membrane associated receptors [Unfried et al 2007]. This specific particle-cell-interaction may also explain observations in other studies where associations between the SSA and specific toxic effects were not as clear, e.g. [Warheit et al 2009].

Alveolar macrophages (AMΦ) are professional phagocytes accounting for approximately 95 % of airspace leukocytes in the healthy lung, which generally represent the first cell type that gets into contact with inhaled pathogens [Martin & Frevert 2005]. The AMΦ cell line NR8383 has been extensively characterized and is widely accepted as a reliable surrogate for freshly obtained primary AMΦ [Helmke et al 1989]. In a previous study, we demonstrated the participation of the classical phagocytosis Fcγ receptor II (FcγRII) in the uptake of fine crystalline silica particles (with a mean geometric diameter of about 1 µm) by NR8383 AMΦ [Haberzettl et al 2008]. Other studies have shown an association between FcγRII stimulation by interferon γ in the monocyte cell line U937 as well as in primary human blood monocytes, and the induction of a signal cascade which is connected to phospholipase Cγ 1 (PLCγ-1). Activation of PLCγ-1 is known to increase the concentration of intracellular calcium ($[Ca^{2+}]_i$) which in turn can activate nicotineamide adenine dinucleotid phosphat (NADPH)-oxidases and thus the generation of reactive oxygen species (ROS) via the so-called oxidative burst [Rada & Leto 2008; Dai et al 2009]. Participation of other membrane receptors including the class A scavenger receptor (SR-A) and the MΦ receptor with collagenous structure (MARCO) has also been described to be of importance for the uptake of fine-sized TiO_2 and silica particles, but not for the internalization of carbonaceous particles [Kobzik 1995; Thakur et al 2008]. Taken together, these observations provide strong evidence that particle type-specific mechanisms of uptake exist in MΦ. However, the exact route(s) by which NP can enter these cells and their impact on subsequent cellular responses are still poorly understood. Elucidation of these mechanisms will provide an important step for the risk assessment of NP and for potential medical and pharmaceutical applications of newly engineered NP.

Interaction of AMΦ with respirable particles can lead to the production of ROS and secretion of a large variety of cytokines, chemokines and other, typically pro-inflammatory mediators. These include TNF-α and IL-1β, both early pro-inflammatory cytokines which in turn are capable to activate various secondary mediators and as such orchestrate the recruitment of further immune cells, like neutrophilic granulocytes [Akagawa 2002]. Many of these cytokines and chemokines are regulated by redox-sensitive transcription factors like NF-κB and/or activator protein 1 (AP-1), which in turn are regulated by second messengers including calcium and ROS [Schulze-Osthoff et al 1995; Brown et al 2004]. Enhanced $[Ca^{2+}]_i$ levels are known leading to the activation of protein kinase C (PKC) which is involved in the activation of NF-κB [Kang et al 2000; Shukla et al 2003]. The involvement of $[Ca^{2+}]_i$ in the pro-inflammatory responses of AMΦ has recently been established for fine crystalline silica particles [Tian et al 2010] as well as for carbonaceous NP, i.e. ultrafine carbon black [Brown et al 2004].

In our current study, two types of TiO_2 with different size distributions were investigated, i.e. fine ($fTiO_2$) and ultrafine ($ufTiO_2$). The aims of our study were to analyze (i) differences in uptake mechanisms for these samples in AMΦ, and (ii) how the uptake associates with various cellular responses in AMΦ that are considered to play a role in the adverse health effects of inhaled particles. The established inflammogenic and fibrogenic crystalline silica sample DQ12 was used as reference particle [Castranova & Vallyathan 2000; Donaldson et al 2001; Albrecht et al 2004; 2005; Rimal et al 2005]. Intra- and extracellular responses of AMΦ were investigated via the analysis of particle uptake, cytotoxicity, changes in $[Ca^{2+}]_i$, ROS generation as well as the induction of various markers of inflammation and oxidative stress, i.e. NF-κB, TNF-α, IL-1β, inducible nitric oxide synthase (iNOS) and heme oxygenase-1 (HO-1). Particle type-specificity of internalization by AMΦ was investigated by uptake analysis in the absence or presence of specific inhibitors, i.e. cytochalasin D (CytD), chlorpromazine (Chl), Filipin III, FcγRII antibody as well as by evaluation of uptake at 4 versus 37 °C. Since former studies have shown that TiO_2 particles tend to reside as aggregates as well as to form larger agglomerates in suspension depending on the type of buffers [Warheit et al 2007], in the present study special emphasis was also put on the characterization of the specific particle suspensions used for the various biological tests. Elemental analysis (EA) and thermogravimetric analysis (TGA) have been employed to exclude the presence of organic residues in the investigated powders that could impact on MΦ responses. Morphology and dispersion behavior of the samples in the different media was evaluated by means of transmission electron microscopy (TEM), dynamic light scattering (DLS) and dark field light scattering microscopy (DF-LSM).

2.2 MATERIALS & METHODS

Particle samples used

Three types of particles were used in this study, i.e. ultrafine ($ufTiO_2$) and fine ($fTiO_2$) titanium dioxide and a respirable quartz sample (DQ12). $fTiO_2$ was obtained from Sigma-Aldrich and is a pure anatase sample with a reported mean diameter of about 250 nm [Singh et al 2007]. The $ufTiO_2$ sample originates from Degussa (Hanau, Germany) and represents a mixture of 80 % anatase and 20 % rutile with a reported mean particle size of 25 nm [Singh et al 2007]. The DQ12 sample originates from Dörentrup, Germany (IUF batch 6) and represents a highly pure quartz (99.1 %) with a mean particle diameter of 960 nm [Albrecht et al 2004]. The specific surface areas of the samples measured according to the method of Brunauer, Emmert and Teller [Brunauer et al 1938] are 50 m^2/g, 10 m^2/g and 9.6 m^2/g for $ufTiO_2$, $fTiO_2$ and DQ12,respectively.

Particle characterization

In order to obtain additional information on particle composition and size, the batches were subjected to TGA, EA, DLS, DF-LSM, and TEM. EA of the powders was carried out with a Perkin-Elmer Analyzer 2400 with an accuracy of measurement of 0.3 %. TGA experiments were performed on powder samples on a Netsch STA 449C Jupiter at a constant heating rate of 10 K min^{-1} in argon atmosphere between 30 and 600 °C. The solid residues at 600 °C are attributed to the inorganic component. TEM images were taken using a Philips EM 208S. DLS measurements were performed on a High-Performance Particle Sizer HPP5002 (Malvern Instruments) in water, $HBSS^{(+/+)}$ (phenol red free, with Mg^{2+} and Ca^{2+}; Invitrogen GmbH, Karlsruhe, Germany) and cell culture medium at 25 °C, using 1 x 1 cm^2 polystyrene cuvettes. Particle size distributions were derived from a deconvolution of the measured intensity autocorrelation function by the non-negative least-squares algorithm included in the DTS software. The suspensions used for this analysis were prepared in the same way as those used for the biological testing as described below. DLS analysis of the $ufTiO_2$ particle suspension was also performed after filtration through a 450 nm membrane filter to further evaluate the influence of aggregate/agglomerate formation on this method.

Preparation of the particle suspensions and cell treatments

NR8383 rat AMΦ (ATCC, Manassas, USA) were cultured in Kaighn's modified medium (F12-K Nutrient Mixture, Gibco, Eggenstein, Germany) containing 15 % FCS, 1 % penicillin/ streptomycin and 1 % glutamine (all purchased from Sigma-Aldrich, Taufkirchen, Germany) and incubated in a humidified incubator (Heraeus, BB 6060 CU) at 37 °C and 5 % CO_2.

Three days before each experiment, cells were seeded in a concentration of 1.25 x 10^5 cells/cm^2 in the indicated culture dishes. If not otherwise mentioned, incubations took place at 37 °C and 5 % CO_2.

Particles were heated at 220 °C for 16 h in order to destroy potential endotoxins, which are known to be potent activators of AMΦ. Immediately before the experiment, particles were freshly suspended either in complete cell culture medium see above] or $HBSS^{(+/+)}$ or $HBSS^{(-/-)}$ (phenol red free, with or without Mg^{2+} and Ca^{2+}) depending on the specific experimental setup. All suspensions were sonicated in a water bath for 10 min (Sonorex TK 52, Schaltech, Mörfelden-Walldorf, Germany) immediately prior to addition to the cells. Particles were added to the AMΦ at concentrations of 10, 20, 40, 80 µg/cm^2 for 1, 4 or 24 h as indicated.

Measurement of particle uptake by flow cytometry

The uptake of particles by the AMΦ was analyzed via flow cytometry. Measurement was performed with a FACSCalibur (Becton Dickinson, Heidelberg, Germany). The sideward scatter (SSC) which is directly related to cell granularity was used as a marker of particle uptake [Palecanda & Kobzik 2000], whereas the forward scatter (FSC) mainly correlates to the cell size.

For inhibition experiments, cells were preincubated for 30 min with the following substances: Cytochalasin D (CytD) (1.5 µg/mL; Sigma, Taufkirchen, Germany) to inhibit actin recruitment, chlorpromazine (Chl) (5 µg/mL; Sigma-Aldrich, Taufkirchen, Germany) to disable the formation of clathrin-coated pits (CCP), and an antibody against the phagocytotic FcγRII (CD32) (5 µg/mL; BD Biosciences, Heidelberg, Germany) to avoid specific receptor binding. DMSO (0.1 %; Sigma, Taufkirchen, Germany) was applied as vehicle control for CytD. The IgG1κ monoclonal antibody was used as isotype control (5 µg/mL; BD Biosciences, Heidelberg, Germany) for the FcγRII antibody experiments.

Cells were treated with particles at concentrations of 10, 20 or 40 µg/cm^2 for 1 or 3 h. NR8383 cells were gently scraped from the culture dishes on ice, centrifuged (200 x g, 10 min, 4 °C), washed with 300 µL of ice cold $HBSS^{(-/-)}$ and centrifuged again. The pellet was resuspended in 200 µL ice cold $HBSS^{(-/-)}$. In total 15,000 events were counted. For calculation cell debris and free particles were excluded by an electronical gate containing AMΦ of all sizes and granularities in a FSC-SSC-histogram. Univariant histograms of SSC determined the median of cell granularity used as measure of particle uptake by AMΦ. Data were detected with CellQuest 3.3 and analyzed using CellQuest Pro (Becton Dickinson, Heidelberg, Germany).

Microscopical evaluation of uptake

In order to microscopically investigate AMΦ after a 24 h treatment with particles cytospin slides were prepared. Therefore, NR8383 cells were scraped, centrifuged (200 x g, 5 min, 4 °C), washed and resuspended in sterile, ice cold PBS. Then 2 x 10^5 cells were spun onto glass slides (600 rpm, 5 min) using a Cytospin3 (Shandon GmbH, Frankfurt, Germany). After drying and May-Grünwald-Giemsa-staining (Merck, Darmstadt, Germany) preparations were analyzed via light microscopy (Olympus BX60, Hamburg, Germany).

Cytotoxicity

Effects of particles on cell viability were determined using the WST-1 assay (Roche Diagnostics GmbH, Mannheim, Germany) which is based on the principle of the reduction of the stable tetrazolium salt WST-1 to a soluble violet formazan product within the mitochondria of viable cells. For this assay, NR8383 cells were seeded in octoplicate in 96-well microtiter plates. After 24 h of particle treatment, 10 µL WST-1 solution (Roche Diagnostics GmbH, Mannheim, Germany) was added to 5 wells per treatment or control and incubated for further 2 h. The other three wells were used as controls for the absorption by the particles and therefore measured without WST-1 substrate application. Optical density was detected at 450 nm using the Multiskan ELISA reader (Thermo Fisher Scientific, Dreieich, Germany). For data calculation, the mean of the obtained values of the wells without WST-1 was subtracted from the mean of the WST-1 substrate treated samples and expressed as percentage of control cells.

Calcium imaging

In order to investigate the relation between particle exposure and intracellular calcium, wide-field fluorescent imaging was employed to measure changes in $[Ca^{2+}]_i$ in individual cultured AMΦ upon particle treatment. NR8383 cells were seeded onto sterile coverslips coated with poly-D-lysine hydrobromide (Sigma-Aldrich, Taufkirchen, Germany) and used for experiments after 3 - 4 days. Loading with the Ca^{2+} sensitive fluorescent dye Fura-2 and fluorescence measurements were performed in saline containing (in mM): NaCl 125, KCl 3, NaH_2PO_4 1.25, $MgSO_4$ 2, $CaCl_2$ 2, HEPES 25, D-glucose 10 (pH 7.4). The acetoxymethyl (AM) ester form of the fluorophore was dissolved as 5 mM stock solution in 20 % Pluronic acid in DMSO and stored at -20 °C. For dye loading coverslips were incubated for 90 min at room temperature in saline containing 0.5 mM Fura-2-AM. Following loading, cells were kept in dye-free saline for at least 30 min to ensure de-esterification of the dye before starting the imaging experiments.

Conventional wide-field fluorescent imaging was performed employing an imaging system (Till Photonics GmbH, Munich, Germany) in conjunction with an upright microscope (Axioskop, Zeiss, Oberkochen, Germany) equipped with a cooled CCD camera (SensiCam QE, PCO, Kelheim, Germany). Cells loaded with Fura-2 were excited every 5 seconds using a monochromator (polychrome V, Till Photonics GmbH); fluorescence emission from regions of interest (ROIs) placed around AMΦ somata was detected by the camera. Emission intensities > 440 nm were collected after alternate excitation at 357 and 380 nm, and background-corrected fluorescent ratios (F357/380) were calculated. Background fluorescence was determined from coverslip areas devoid of cellular material.

Baseline $[Ca^{2+}]_i$ was recorded under control conditions and for at least 70 min during exposure to either ufTiO_2 or fTiO_2 particles at concentrations of 10 or 20 µg/cm^2. To quantitatively analyze and compare calcium fluctuations in response to different particles, integrals for ratio values for specific 10 min time windows (one for control experiments; 15 - 25 min and 55 - 65 min after particle application) were calculated for each individual cell employing OriginPro Software (OriginLab Corporation, Northampton, MA).

Intracellular ROS measured by DCFH-DA

To quantify intracellular ROS the cell-permeable non-fluorescent probe 2',7'-dichlorodihydrofluorescein diacetate (DCFH-DA; Sigma, Saint-Louis, Missouri, USA) was used. After entering the cell, DCFH-DA loses its diacetate group by the action of esterases. The oxidation of this probe leads to the highly fluorescent DCF. Prior to particle treatment, NR8383 cells seeded in 96-well plates were washed and replaced by HBSS$^{(+/+)}$ to avoid scavenging effects of DCFH-DA by medium components. After a recovery time of 30 min, AMΦ were pre-incubated with 100 µM DCFH-DA for another 20 min in the incubator. Afterwards cells were washed and allowed to recover for another 30 min before they were treated with 40 µg/cm^2 of particles. The change in DCFH-DA fluorescence over time was detected via fluorescence reader (Synergy2, BioTek Instruments Inc., Bad Reichenhall, Germany) for 3 h at 37 °C.

Measurement of extracellular ROS by Electron Paramagnetic Resonance (EPR) spectroscopy with spin trapping

For the analysis of extracellular ROS, NR8383 cells were seeded in 96 well plates. Cells were washed and the medium was replaced by HBSS$^{(+/+)}$ followed by a recovery time of 30 min. AMΦ were treated with particles at concentrations of 10 or 40 µg/cm^2. The spin trapping agent 5,5-dimethyl-1-pyrroline-N-oxide (DMPO, 0.11 M, Sigma-Aldrich, Taufkirchen,

Germany) was added simultaneously with the particles; cells were incubated for 3 h. Cell-free supernatants were harvested and immediately measured for radical formation using a MiniScope MS200 Spectrometer (Magnettech, Berlin, Germany) with the following instrumental settings: room temperature, microwave frequency = 9.39 GHz, magnetic field = 3360 G, sweep width = 100 G, scan time = 30 s, number of scans = 3, modulation amplitude = 2 G, receiver gain = 900. Quantification was carried out on first derivation of EPR signal of the characteristic DMPO–OH quartet, as the mean of amplitudes, and outcomes are expressed in arbitrary units (a.u.). DQ12 and the well-known PKC activator PMA were used as positive controls.

Immunocytochemistry (IHC) for NF-κB

Transcriptional activation of the nuclear factor κB was microscopically analyzed by the nuclear translocation of the p65 subunit. Therefore, cells were seeded into 4-chamber slides and treated with 40 µg/cm^2 of particles. After 1 h, NR8383 cells were fixed (4 % paraformaldehyde/PBS, pH 7.4) and permeabilized (0.1 % TritonX-100, 5 min). Unspecific binding sites were blocked by goat normal serum followed by an overnight incubation with anti-NF-κB (p65) antibody (1:500; Santa Cruz Biotechnology, CA, USA). Slides were incubated with secondary antibody Alexa-488 (1:200; Molecular Probes, OR, USA) for 1 h before mounting the cover slip with Ultra Cruz Mounting Medium containing DAPI (Santa Cruz Biotechnology, CA, USA). Fluorescence images were taken with the Axio Observer.D1 fluorescence microscope (Carl Zeiss MicroImaging GmbH, Göttingen, Germany).

TNF-α and IL-1β release

NR8383 cells were seeded onto 24-well microtiter plates. After 24 h of particle treatment, cell-free supernatant was collected, centrifuged (200 x g, 10 min, 4 °C) and aliquots were stored at -20 °C. Supernatants were analyzed using a TNF-α or IL-1β ELISA kit (R&D Systems, Wiesbaden, Germany) according to the manufacturer's manual and using a Multiskan ELISA reader (Thermo Fisher Scientific, Dreieich, Germany).

Quantitative RT-PCR analysis of gene expression

NR8383 cells were seeded in 6-well plates, treated with particles for 4 h, scraped and centrifuged (200 x g, 5 min, 4 °C). The pellet was resuspended in 0.5 mL Trizol® Reagent (Invitrogen GmbH, Karlsruhe, Germany) and stored at -20 °C until further use. The RNeasy® mini kit (Qiagen, Hilden, Germany) coupled to DNAse treatment was used to purify total RNA from salts and residual DNA. Quantity and purity of RNA were evaluated using

spectrophotometry at 230, 260, 280, and 320 nm. cDNA was synthesized using the iScript™ cDNA Synthesis kit (BioRad, CA, USA), starting from 0.5 µg of RNA. cDNA was diluted 15 x in RNAse-free water before use. PCR primers for rat HO-1, iNOS and the housekeeping gene GAPDH were designed using Primer Express software (Applied Biosystems). Primer sequences for HO-1 were 5'-GGG AAG GCC TGG CTT TTTT -3' (forward) and 5'-CAC GAT AGA GCT GTT TGA ACT TGGT -3' (reverse), for iNOS 5'-AGG AGA GAG ATC CGG TTC ACA GT-3' (forward) and 5'-ACC TTC CGC ATT AGC ACA GAA-3' (reverse) and for GAPDH 5'-TGA TTC TAC CCA CGG CAA GTT-3' (forward) and 5'-TGA TGG GTT TCC CAT TGA TGA-3' (reverse). qRT-PCR was performed with a MyiQ Single Color real time PCR detection system (BioRad) using iQ™ SYBR® Green Supermix (Biorad), 5 µL diluted cDNA, and 2.5 µL of 0.3 µM forward and reverse primer in a total volume of 25 µL. PCR was conducted as follows: a denaturation step at 95 ºC for 3 min was followed by 40 cycles at 95 ºC (15 seconds) and 60 ºC (45 seconds). After PCR, a melt curve (60 - 95 ºC) was generated for product identification and purity. PCR efficiency of all four primer sets, as assessed by the use of cDNA dilution curves, was 90 - 100 %. Data were analyzed using the MyiQ Software system (BioRad) and were expressed as relative gene expression (fold increase) using the $2^{-\Delta\Delta Ct}$ method [Livak & Schmittgen 2001].

Statistical Analysis

All biological assays were performed in at least three independent experiments. Data are presented as mean ± SEM unless indicated otherwise. Statistical analysis was performed using SPSS 18.0 for Windows using analysis of variance (ANOVA) with Dunnett or LSD post hoc comparison as indicated for the specific data. Differences compared to untreated control cells were considered significant at * $p < 0.05$, ** $p < 0.01$ and *** $p < 0.001$. Differences in inhibition experiments compared to the appropriate particle treatment were indicated as # $p < 0.05$, ## $p < 0.01$ and ### $p < 0.001$.

2.3 RESULTS

Particle sample characteristics

In order to verify the absence of organic residues in the particle samples, we performed EA and TGA in the powders. In the former, no carbon content was detected within the experimental error, and in the latter, no significant weight loss was found attributable to organic combustible contents, up to a temperature of 600 °C [data not shown]. The morphology of the samples was investigated by means of TEM. Representative images [Figure 2.1] showed for the TiO_2 samples individual particles of nearly spherical shape and moderate size distribution. From the images, particle size histograms were extracted [Figure 2.1 D], revealing a number-average particle diameter of 69.1 nm (± 39.9 nm SD) for $ufTiO_2$ particles and of 194.9 nm (± 60.8 nm SD) for $fTiO_2$, respectively. Figure 2.1C shows a representative image of the control sample DQ12. A detailed characterization of this sample has been performed in a previous study, revealing a mean diameter of 960 nm [Albrecht et al 2004].

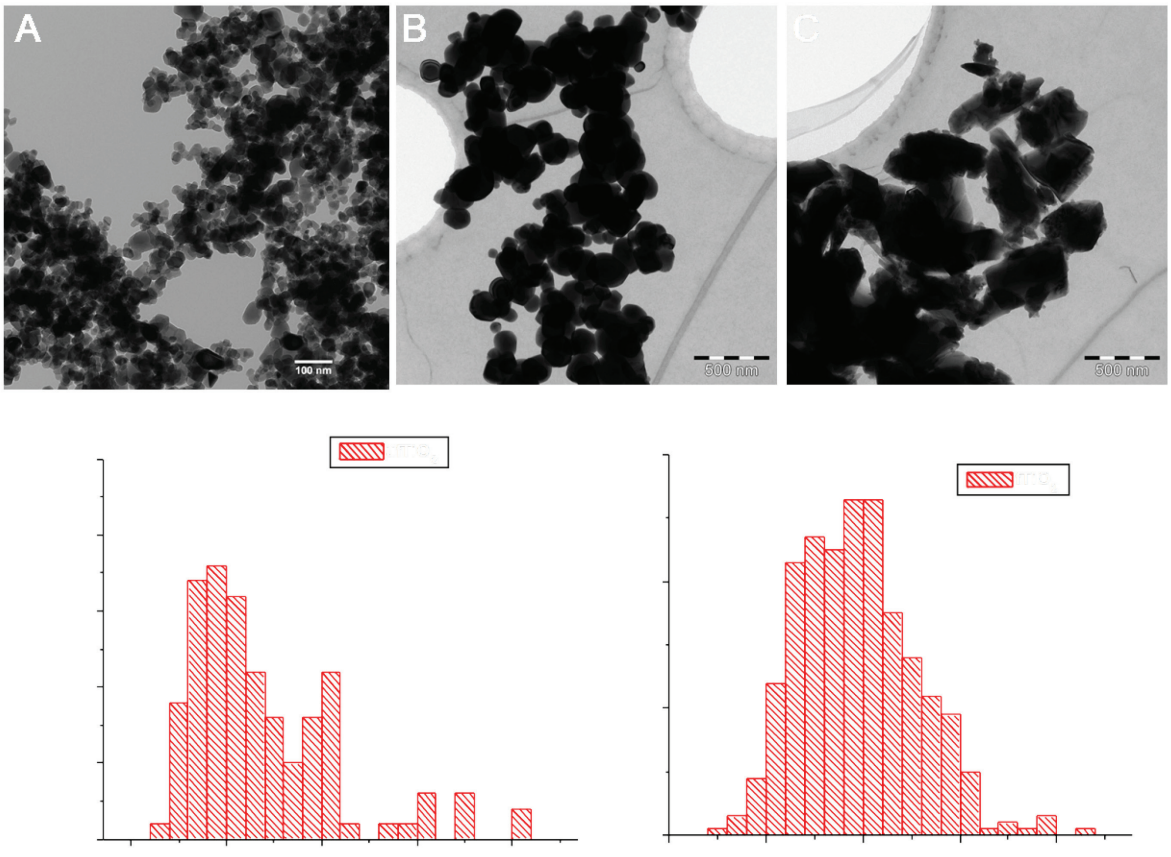

Figure 2.1 TEM images and size distribution of particles.
Particles were suspended and prepared for TEM measurements in deionized water. (A) $ufTiO_2$ and (B) $fTiO_2$ are regular and spherical particles in contrast to (C) crystalline silica DQ12 particles that display a very irregular shape. (D) Particle size histograms are derived from the appropriate TEM analysis for primary particles of $ufTiO_2$ and $fTiO_2$.

Evaluation of particle suspensions used for biological testing

It is well-known that for (nano)particle dispersions the actual object size can differ significantly from the size of the primary particles and their aggregates due to agglomeration processes. Therefore, we compared the core size of the primary particles obtained from TEM with results from dispersion-based methods. For this purpose, DLS and DF-LSM experiments were carried out. Both methods are based on the analysis of the distribution of the diffusion coefficient measured from scattered light signals. While in DLS the signal fluctuations are used directly to obtain information on the autocorrelation function, in DF-LSM the signals are used to track individual objects and analyze their Brownian diffusion perpendicular to the laser direction. For $ufTiO_2$ as well as $fTiO_2$, particle dynamics as examined by DLS were in accordance with the presence of predominantly primary particles or small aggregates in water dispersion after ultrasonification and partly filtration by a 450 nm microfilter. This is evident from the high correlation of the number-average hydrodynamic particle diameter as extracted by DLS [Table 2.1] with the average core diameter as observed by TEM.

Table 2.1 Characteristics of particle dispersions measured by DLS.

Sample	Dispersant	d_h[a]	PDI[b]
$ufTiO_2$	water	55.4[c] (891.2)	0.22
	cell culture medium	57.5	0.33
	buffer	164.2[c] (2018)	0.26
$fTiO_2$	water	321.2	0.18
	cell culture medium	448.6	0.16
	buffer	936.6	0.64

[a] number-average hydrodynamic diameter [nm]
[b] polydispersity index
[c] sample was filtered (450 nm microfilter) prior to experiment
in brackets: results of the comparable measurement of unfiltered sample

Similar values were also obtained for the cell culture-based particle dispersions. In the latter, after filtration which was performed to investigate the impact of aggregate/agglomerate formation on the DLS measurements, the scattering signal was dominated by small colloids (~ 6 nm). This signal could be attributed to proteins which are abundant in the FSC containing medium. The proteins contained within the FCS stabilize the particles in the dispersion and hence prevent their sedimentation. In the HBSS-based suspensions, however,

the DLS measurements indicated the presence of agglomerates with a diameter of up to the micrometer range [Table 2.1, values in brackets]. The findings are in accordance with the observation of a lower sedimentation stability of these buffer-based samples compared to water- or complete culture medium-based dispersions.

Importantly, for the $ufTiO_2$ particles the mass percentage of the filtered fraction was 20 % of the total mass [data not shown]. The large fraction of the non-filtered material at least in part accounts for larger agglomerates which may be inappropriately measured by the DLS method. As such, the data of the unfiltered samples have to be interpreted with caution. Nevertheless, the measurements of the unfiltered suspensions [Table 2.1] showed that the ultrafines tended to from larger agglomerates than their fine counterparts. These findings were also supported by data obtained from DF-LSM [not shown], and are important in view of the cell based assays.

Dose-dependent particle uptake in alveolar macrophages

The uptake of particles by NR8383 AMΦ was determined by measuring the granularity of the cells via flow cytometry. These measurements revealed a dose-dependent uptake (10, 20 or 40 µg/cm^2) of all tested particles after 1 as well as 3 h [Figure 2.2 A-C].

Comparison of the SSC results also indicates that the smaller the ingested particles, the higher is the light scattering caused by the elevated granularity of the cells. This was confirmed by comparison of cell free particle suspensions revealing a median SSC of 885, 728 or 228 for $ufTiO_2$, $fTiO_2$ or DQ12, respectively. Uptake was also verified by light microscopy of treated NR8383 cells [Figure 2.2 D].

Figure 2.2 Concentration- and time-dependent particle uptake by NR8383 cells [on page 54].
Results of FACS analysis demonstrate increased particle uptake by AMΦ based on SSC of laser light indicating cellular granularity. AMΦ were treated with (A) $ufTiO_2$, (B) $fTiO_2$ and (C) DQ12 particles in concentrations of 10, 20 or 40 µg/cm^2 for 1 or 3 h. (D) Particle internalization by NR8383 cells demonstrated in MGG-stained cytospin preparations. Light microscopic images show AMΦ either untreated or treated with 10 µg/cm^2 of particles for 4 h (upper panel) or 24 h (lower panel). Original magnification 1000-fold (Olympus BX60). Figure A - C represent median ± SEM of three independent experiments, with * $p < 0.05$, ** $p < 0.01$ and *** $p < 0.001$ vs. control (ANOVA with Dunnett post-hoc comparison).

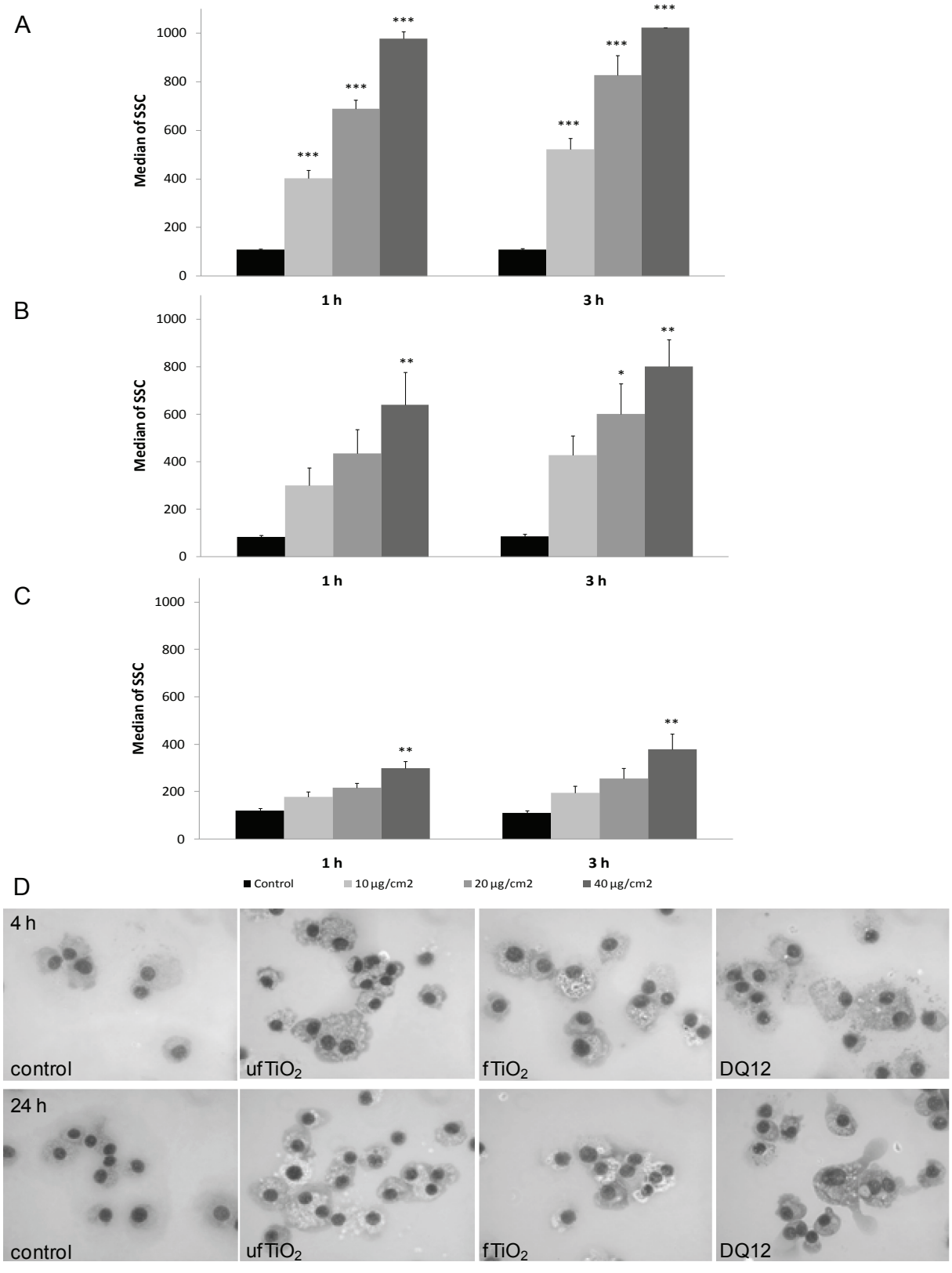
A
B
C
D
Median of SSC
1 h
3 h
Control
10 µg/cm2
20 µg/cm2
40 µg/cm2
4 h
24 h
control
ufTiO2
fTiO2
DQ12

Cell toxicity following particle exposure

Viability of AMΦ after 4 and 24 h of particle treatment was determined by measurement of mitochondrial dehydrogenase activity. This investigation showed no cytotoxic effects after 4 h for all three tested particles [Figure 2.3 A] but marked differences between $fTiO_2$ and $ufTiO_2$ particles after 24 h [Figure 2.3 B]. Treatment of the AMΦ with $ufTiO_2$ particles already caused toxic responses at a concentration of 20 µg/cm^2 which was comparable to the responses of the positive control DQ12. For $fTiO_2$ particles no effects on cell viability were found up to the highest tested concentration of 80 µg/cm^2.

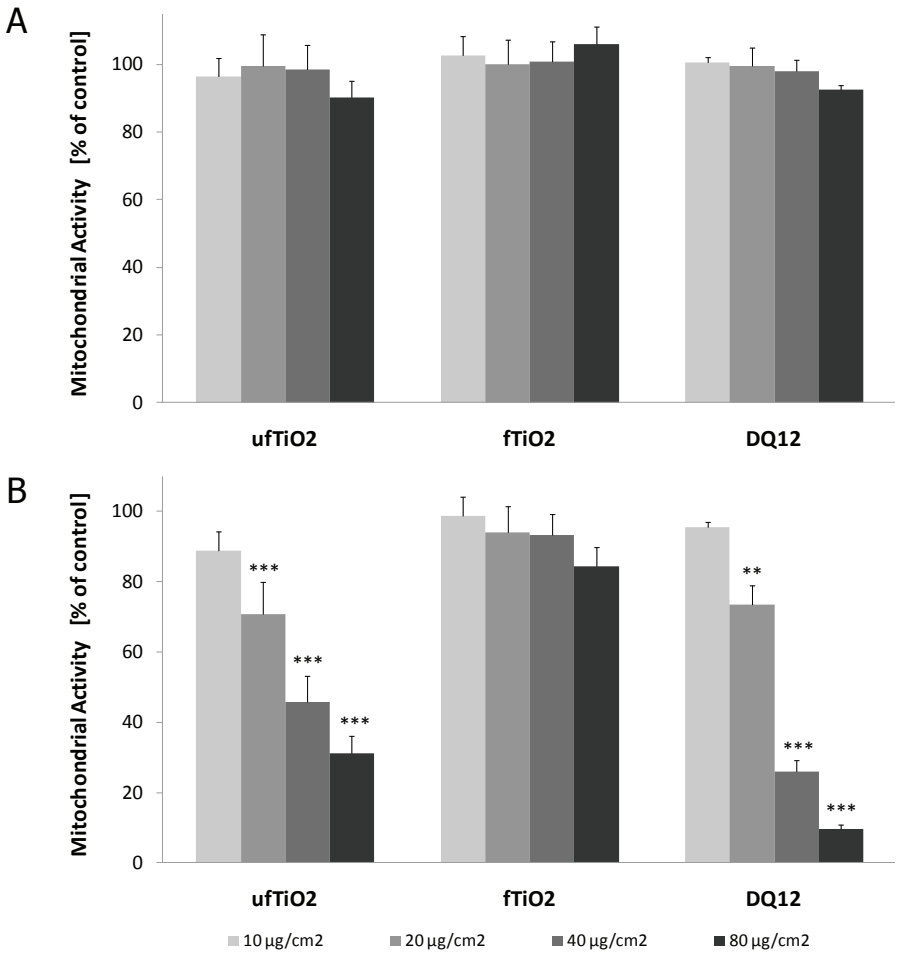

Figure 2.3 Particle-dependent effects on cell viability in NR8383 cells.
Mitochondrial activity of particle-treated AMΦ shows (A) no impairment of cell viability after 4 h. (B) Particle treatment of 24 h reveals toxicity for $ufTiO_2$ and DQ12 particles at concentrations of 20 µg/cm^2 and above, whereas $fTiO_2$ does not result in toxicity up to 80 µg/cm^2. Figures represent mean ± SEM of three independent experiments, with ** $p < 0.01$ and *** $p < 0.001$ vs. control (ANOVA with LSD post-hoc comparison).

Ultrafine and fine TiO_2 exposure induce intracellular increase of calcium

Calcium is an important second messenger involved in a multitude of intracellular signaling pathways. We, therefore, investigated the impact of exposure to TiO_2 particles on the calcium concentration ($[Ca^{2+}]_i$) of individual AMΦ by performing ratiometric imaging with Fura-2 [Figure 2.4 A]. Under control conditions with no added particles, baseline calcium concentration was stable [Figure 2.4 B]. Addition of either $ufTiO_2$ or $fTiO_2$ caused an increase in the intracellular calcium concentration in a large number of cells in the field of view, some cells responded with large and random calcium oscillations [Figure 2.4 C].

To quantitatively analyze and compare calcium fluctuations in response to different particles and different concentrations, integrals for ratio values for specific 10 min time windows (one for control experiments; 15 - 25 min and 55 - 65 min after particle application) were calculated for each individual cell [Figure 2.4 D]. The resulting integral values were normalized to the mean of control values (obtained in the absence of particles). Cells, displaying values not covered by the standard deviation of control, were classified as "activated". A small number of such activated cells (8 - 10%) were already found in the control [Figure 2.4 D, upper histograms]. After addition of particles, however, the number of activated cells increased to 30 - 70% [Figure 2.4 D]. No consistent differences in percentage of activated cells nor amplitude of calcium fluctuations was found between $ufTiO_2$ and $fTiO_2$.

Figure 2.4 Increase of $[Ca^{2+}]_i$ after exposure of NR8383 cells to TiO_2 samples [on page 57].
(A) Transmission image of AMΦ (left) and image of Fura-2 fluorescence (excitation at 357 nm) (right). (B) Control experiments showing Fura-2 fluorescence ratio of untreated AMΦ. (C) Calcium fluctuations in individual cells in response to particle application ($ufTiO_2$ 20 µg/cm^2) over time. Some cells exhibit large calcium fluctuations, while others do not respond. Grey boxes indicate the time windows for which quantitative analysis shown in D was performed. (D) Quantitative analysis of calcium fluctuations: The integral of ratio traces was calculated for 10 min time windows for each individual cell. The resulting integral values were normalized to the mean of control values obtained in the absence of particles. Histograms show the percentage of cells exhibiting a 1.5 to 12 fold increase in calcium ratio integrals relative to controls. Light gray columns represent integral values within the standard deviation of controls. Dark columns represent signals of activated cells. Data are from 57 experiments on 39 coverslips, number of cells for each group: n = 198 - 443.

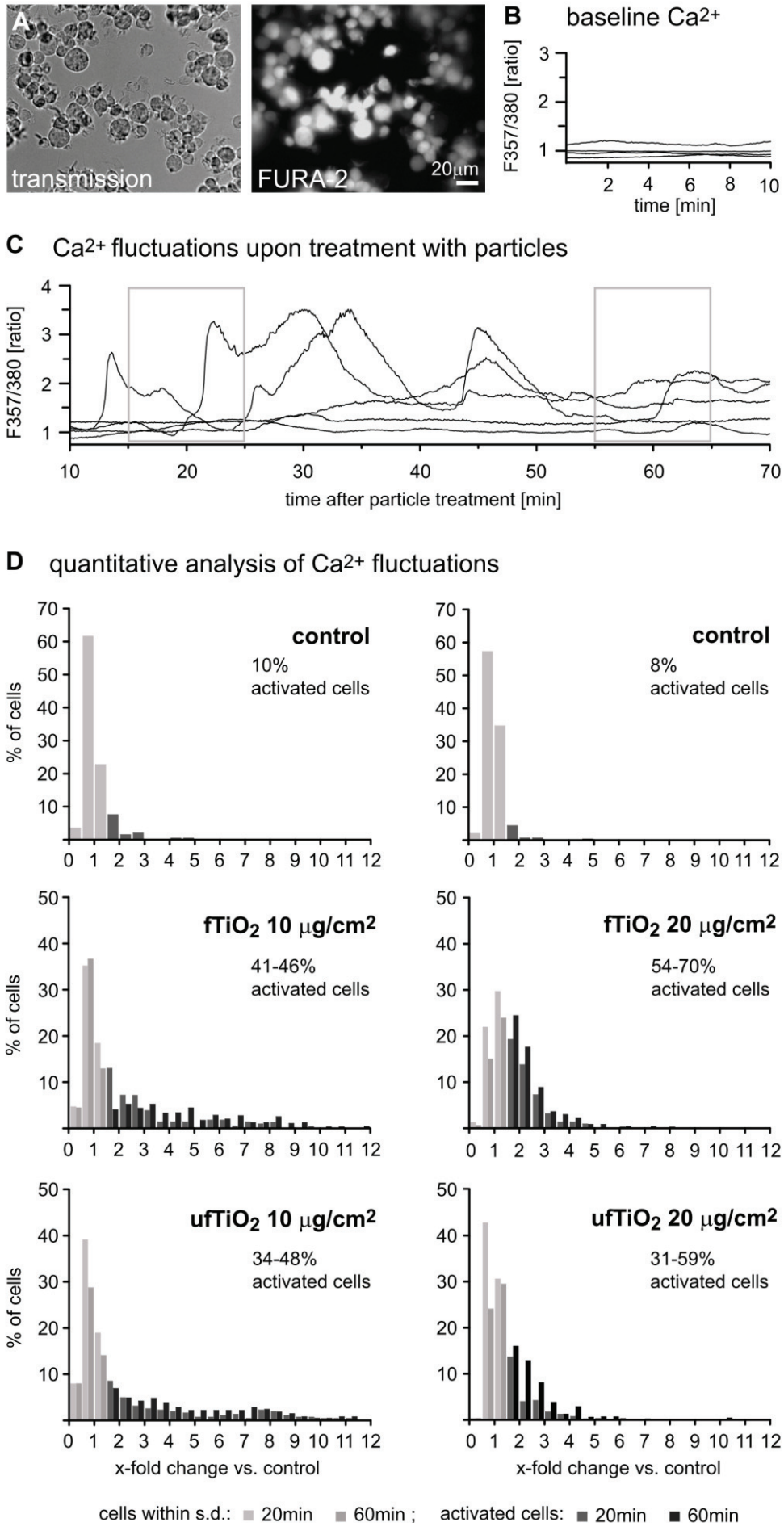
A
transmission
FURA-2
20µm
B
baseline Ca2+
F357/380 [ratio]
time [min]
C
Ca2+ fluctuations upon treatment with particles
F357/380 [ratio]
time after particle treatment [min]
D
quantitative analysis of Ca2+ fluctuations
control
10%
activated cells
control
8%
activated cells
fTiO2 10 µg/cm2
41-46%
activated cells
fTiO2 20 µg/cm2
54-70%
activated cells
ufTiO2 10 µg/cm2
34-48%
activated cells
ufTiO2 20 µg/cm2
31-59%
activated cells
% of cells
x-fold change vs. control
cells within s.d.: 20min 60min ; activated cells: 20min 60min

Particle-induced ROS generation

To study the ability of $ufTiO_2$, $fTiO_2$ and DQ12 particles to cause ROS generation in the NR8383 cells, measurements were conducted over a period of 3 h.

Formation of the fluorescent DCF, representing intracellular ROS formation within the particle treated AMΦ is shown in Figure 2.5 A. Intracellularly generated ROS were clearly observed upon particle treatment compared to untreated NR8383 cells. No significant differences were found between the different types of particles.

Extracellular ROS were detected upon 3 h of particle treatment in the supernatant of NR8383 cells by EPR coupled to spin trapping with DMPO [Figure 2.5 B]. A clear dose dependency was observed for all three particle types, with effects reaching statistical significance for $ufTiO_2$ and DQ12 at the higher concentration of 40 µg/cm^2.

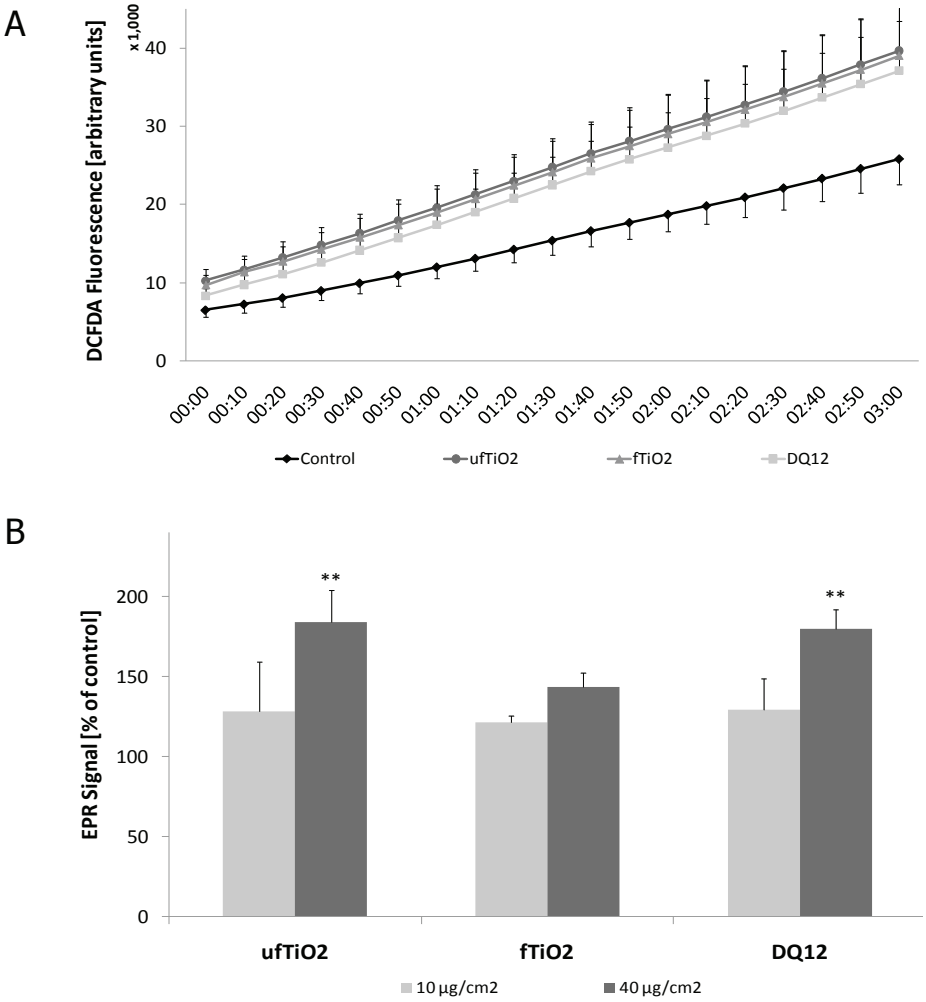

Figure 2.5 ROS generation by NR8383 cells after particle treatment.
(A) Intracellular ROS were measured via fluorescence of DCFH-DA after particle treatment of 40 µg/cm^2. (B) EPR measurements in NR8383 supernatant using the spintrap DMPO show a concentration-dependent generation of ROS induced by treatment with both TiO_2 and DQ12 particles. In both experiments AMΦ were treated for 3 h. Figures represent mean ± SEM of four independent experiments, with * $p < 0.05$ and ** $p < 0.01$ vs. untreated control (ANOVA with LSD post-hoc comparison) in Figure B.

Induction of markers of oxidative stress and inflammation

ROS as well as intracellular calcium are known to play an important role in activating several signaling pathways such as MAP kinases and redox-sensitive transcription factors including NF-κB, which can lead to the production of pro-inflammatory molecules and mediators. Therefore, we investigated the effects of the different particles on NF-κB activation, the release of TNF-α and IL-1β as well as changes in mRNA expression of HO-1 and iNOS in the NR8383 cells. In non-activated cells, NF-κB-specific fluorescence, reported by an antibody against the RelA(p65), was located in the cytoplasm of the AMΦ [Figure 2.6 A]. Distinct increase in nuclear fluorescence staining, indicating activation of the NF-κB pathway, was seen after treatment with the positive control DQ12 [Figure 2.6 B]. Treatment of NR8383 cells with $ufTiO_2$ [Figure 2.6 D] was found to cause an increase in the nuclear p65 staining albeit less strong than that following DQ12 treatment. The treatment with $fTiO_2$ showed a weak signal [Figure 2.6 C].

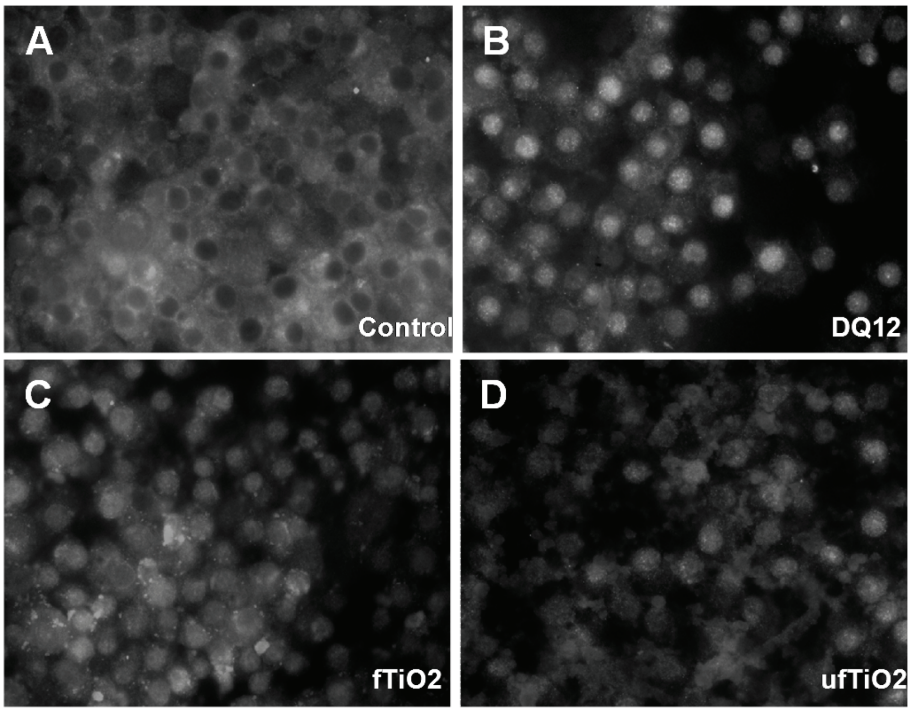

Figure 2.6 Induction of NFκB signaling after particle treatment.
NR8383 cells were treated with particles as indicated in concentrations of 40 µg/cm^2 for 1 h. Compared to (A) untreated AMΦ, (B) DQ12-treated cells show the strongest nuclear staining, while (C) $fTiO_2$ and (D) $ufTiO_2$ particles demonstrate a lower nuclear staining. Original magnification: 400-fold (Zeiss Axio Observer.D1).

The ability of the different particle types to induce TNF-α and IL-1β release from NR8383 cells is shown in Figure 2.7. TNF-α release was found to be induced by $ufTiO_2$ particles in a concentration-dependent manner, but not by $fTiO_2$ particles [Figure 2.7 A]. DQ12 was the most potent particle type, showing a significantly increased TNF-α release at 40 µg/cm^2, whereas a significant effect for $ufTiO_2$ was only found at the highest concentration tested (80 µg/cm^2). In contrast to the observations for TNF-α, the release of IL-1β from NR8383 cells was only increased after treatment with DQ12 particles [Figure 2.7 B]. Neither $ufTiO_2$ nor $fTiO_2$ were capable of initiating an increased IL-1β release from the NR8383 cells at the concentrations tested.

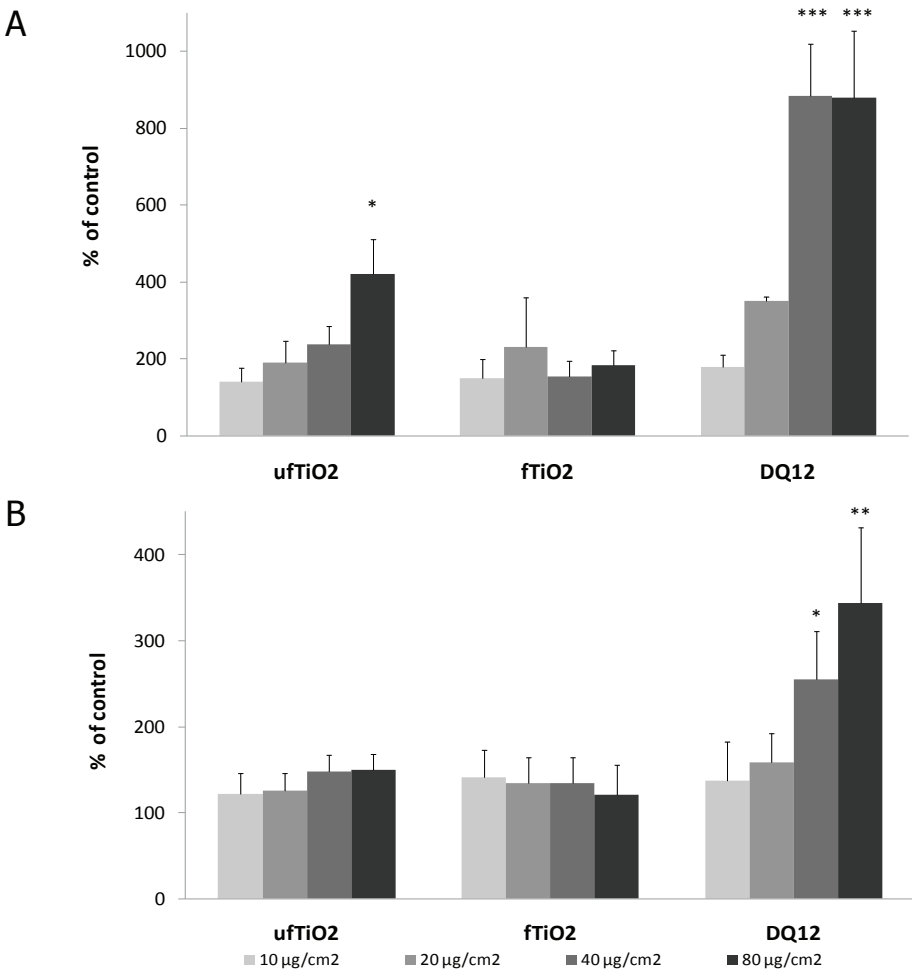

Figure 2.7 Particle-dependent release of TNF-α and IL-1β.
(A) $ufTiO_2$ and DQ12 particles trigger the release of TNF-α by AMΦ in a concentration- dependent manner. (B) Only DQ12 particles cause the release of IL-1β by AMΦ at the highest concentrations. Data are presented as mean ± SEM of three independent experiments, with * $p < 0.05$, ** $p < 0.01$ and *** $p < 0.001$ vs. medium control (ANOVA with LSD post-hoc comparison).

Results of the qRT-PCR analyzes of the mRNA levels of the stress response gene HO-1 and the inflammatory gene iNOS on the mRNA level by qRT-PCR are shown in Figure 2.8. A significantly higher HO-1 mRNA expression was observed after 4 h incubation with 40 µg/cm^2 ufTiO$_2$ as well as DQ12 [Figure 2.8 A], whereas iNOS mRNA expression was only significantly increased upon treatment with 40 µg/cm^2 ufTiO$_2$ [Figure 2.8 B]. In contrast, fTiO$_2$ particles showed no notable effect on the mRNA expression of either gene.

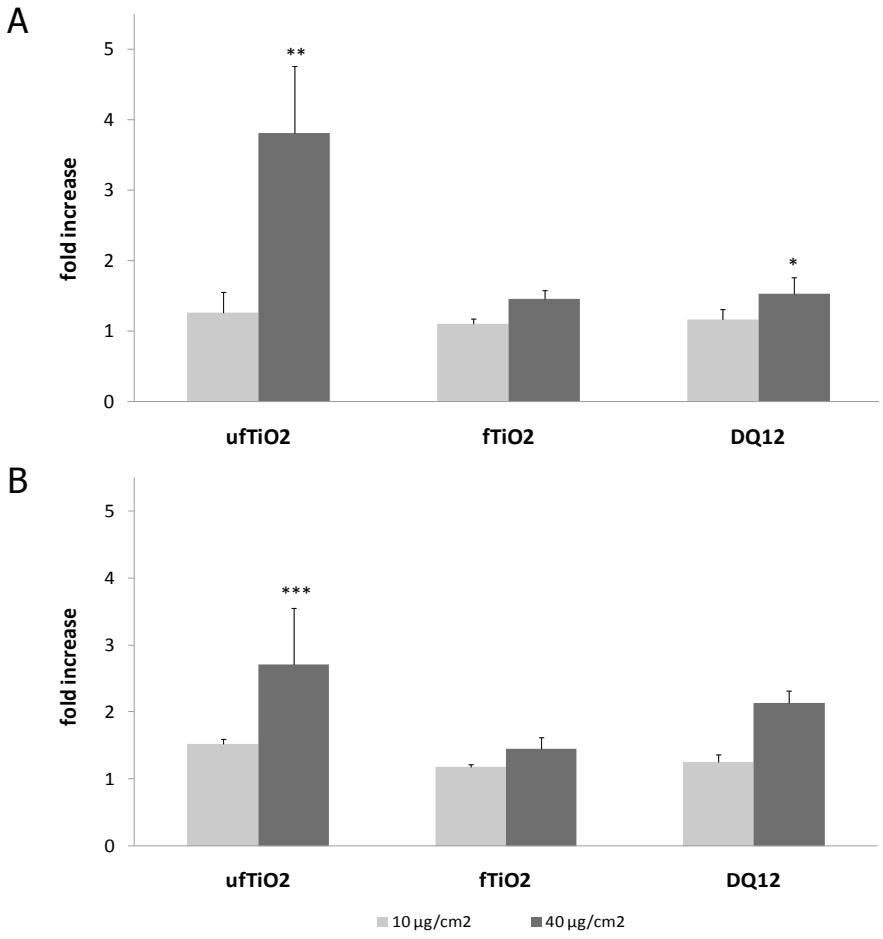

Figure 2.8 Particle-dependent impact on the mRNA regulation of HO-1 and iNOS.
NR8383 cells were treated with 10 or 40 µg/cm^2 of the indicated particles for 4 h. (A) ufTiO$_2$ and DQ12 trigger mRNA upregulation of the stress-response gene HO-1 in a concentration-dependent manner. (B) Synthesis of the inflammatory marker iNOS is strongly induced on the mRNA level by ufTiO$_2$ at a concentration of 40 µg/cm^2. Figures represent mean ± SEM of four independent experiments, with * $p < 0.05$, ** $p < 0.01$ and *** $p < 0.001$ vs. medium control (ANOVA with LSD post-hoc comparison).

Determination of specific internalization routes for the investigated particles.

In order to investigate internalization pathways for the different particle types in NR8383 cells, various approaches were used. Passive translocation was addressed by comparative evaluation of uptake at temperatures of 37 and 4 °C [Figure 2.9 A]. Irrespective of their size, approximately 50 % of the TiO_2 particles entered the cell by non-active routes of uptake, whereas for DQ12 particles a lower percentage was detected. However, it is important to note that the increased granularity of NR8383 cells at 4 °C may also - at least partially - reflect a fraction of particles that was not internalized but merely adherent to the cell.

For the evaluation of specific mechanisms of active uptake a set of specific inhibitors was used. Comparison of the FACS analysis data at 1 and 3 h show that the majority of particle uptake takes place within the first hour after particle treatment [Figure 2.2 A-C]. Hence, the particle treatment time for the inhibition experiments was set to 1 h [Figure 2.9 B-D]. Actin-dependent phagocytosis and macropinocytosis using CytD reduced the uptake of $fTiO_2$ and DQ12 particles, but not of $ufTiO_2$ particles. Whereas inhibition of actin in NR8383 cells was able to abrogate active DQ12 uptake, internalization of $fTiO_2$ could not be blocked completely via this mechanism. The uptake of $fTiO_2$ and DQ12 particles was significantly reduced at a particle concentration $\geq$ 20 µg/cm^2 upon inhibition of the formation of CCP by Chl. Inhibition of CPP-mediated internalization of $ufTiO_2$ particles was only significant at the highest concentration tested. In contrast to these findings, treatment of NR8383 cells with an antibody against the phagocytosis receptor FcγII had a strong influence on the uptake of $ufTiO_2$ but not of $fTiO_2$ particles. To inhibit the formation of caveolae, the inhibitor Filipin III was used. However, these experiments did not demonstrate any effect on particle uptake data not shown], which suggests that caveolae-mediated endocytosis is not involved in the uptake of any of the tested particles in NR8383 cells. No significant effects on particle uptake were observed upon treatment of the cells with the vehicle control DMSO as well as with the IgG control that was used for the FcγRII antibody treatment experiments.

Figure 2.9 Particle-specific mechanisms of internalization [on page 63].
(A) Assessment of the percentage of passively entered particles by measuring at 4 °C. The results are depicted as increase of SSC median compared to untreated NR8383 cells. (B - D) Preincubation for 30 min with CytD, Chl or an antibody against FcγRII (FcR ab) in order to block active uptake mechanisms, i.e. actin cytoskeleton-dependent uptake, uptake via CCP formation and FcγRII-mediated internalization, respectively. Treatment with (B) $ufTiO_2$, (C) $fTiO_2$ or (D) DQ12 particles in concentrations of 10, 20 or 40 µg/cm^2 for 1 h shows particle-specific internalization routes. Figures represent median ± SEM as percentage of untreated or vehicle (DMSO) control cells of three independent experiments, with * $p < 0.05$, ** $p < 0.01$ and *** $p < 0.001$ (ANOVA with Dunnett post-hoc comparison); as well as # $p < 0.05$, ## $p < 0.01$ and ### $p < 0.001$ for reduced granularity vs. appropriate particle treated cells (ANOVA with LSD post-hoc comparison), respectively.

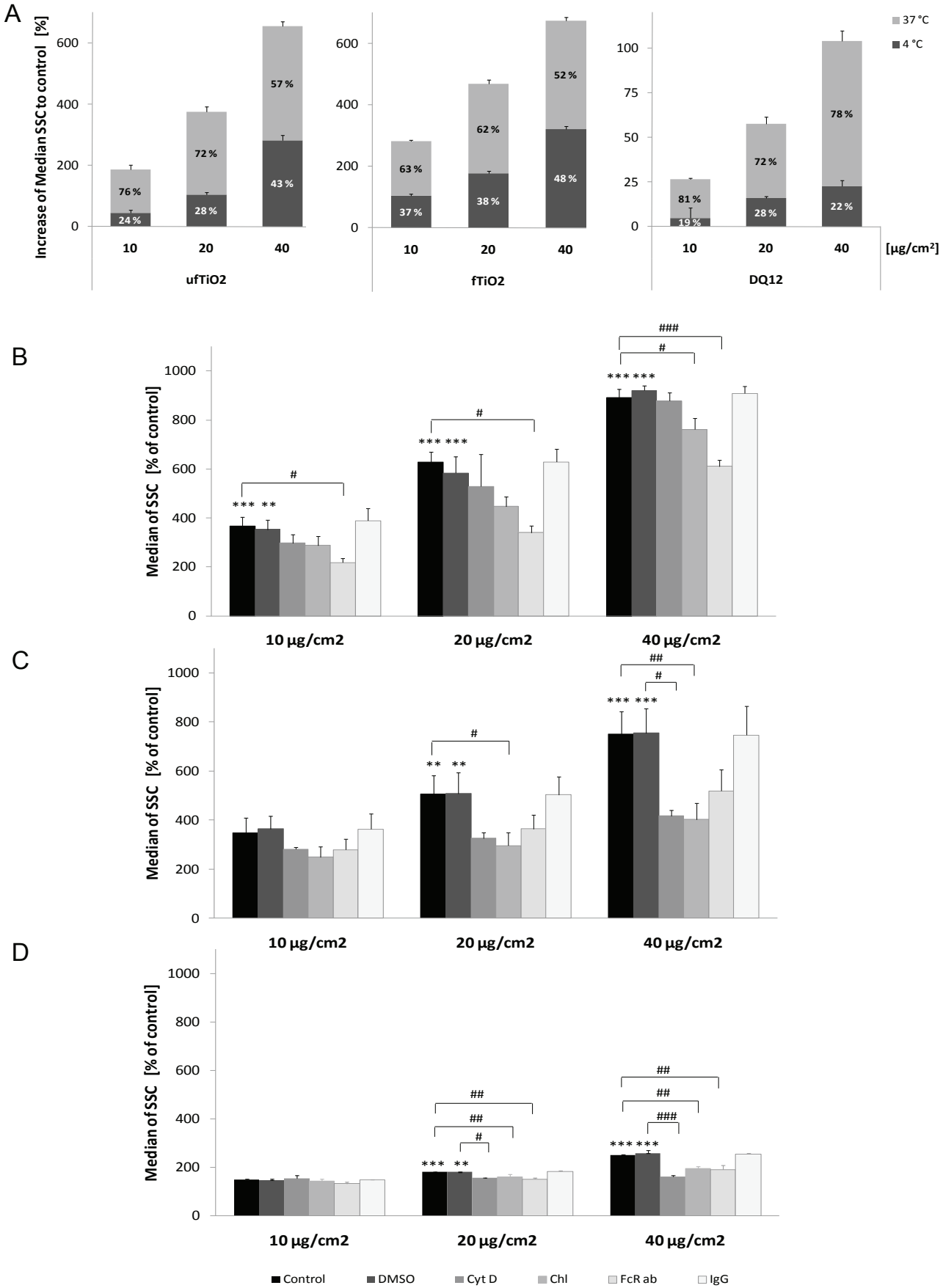
A
Increase of Median SSC to control [%]
37 °C
4 °C
76 %
24 %
72 %
28 %
57 %
43 %
63 %
37 %
62 %
38 %
52 %
48 %
81 %
19 %
72 %
28 %
78 %
22 %
10
20
40
[µg/cm²]
ufTiO2
fTiO2
DQ12
B
C
D
Median of SSC [% of control]
10 µg/cm2
20 µg/cm2
40 µg/cm2
Control
DMSO
Cyt D
Chl
FcR ab
IgG

2.4 DISCUSSION

In various studies ufTiO$_2$ particles have been shown to possess increased inflammogenic potential in comparison to fTiO$_2$ [Oberdörster et al 1994; 2005; Singh et al 2007; Sager & Castranova 2009]. Physiologic and systemic reactions towards NP exposure have been shown in several *in vivo* studies [Ferin & Oberdörster 1985; Lindenschmidt et al 1990; Oberdörster 2001; van Ravenzwaay et al 2009]. However, for the investigation of underlying basic cellular mechanisms and pathways, *in vitro* studies are necessary with established cell lines, e.g. NR8383 cells [Helmke et al 1989]. Responses of these cells to various toxicants such as PMA, endotoxin and DQ12 have shown to be highly comparable to those in primary AMΦ obtained from rat lungs by bronchoalveolar lavage [Albrecht et al 2009; van Berlo et al 2010].

In the present study we observed internalization of fTiO$_2$, ufTiO$_2$ and DQ12 by AMΦ in a clear dose-dependent manner. Direct comparison between the specific particles was not possible, because of their differing light scattering properties as observed under cell free testing conditions. However, our study demonstrates that, although all three particle types are taken up, the cellular responses of the AMΦ are substantially different. DQ12 and ufTiO$_2$ showed similar cytotoxicity, while significant effects for fTiO$_2$ were absent. This confirms the accepted view in particle toxicology that uptake of inorganic poorly soluble particles does not necessarily culminate in a toxic response in AMΦ. Our findings also show that particle uptake *per se* does not dictate oxidative stress and the induction of inflammatory mediators. DQ12 represented the most potent sample in inducing NF-κB activation and release of TNF-α and IL-1β from the AMΦ. However, HO-1 and iNOS mRNA expression levels in AMΦ were most pronounced after treatment with ufTiO$_2$. Remarkably also, both DQ12 and ufTiO$_2$ triggered TNF-α release, while only DQ12 induced IL-1β release. Finally, calcium influx and intracellular ROS generation were observed in AMΦ with all three particle types to a similar extent, although both are considered as key mechanisms for adverse particle effects [Donaldson et al 2003].

Tian and colleagues [2010] recently demonstrated that ROS do not modulate $[Ca^{2+}]_i$ in quartz-treated rat AMΦ, however, calcium increase in the cytoplasm causes ROS generation after silica treatment. Enhanced $[Ca^{2+}]_i$ in relation to pro-inflammatory signaling pathways has also been observed after treatment of MΦ with ultrafine carbon black (CB) particles in contrast to fine CB [Brown et al 2004]. To the best of our knowledge, a comparison of effects between ufTiO$_2$ and fTiO$_2$ on calcium homeostasis in MΦ has not yet been investigated. We observed no clear difference between both particle types in terms of the number of activated cells or the intensity of activation. In line with this, intracellular ROS levels also did not differ after treatment with both types of TiO$_2$. Our findings are in contrast to observations with CB

[Brown et al 2004], and suggest that particle size- and/or surface area-dependent effects on calcium influx and ROS formation are (nano)particle type-specific.

Besides intracellular ROS by DCFH-DA assay, we also determined extracellular ROS levels by means of EPR. Significant increases were observed here after treatment with DQ12 and $ufTiO_2$, but not after $fTiO_2$. Previous studies indicate that $fTiO_2$ and $ufTiO_2$ samples do not markedly differ in their intrinsic ROS capacity, when measured in cell free assays in the absence of photosensitization [Singh et al 2007; Fenoglio et al 2009; Jin et al 2010]. In concordance with our current findings in NR8383 cells, we could previously also show that $ufTiO_2$, unlike $fTiO_2$, caused enhanced ROS formation in supernatants of A549 human lung epithelial cells. This suggests that ROS predominantly originate from interactions between $ufTiO_2$ and cellular constituents and compartments rather than from the particles themselves. Potentially relevant sources herein include NADPH-oxidase enzyme family members as well as mitochondria [Singh et al 2007]. Our findings indicate that different ROS-generating mechanisms exist in AMΦ, with a selective sensitivity towards particle size or chemical composition as already concluded by Dick and colleagues [Dick et al 2003]. At this stage however, it should be emphasized that the calcium imaging experiments and both ROS assays were not performed in complete culture medium, but in saline, or $HBSS^{+/+}$, respectively. This was required to minimize potent radical scavenging properties of various (protein) constituents in the FCS-containing medium that can interfere with the assays. DLS measurements demonstrated that both $fTiO_2$ and $ufTiO_2$, when suspended in HBSS, reside as large agglomerates, unlike in FCS containing medium. Lacking differences in calcium influx and intracellular ROS between $fTiO_2$ and $ufTiO_2$ may therefore reflect an "agglomeration"-response of NR8383 cells. Interestingly though, increased extracellular ROS levels could be shown for $ufTiO_2$ by EPR analysis, despite its agglomeration. All other parameters in our study were evaluated using FCS-containing culture medium, in which the number-average diameter of $ufTiO_2$ sample was well within the nanosize range.

The contrasting abilities of DQ12, $ufTiO_2$ and $fTiO_2$ to induce IL-1β and/or TNF-α release can likely be explained by underlying differences in signaling pathways of activation of both inflammatory genes. NF-κB, a key regulator in the pathogenesis of particle-induced diseases [Donaldson & Stone 2003; Rimal et al 2005], regulates the expression of cytokines, growth factors and distinct enzymes in response to ligation of many receptors involved in immunity [Memet 2006]. A clear association between TNF-α levels in the supernatants from AMΦ upon particle treatment at equal mass (i.e. DQ12 > $ufTiO_2$ > $fTiO_2$) and their abilities to cause NF-κBp65 nuclear translocation was found. The exclusive effect of DQ12 on IL-1β release is likely to be explained by the recently unraveled mechanism of its cellular activation via the

inflammasome: IL-1β is produced as the inactive cytoplasmic precursor proIL-1β which has to be cleaved by caspase-1 to generate the mature active form of the protein [Dinarello 1998; Thornberry & Lazebnik 1998; Agostini et al 2004]. In turn, caspase-1 is regulated by the inflammasome protein complex NALP3 [Martinon & Tschopp 2007], which has been proposed to be activated by crystalline silica particles following lysosomal rupture [Hornung et al 2008] or by NADPH-oxidase-generated ROS upon phagocytosis of these particles [Dostert et al 2008]. A recent study has revealed that upon priming with LPS to induce proIL-1β, both DQ12 and ufTiO$_2$ do trigger IL-1β-secretion from bone marrow derived dendritic cells from wild-type but not caspase-1 or NLRP3-deficient mice [Winter et al in press]. This may suggest that the contrasting IL-1β responses observed with NR8383 cells may be due to differences in the abilities of specific types of poorly soluble particles to act on proIL-1β activation, i.e. upstream of the inflammasome activation.

A further remarkable observation in our study concerned the mRNA expression of HO-1 and iNOS. The positive control DQ12 appeared to be even less potent than ufTiO$_2$ with regard to the mRNA expression of both genes. HO-1 is considered as a sensitive marker of oxidative stress and has shown to be induced by inhaled ambient ultrafine particles [Li et al 2003] as well as by DQ12 quartz [Li et al 2008; van Berlo et al 2010]. The induction of iNOS in MΦ has been well-established in previous studies for crystalline silica particles, and this is considered to play a major role in its pulmonary toxicity [Porter et al 2002]. The contrasts in nuclear translocation of NF-κBp65, iNOS and HO-1 mRNA expression in NR8383 cells in response to ufTiO$_2$ and DQ12 suggests that particle-induced iNOS activation in MΦ can occur NF-κB-independently. While ufTiO$_2$ and DQ12 both trigger pro-inflammatory effects in MΦ unlike fTiO$_2$, these likely operate through different mechanisms.

The contrasting cellular responses observed by the three types of particles could not be explained by uptake by the AMΦ *per se*. Therefore, investigations were performed addressing the underlying cellular mechanisms of particle internalization. Herein, the importance of particle size and distribution as well as of agglomeration behavior in cell culture medium suspensions was taken into account using TEM, DLS and DF-LSM. We also specifically compared the uptake mechanisms of both TiO$_2$ samples with those that we previously investigated with DQ12 in NR8383 cells [Haberzettl et al 2007; 2008]. Evaluation of uptake at 4 °C indicates a passive, energy-independent entrance of particles into cells and/or their adherence to outer membranes of AMΦ. For both TiO$_2$ samples the proportion was found to be higher than for DQ12. However, no clear difference could be seen between fTiO$_2$ and ufTiO$_2$ despite the marked differences in their size distributions in complete culture medium used for the uptake experiments. Churg and colleagues found in a rat tracheal

explant model that $ufTiO_2$ particles readily formed agglomerates that persisted within the epithelium, whereas agglomerates of $fTiO_2$ became smaller over time, i.e. after 4 to 7 days [Churg et al 1998].

A series of specific inhibition experiments were performed to investigate the various active uptake routes in NR8383 cells. A combination between different uptake mechanisms in our study can be reasoned by the findings of Rothen-Rutishauser and colleagues [2007] showing TiO_2 particles in a three-dimensional cell culture model free in the cytoplasm as well as membrane-bound. Our own findings indicate that the active internalization of $ufTiO_2$ particles in AMΦ is mainly performed via a FcγRII-mediated mechanism and, to a lesser extent, by CCP which exhibit a vesicle diameter of 100 - 120 nm [Geiser 2010]. Uptake of $fTiO_2$ particles also took place via CCP, but in addition an actin-dependent uptake mechanism was equally involved. This may include macropinocytosis, by which large vesicles between 0.2 - 10 µm are formed spontaneously or upon stimulation [Swanson 2008]. Actin-mediated endocytosis is connected to receptor activation like MARCO and SR-A mediated processes, as previously shown by Kobzik and co-workers for primary AMΦ of different species [Palecanda et al 1999; Arredouani et al 2004; 2005]. The prominent receptor-mediated uptake mechanism for $fTiO_2$ and DQ12 by human MΦ via SR-A reported by Thakur et al. [2008] is beyond all question for our study, since NR8383 cells lack this receptor as determined by PCR analysis data not shown]. As expected from their size distribution, the DQ12 particles were taken up by actin-dependent classical phagocytosis which is described to be mediated by FcγRII [Haberzettl et al 2007]. Phagocytosis is the most effective clearance mechanism for particles between 1 - 5 µm in diameter [Geiser 2010]. Inhibition experiments with Filipin III were found to be unsuccessful in reducing particle uptake in NR8383 cells. For DQ12 and $fTiO_2$ this could be anticipated in view of their size distributions and the typical diameter of 50 - 100 nm of the caveolae vesicles. However, Filipin III was also ineffective for $ufTiO_2$, despite the fact that its number-average hydrodynamic diameter falls into the vesicle size range of caveolae. This suggests that even for these smaller particles/aggregates alternative uptake pathways such as CCP dominate. Another explanation may be related to the specific method of particle uptake used in the present study. In relation to the relative contribution of particle number and particle mass to changes in AMΦ granularity it is possible that the uptake of the smallest particles is underestimated in the flow cytometry approach. A major conclusion that can be drawn from the uptake experiments is that $fTiO_2$ and DQ12 which are both classified as "fine" particles show a specificity and size-dependency with regard to the tested cellular uptake mechanisms. Our observation that multiple uptake mechanisms may be relevant for one specific type of particle can be explained by the size-

distribution of the specific samples and, likely of more importance, their agglomeration behavior when suspended in culture media. Regarding agglomerate sizes of immune complexes and their internalization pathways, Tse and colleagues [2003] demonstrated the existence of different FcγRIII-mediated uptake mechanisms in mouse MΦ.

In conclusion, the data from our study indicate that the specific physico-chemical properties of quartz, $fTiO_2$ and $ufTiO_2$ particles are responsible for qualitative as well as quantitative differences in oxidative stress and inflammatory responses in AMΦ. In contrast to $fTiO_2$ which was relatively inert, both DQ12 and $ufTiO_2$ increased extracellular ROS and TNF-α release, while only $ufTiO_2$ enhanced iNOS mRNA expression, and DQ12 exclusively triggered IL-1β release. These outcomes may relate to differences in the involvement of specific uptake mechanisms, i.e. actin cytoskeleton, CCP formation and FcγRII internalization. In contrast, intracellular ROS and calcium influx were observed with all three particle types to a similar extent, and thus could not explain for their differential uptake mechanisms and pro-inflammatory responses.

ACKNOWLEDGEMENTS

We are grateful to Christel Weishaupt (IUF) for technical assistance. Furthermore, we thank Claudia Roderigo (Heinrich-Heine-University Düsseldorf) for performing the calcium imaging experiments and Dr. Lhoussaine Belkoura (University of Cologne) for the performance of TEM analysis.
The current address of P.H. is the Division of Cardiology, University of Louisville, USA.

GRANTS

This work was financially supported by the Federal Ministry of the Environment (BMU) as well as by the Graduate School GRK1427 of the German Research Council (DFG).

2.5 REFERENCES

Agostini L, Martinon F, Burns K, McDermott MF, Hawkins PN, Tschopp J. NALP3 forms an IL-1beta-processing inflammasome with increased activity in Muckle-Wells autoinflammatory disorder. Immunity 2004, 20(3):319-25.

Akagawa KS. Functional heterogeneity of colony-stimulating factor-induced human monocyte-derived macrophages. Int J Hematol 2002, 76(1):27-34.

Albrecht C, Knaapen AM, Becker A, Höhr D, Haberzettl P, van Schooten FJ, Borm PJ, Schins RP. The crucial role of particle surface reactivity in respirable quartz-induced reactive oxygen/nitrogen species formation and APE/Ref-1 induction in rat lung. Respir Res 2005, 6:129.

Albrecht C, Scherbart AM, van Berlo D, Braunbarth CM, Schins RP, Scheel J. Evaluation of cytotoxic effects and oxidative stress with hydroxyapatite dispersions of different physicochemical properties in rat NR8383 cells and primary macrophages. Toxicol In Vitro 2009, 23(3):520-30.

Albrecht C, Schins RP, Höhr D, Becker A, Shi T, Knaapen AM, Borm PJ. Inflammatory time course after quartz instillation: role of tumor necrosis factor-alpha and particle surface. Am J Respir Cell Mol Biol 2004, 31(3):292-301.

Arredouani M, Yang Z, Ning Y, Qin G, Soininen R, Tryggvason K, Kobzik L. The scavenger receptor MARCO is required for lung defense against pneumococcal pneumonia and inhaled particles. J Exp Med 2004, 200(2):267-72.

Arredouani MS, Palecanda A, Koziel H, Huang YC, Imrich A, Sulahian TH, Ning YY, Yang Z, Pikkarainen T, Sankala M, Vargas SO, Takeya M, Tryggvason K, Kobzik L. MARCO is the major binding receptor for unopsonized particles and bacteria on human alveolar macrophages. J Immunol 2005, 175(9):6058-64.

Bermudez E, Mangum JB, Wong BA, Asgharian B, Hext PM, Warheit DB, Everitt JI. Pulmonary responses of mice, rats, and hamsters to subchronic inhalation of ultrafine titanium dioxide particles. Toxicol Sci 2004, 77(2):347-57.

Brown DM, Donaldson K, Borm PJ, Schins RP, Dehnhardt M, Gilmour P, Jimenez LA, Stone V. Calcium and ROS-mediated activation of transcription factors and TNF-alpha cytokine gene expression in macrophages exposed to ultrafine particles. Am J Physiol Lung Cell Mol Physiol 2004, 286(2):L344-53.

Brunauer S, Emmert PH, Teller E. Adsorption of gases in multimolecular layers. J Amer Chem Soc 1938, 60:309-19.

Castranova V, Vallyathan V. Silicosis and coal workers' pneumoconiosis. Environ Health Perspect 2000, 108 Suppl 4:675-84.

Churg A, Stevens B, Wright JL. Comparison of the uptake of fine and ultrafine TiO2 in a tracheal explant system. Am J Physiol 1998, 274(1 Pt 1):L81-6.

Dai X, Jayapal M, Tay HK, Reghunathan R, Lin G, Too CT, Lim YT, Chan SH, Kemeny DM, Floto RA, Smith KG, Melendez AJ, MacAry PA. Differential signal transduction, membrane trafficking, and immune effector functions mediated by FcgammaRI versus FcgammaRIIa. Blood 2009, 114(2):318-27.

Dick CA, Brown DM, Donaldson K, Stone V. The role of free radicals in the toxic and inflammatory effects of four different ultrafine particle types. Inhal Toxicol 2003, 15(1):39-52.

Dinarello CA. Interleukin-1 beta, interleukin-18, and the interleukin-1 beta converting enzyme. Ann N Y Acad Sci 1998, 856:1-11.

Donaldson K, Stone V. Current hypotheses on the mechanisms of toxicity of ultrafine particles. Ann Ist Super Sanita 2003, 39(3):405-10.

Donaldson K, Stone V, Borm PJ, Jimenez LA, Gilmour PS, Schins RP, Knaapen AM, Rahman I, Faux SP, Brown DM, MacNee W. Oxidative stress and calcium signaling in the adverse effects of environmental particles (PM10). Free Radic Biol Med 2003, 34(11):1369-82.

Donaldson K, Stone V, Duffin R, Clouter A, Schins R, Borm P. The quartz hazard: effects of surface and matrix on inflammogenic activity. J Environ Pathol Toxicol Oncol 2001, 20 Suppl 1:109-18.

Donaldson K, Tran CL. Inflammation caused by particles and fibers. Inhal Toxicol 2002, 14(1):5-27.

Dostert C, Petrilli V, Van Bruggen R, Steele C, Mossman BT, Tschopp J. Innate immune activation through Nalp3 inflammasome sensing of asbestos and silica. Science 2008, 320(5876):674-7.

Fenoglio I, Greco G, Livraghi S, Fubini B. Non-UV-induced radical reactions at the surface of TiO2 nanoparticles that may trigger toxic responses. Chemistry 2009, 15(18):4614-21.

Ferin J, Oberdörster G. Biological effects and toxicity assessment of titanium dioxides: anatase and rutile. Am Ind Hyg Assoc J 1985, 46(2):69-72.

Geiser M. Update on macrophage clearance of inhaled micro- and nanoparticles. J Aerosol Med Pulm Drug Deliv 2010, 23(4):207-17.

Haberzettl P, Duffin R, Kramer U, Höhr D, Schins RP, Borm PJ, Albrecht C. Actin plays a crucial role in the phagocytosis and biological response to respirable quartz particles in macrophages. Arch Toxicol 2007, 81(7):459-70.

Haberzettl P, Schins RP, Höhr D, Wilhelmi V, Borm PJ, Albrecht C. Impact of the FcgammaII-receptor on quartz uptake and inflammatory response by alveolar macrophages. Am J Physiol Lung Cell Mol Physiol 2008, 294(6):L1137-48.

Helmke RJ, German VF, Mangos JA. A continuous alveolar macrophage cell line: comparisons with freshly derived alveolar macrophages. In Vitro Cell Dev Biol 1989, 25(1):44-8.

Hornung V, Bauernfeind F, Halle A, Samstad EO, Kono H, Rock KL, Fitzgerald KA, Latz E. Silica crystals and aluminum salts activate the NALP3 inflammasome through phagosomal destabilization. Nat Immunol 2008, 9(8):847-56.

Jin C, Tang Y, Yang FG, Li XL, Xu S, Fan XY, Huang YY, Yang YJ. Cellular Toxicity of TiO(2) Nanoparticles in Anatase and Rutile Crystal Phase. Biol Trace Elem Res 2010.

Johnston H, Hutchison GR, Christensen FM, Peters S, Hankin S, Stone V. Identification of the mechanisms that drive the toxicity of TiO_2 particulates: the contribution of physicochemical characteristic. Part Fib Tox 2010, 6:33.

Kang JL, Pack IS, Hong SM, Lee HS, Castranova V. Silica induces nuclear factor-kappa B activation through tyrosine phosphorylation of I kappa B-alpha in RAW264.7 macrophages. Toxicol Appl Pharmacol 2000, 169(1):59-65.

Kobzik L. Lung macrophage uptake of unopsonized environmental particulates. Role of scavenger-type receptors. J Immunol 1995, 155(1):367-76.

Kuempel ED, Attfield MD, Vallyathan V, Lapp NL, Hale JM, Smith RJ, Castranova V. Pulmonary inflammation and crystalline silica in respirable coal mine dust: dose-response. J Biosci 2003, 28(1):61-9.

Lardot CG, Huaux FA, Broeckaert FR, Declerck PJ, Delos M, Fubini B, Lison DF. Role of urokinase in the fibrogenic response of the lung to mineral particles. Am J Respir Crit Care Med 1998, 157(2):617-28.

Li H, van Berlo D, Shi T, Speit G, Knaapen AM, Borm PJ, Albrecht C, Schins RP. Curcumin protects against cytotoxic and inflammatory effects of quartz particles but causes oxidative DNA damage in a rat lung epithelial cell line. Toxicol Appl Pharmacol 2008, 227(1):115-24.

Li N, Sioutas C, Cho A, Schmitz D, Misra C, Sempf J, Wang M, Oberley T, Froines J, Nel A. Ultrafine particulate pollutants induce oxidative stress and mitochondrial damage. Environ Health Perspect 2003, 111(4):455-60.

Lindenschmidt RC, Driscoll KE, Perkins MA, Higgins JM, Maurer JK, Belfiore KA. The comparison of a fibrogenic and two nonfibrogenic dusts by bronchoalveolar lavage. Toxicol Appl Pharmacol 1990, 102(2):268-81.

Livak KJ, Schmittgen TD. Analysis of relative gene expression data using real-time quantitative PCR and the 2(-Delta Delta C(T)) Method. Methods 2001, 25(4):402-8.

Martin TR, Frevert CW. Innate immunity in the lungs. Proc Am Thorac Soc 2005, 2(5):403-11.

Martinon F, Tschopp J. Inflammatory caspases and inflammasomes: master switches of inflammation. Cell Death Differ 2007, 14(1):10-22.

Memet S. NF-kappaB functions in the nervous system: from development to disease. Biochem Pharmacol 2006, 72(9):1180-95.

Nel A, Xia T, Madler L, Li N. Toxic potential of materials at the nanolevel. Science 2006, 311(5761):622-7.

Oberdörster G. Pulmonary effects of inhaled ultrafine particles. Int Arch Occup Environ Health 2001, 74(1):1-8.

Oberdörster G, Ferin J, Lehnert BE. Correlation between particle size, in vivo particle persistence, and lung injury. Environ Health Perspect 1994, 102 Suppl 5:173-9.

Oberdörster G, Oberdörster E, Oberdörster J. Nanotoxicology: an emerging discipline evolving from studies of ultrafine particles. Environ Health Perspect 2005, 113(7):823-39.

Palecanda A, Kobzik L. Alveolar macrophage-environmental particle interaction: analysis by flow cytometry. Methods 2000, 21(3):241-7.

Palecanda A, Paulauskis J, Al-Mutairi E, Imrich A, Qin G, Suzuki H, Kodama T, Tryggvason K, Koziel H, Kobzik L. Role of the scavenger receptor MARCO in alveolar macrophage binding of unopsonized environmental particles. J Exp Med 1999, 189(9):1497-506.

Porter DW, Millecchia L, Robinson VA, Hubbs A, Willard P, Pack D, Ramsey D, McLaurin J, Khan A, Landsittel D, Teass A, Castranova V. Enhanced nitric oxide and reactive oxygen species production and damage after inhalation of silica. Am J Physiol Lung Cell Mol Physiol 2002, 283(2):L485-93.

Rada B, Leto TL. Oxidative innate immune defenses by Nox/Duox family NADPH oxidases. Contrib Microbiol 2008, 15:164-87.

Rimal B, Greenberg AK, Rom WN. Basic pathogenetic mechanisms in silicosis: current understanding. Curr Opin Pulm Med 2005, 11(2):169-73.

Rothen-Rutishauser B, Muhlfeld C, Blank F, Musso C, Gehr P. Translocation of particles and inflammatory responses after exposure to fine particles and nanoparticles in an epithelial airway model. Part Fibre Toxicol 2007, 4:9.

Sager TM, Castranova V. Surface area of particle administered versus mass in determining the pulmonary toxicity of ultrafine and fine carbon black: comparison to ultrafine titanium dioxide. Part Fibre Toxicol 2009, 6:15.

Schulze-Osthoff K, Los M, Baeuerle PA. Redox signalling by transcription factors NF-kappa B and AP-1 in lymphocytes. Biochem Pharmacol 1995, 50(6):735-41.

Shukla A, Ramos-Nino M, Mossman B. Cell signaling and transcription factor activation by asbestos in lung injury and disease. Int J Biochem Cell Biol 2003, 35(8):1198-209.

Shvedova AA, Castranova V, Kisin ER, Schwegler-Berry D, Murray AR, Gandelsman VZ, Maynard A, Baron P. Exposure to carbon nanotube material: assessment of nanotube cytotoxicity using human keratinocyte cells. J Toxicol Environ Health A 2003, 66(20):1909-26.

Singh S, Shi T, Duffin R, Albrecht C, van Berlo D, Höhr D, Fubini B, Martra G, Fenoglio I, Borm PJ, Schins RP. Endocytosis, oxidative stress and IL-8 expression in human lung epithelial cells upon treatment with fine and ultrafine TiO2: role of the specific surface area and of surface methylation of the particles. Toxicol Appl Pharmacol 2007, 222(2):141-51.

Stoeger T, Reinhard C, Takenaka S, Schroeppel A, Karg E, Ritter B, Heyder J, Schulz H. Instillation of six different ultrafine carbon particles indicates a surface area threshold dose for acute lung inflammation in mice. Environ Health Perspect 2006, 114(3):328-33.

Stone V, Johnston H, Schins RP. Development of in vitro systems for nanotoxicology: methodological considerations. Crit Rev Toxicol 2009, 39(7):613-26.

Swanson JA. Shaping cups into phagosomes and macropinosomes. Nat Rev Mol Cell Biol 2008, 9(8):639-49.

Thakur SA, Hamilton RF, Jr., Holian A. Role of scavenger receptor a family in lung inflammation from exposure to environmental particles. J Immunotoxicol 2008, 5(2):151-7.

Thornberry NA, Lazebnik Y. Caspases: enemies within. Science 1998, 281(5381):1312-6.

Tian F, Zhu T, Shang Y. Intracellular influx of calcium induced by quartz particles in alveolar macrophages. Toxicol Appl Pharmacol 2010, 242(2):173-81.

Tse SM, Furuya W, Gold E, Schreiber AD, Sandvig K, Inman RD, Grinstein S. Differential role of actin, clathrin, and dynamin in Fc gamma receptor-mediated endocytosis and phagocytosis. J Biol Chem 2003, 278(5):3331-8.

Unfried K, Albrecht C, Klotz LO, von Mikecz A, Grether-Beck S, Schins RPF. Cellular responses to nanoparticles: Target structures and mechanisms. Nanotoxicology 2007, 1:20.

van Berlo D, Knaapen AM, van Schooten FJ, Schins RP, Albrecht C. NF-kappaB dependent and independent mechanisms of quartz-induced proinflammatory activation of lung epithelial cells. Part Fibre Toxicol 2010, 7:13.

van Ravenzwaay B, Landsiedel R, Fabian E, Burkhardt S, Strauss V, Ma-Hock L. Comparing fate and effects of three particles of different surface properties: nano-TiO(2), pigmentary TiO(2) and quartz. Toxicol Lett 2009, 186(3):152-9.

Warheit DB, Reed KL, Sayes CM. A role for nanoparticle surface reactivity in facilitating pulmonary toxicity and development of a base set of hazard assays as a component of nanoparticle risk management. Inhal Toxicol 2009, 21 Suppl 1:61-7.

Warheit DB, Webb TR, Reed KL, Frerichs S, Sayes CM. Pulmonary toxicity study in rats with three forms of ultrafine-TiO2 particles: differential responses related to surface properties. Toxicology 2007, 230(1):90-104.

Winter M, Beer HD, Hornung V, Kramer U, Schins RP, Forster I. Activation of the inflammasome by amorphous silica and TiO(2) nanoparticles in murine dendritic cells. Nanotoxicology, in press.

CHAPTER III

SURFACE IRON INHIBITS QUARTZ-INDUCED CYTOTOXIC AND INFLAMMATORY RESPONSES IN ALVEOLAR MACROPHAGES

Mara Ghiazza*, Agnes M. Scherbart*, Ivana Fenoglio, Francesca Grendene, Francesco Turci, Gianmario Martra, Catrin Albrecht, Roel P.F. Schins, Bice Fubini

* equal contributions

Chemical Research in Toxicology, 2011 Jan;24(1):99-110

DECLARATION - STUDY 2

Surface iron inhibits quartz-induced cytotoxic and inflammatory responses in alveolar macrophages.

Declaration:
The manuscript is submitted to a peer-review journal.
Most experimental work presented, was done by Agnes M. Scherbart.
The impact on authoring this paper can be estimated to 50 %.

ABSTRACT

The mechanism of enhancement or inhibition of quartz toxicity induced by iron is still unclear. Here the amount of iron on a fibrogenic quartz (Qz) was increased by impregnation with $Fe(NO_3)_3$ (0.67 and 6.7 % wt). X-ray diffraction (XRD), XRF diffuse reflectance, UV-Vis and infrared (IR) spectroscopies revealed dispersed ferric ions and, only at the higher loading, hematite aggregates. Surface features and cell responses relevant to pathogenicity were compared not only with the original quartz, but also with reference quartz DQ12. Surface charge (ζ-potential) was higher on the original and low loaded specimen than on the high loaded one, as also hematite contributes to the overall charge. DQ12 had a lower ζ-potential than Qz, relatable to the absence of aluminum present at a level of 1.7 % in Qz. Generation of HO· radicals (Fenton activity), measured by the EPR/spin trapping technique, revealed that all quartzes were active, with slight increase in activity upon iron-loading. Rupture of a C-H bond took place on Qz only and was suppressed upon iron deposition. Iron removable by chelators increased with loading but remained below 0.3 %. All quartzes were taken up by alveolar macrophages (AMΦ cell line NR8383) at the same extent, irrespective of their surface state. Conversely, iron-loading increased AMΦ viability (evaluated by cytotoxicity and induction of apoptosis), and Qz was much less toxic than DQ12. Investigation of oxidative stress and inflammatory responses (evaluated by HO-1 mRNA expression and TNF-α mRNA and protein expression) also revealed a reduction in inflammogenicity upon iron-loading and a more inflammogenic potency of DQ12, which may be due to undissociated SiOH interacting via H-bonding with membranes and biomolecules. The results suggest that beside aluminum also iron at the quartz surface may have an inhibitory effect on adverse health responses.

3.1 INTRODUCTION

It is well-known that exposure to silica dusts causes silicosis - the most ancient occupational disease - but also lung cancer and several autoimmune diseases [IARC 1997, 2010]. In spite of a large number of *in vivo* and *in vitro* studies, the detailed mechanism of quartz toxicity at the molecular level is still not fully understood. Toxicity has been traditionally ascribed only to crystalline silica polymorphs, even if recently vitreous silica showed strong similarities with quartz in physico-chemical features and cellular responses [Ghiazza et al 2010]. Quartz is the most common form of particulate silica to which workers are exposed [Iler 1979; Green & Vallyathan 1996; IARC 1997; Fubini 1998a; Donaldson & Borm 1998] but other polymorphs such as tridimite and cristobalite are equally or even more toxic [Castranova et al 1996b; IARC 1997]. Extensive investigations of several quartz samples from different sources revealed a wide variability in quartz hazard [Donaldson & Borm 1998; Fubini 1998b; Bruch et al 2004; Cakmak et al 2004]. The origin, the mechanical history of the dusts and the different level of contaminants, associated either with the original mineral or acquired during the industrial processes, have been recognized as important factors in determining such variability [IARC 1997; Fubini 1998a; Fubini et al 2004]. The scientific community became aware of differences first among the various crystalline polymorphs, then among the same polymorph but with different origin [Fubini 1998b] and among particles modified in their surface properties, e.g. by aluminum ions [Schins et al 2002] or by contaminating metals [Fenoglio et al 2001; Fubini et al 2004; Bruch et al 2004; Cakmak et al 2004; Seiler et al 2004]. There is a general agreement that many different physico-chemical features contribute to the overall toxicity of given crystalline silica particulate.

The most common metal contaminant in commercial quartz dusts is iron which may be present at the surface in different oxidative states. The role of iron has been a matter of debate for many years in particle toxicology [Kamp & Weitzman 1999]. It is well-known that iron plays an important role in the toxicity of asbestos [Hardy & Aust 1995; Fubini & Otero-Aréan 1999], coal fly ashes [Smith et al 1998; van Maanen et al 1999; Smith et al 2000], airborne particulate matter [Donaldson et al 1997] and silicas [Hetland et al 2001; Fubini et al 2001; Elias et al 2002a, 2002c]. Iron has been shown to play an important role in modulating the quartz toxicity; contrasting results, however, have been reported in the literature: Metallic iron associated to quartz was found to inhibit lung inflammation in rats [Cullen et al 1997], and iron salts decreased the ability of quartz to damage the membranes of erythrocytes [Nolan et al 1981]. Conversely, Castranova and co-workers reported that quartz particles contaminated with iron during the milling processes were more inflammogenic in rats [Castranova et al 1997], while ferrous and ferric iron ions increase the

reactivity of the quartz surface by leading to Fenton chemistry-mediated generation of radicals [Vallyathan 1994; Castranova et al 1996a; Fenoglio et al 2001]. The presence of Fe(III) ions was also reported to enhance the ability of quartz to consume endogenous antioxidants [Fenoglio et al 2003]. Furthermore, some of us have shown in a previous study, that enrichment of quartz dust with a high amount of iron decreased both the HO· yield of the dust and its effect on cell transformation in Syrian hamster embryo (SHE) cells [Fubini et al 2001]. However, amelioration also took place when traces of iron were removed by chelators suggesting that iron might increase the toxicity when present in traces but decrease it when in substantial amounts at the surface. Such differences may be partially ascribed to the amount of iron at the surface [Donaldson & Borm 1998], its oxidative state but also to different coordinative sphere of iron ions. In heterogeneous catalysis, the coordination state of metals is known to modulate the reactivity of the catalyst, poorly coordinated metal ions acting as active sites in different reactions [Somorjai et al 2002]. Castranova et al [1997] showed that iron-coating augmented the *in vivo* response to quartz as demonstrated by several parameters such as recruitment of leukocytes and lipid peroxidation. Specifically for alveolar macrophages (AMΦ) obtained by bronchoalveolar lavage, high iron addition increased NO-dependent and zymosan-stimulated chemiluminescence. In contrast, Cullen et al showed a protection by ferrous or ferric iron coating on quartz induced cellular response [Cullen et al 1997]. To date, only few studies have been designed to elucidate the role of the coordinative state of iron ions on the toxic potential of quartz particulates.

AMΦ are phagocytic active cells that play a major role in host defence in the alveolar region of the respiratory system and they represent the common link between the innate and the acquired immune system. AMΦ are the first cell type getting into contact with inhaled pathogens, which makes them important to study in pathologies associated with e.g. silica exposure [Gwinn & Vallyathan 2006]. Uptake of pathogens, including particles, may lead to MΦ activation resulting in the release of reactive oxygen/nitrogen species as well as inflammatory mediators [Kanj et al 2005; Azad et al 2008]. In the present study NR8383 cells were used as a well-established and well-investigated cellular model for AMΦ [Helmke et al 1989; Lane et al 1998]. The suitability of this cell line to investigate mechanisms of toxicity of particles, including quartz, has been demonstrated in several studies [Albrecht et al 2007; Haberzettl et al 2008; van Berlo et al 2009, 2010; Lison et al 2009].

To investigate the influence of iron ions on the reactivity of quartz particles, we have prepared *ad hoc* quartz samples impregnated with two different amounts of iron and compared their activity in cell free and cellular tests with that of the original quartz sample.

We report here the potential of these modified quartz samples differing in loading and coordinative state of surface iron to generate hydroxyl and carbon centered free radicals in a cell-free system and to induce biological responses in NR8383 rat AMΦ. In this cell line we investigated the role of iron in the uptake of quartz particles, cytotoxicity, apoptosis, the induction of the oxidative stress marker heme oxygenase-1 (HO-1) and the pro-inflammatory cytokine tumor necrosis factor-alpha (TNF-α). The well-known cytotoxic, inflammogenic and fibrogenic quartz sample DQ12 was included as a positive control in these experiments [Huaux et al 1995; Bruch et al 2004; Albrecht et al 2004; Haberzettl et al 2008]. Unfortunately, few laboratories still hold substantial amounts of this material (largely used in past European studies), which exhibits a much higher fibrogenic activity than most other quartz specimens [Clouter et al 2001; Bruch et al 2004]. Physico-chemical reasons for such high activity were never assessed, even if they may yield a clue to the understanding of the molecular mechanisms taking place. Therefore, we have examined in some detail the physico-chemical features of this specimen, also in the view of preparing a new controlled reference material.

3.2 MATERIALS & METHODS

Preparation of iron loaded quartz dusts

Quartz dusts employed

Natural microcrystalline quartz (Qz), with a relative low amount of iron and aluminum as trace contaminants, purchased from Sigma-Aldrich was employed. The particle size distribution reported by the supplier falls in the range 0.5 - 10 µm, with 80 % of particles comprised between 1 and 5 µm. The surface area is 7.5 m^2/g a value close to that of most common industrial dusts [Hyun et al 2003], with no appreciable amount of meso- or micropores. This quartz dust was chosen because of its reported fibrogenicity in rats [Corsini et al 2003]. Quartz DQ12 (Dörentrup, Germany, batch 6, mean diameter 0.96 µm) was employed as positive control [Albrecht et al 2004; Albrecht et al 2005] in view of its well-established ability to activate MΦs *in vitro* [Bruch et al 2004; Albrecht et al 2009; van Berlo et al 2009, 2010].

Impregnation with Fe(III)

A wet impregnation method was used. 1 g of quartz was impregnated with 3 mL of an aqueous solution of $Fe(NO_3)_3$, either 0.002 or 0.2 M, that correspond to 0.67 and 6.7 wt % of Fe(III), respectively. These samples are denoted hereafter as low loading sample (QzFe/ll) and high loading sample (QzFe/hl). The suspension was dried at 40 °C for 24 h then the procedure was carried out a second time. The product obtained was washed three times with distilled water to eliminate any iron not firmly bound to the surface. The samples were then dried at 100 °C and subsequently calcinated at 600 °C for 16 h [El Malki et al 2000; Berlier et al 2002].

Elemental analysis

The elemental analysis of the samples was performed by means of X-ray fluorescence (XRF) spectroscopy. The samples were analyzed using an EDAX Eagle III energy-dispersive micro-XRF (µXRF) spectrometer equipped with a Rh x-ray tube and a polycapillary exiting a circular area of nominally 30 µm diameter. Data collection occurred at each point for 45 s detector live time, with x-ray tube settings adjusted for 30 % dead time. Under this experimental condition, about 1 x 10^6 counts were collected per scan. A matrix of at least 25 spots was analyzed for each sample.

ζ-potential

The ζ-potential was evaluated by means of electrophoretic light scattering (ELS) (Zetasizer Nano-ZS, Malvern Instruments, Worcestershire, U.K.). In this technique, the velocity of particles in an oscillating electric field, which is proportional to their ζ-potential, was measured by light scattering. The quartz specimens (6 mg/10 mL) were suspended in ultrapure water and the ζ-potential was measured after adjusting the pH to 5.0 (a value close to that of lysosomal fluids) with 0.1 M HCl or 0.1 M NaOH.

Diffuse Reflectance UV-Vis Spectroscopy

UV-Vis diffuse reflectance (DR UV-Vis) was employed to identify both oxidative and coordinative state and the surface dispersion of iron ions. DR UV-Vis measurements were performed on fine powders of the samples put into a cell with optical quartz walls. The spectra were collected in the reflectance mode with a Perkin-Elmer Lambda 19 instrument equipped with an integrating sphere (using $BaSO_4$ as reference) and then converted by using the Kubelka-Munk function to obtain an absorbance-like pattern.

X-Ray diffraction (XRD)

The presence of iron oxides nanoparticles in the impregnated quartz samples has been evaluated by means of X-ray diffraction (XRD). Patterns have been collected with a PW3050/60 X'Pert PRO MPD diffractometer from PANalytical working in Debye-Scherrer geometry, using as source the high power ceramic tube PW3373/10 LFF with a Cu anode equipped with Ni-filter to attenuate K_β and focused by X-ray mirror PW3152/63. Scattered photons have been collected by a RTMS (Real Time Multiple Strip) X'celerator detector. Powdered samples have been hosted inside a 1.0 mm boron-silicate capillary and mounted on a rotating goniometer head. The patterns obtained were compared to those reported in the J.C.PDS (Joint Committee of Powder Diffraction Standard) archives.

IR spectroscopy

IR spectroscopy was employed to investigate the coordinative state of iron ions at the surface of quartz dusts using nitric oxide (NO) as a probe molecule. The samples were pressed in self supporting pellets and placed in a quartz cell for measurements in the transmission mode, equipped with KBr windows. The cell was permanently attached to a high vacuum line (residual pressure: 1×10^{-6} Torr; 1 Torr = 133.33 Pa) allowing outgassing at increasing temperature and adsorption-desorption experiments to be carried out *in situ*. The adsorption of NO was carried out after outgassing the samples at 400 °C for 45 min in

order to remove water and/or hydroxyls coordinated to surface iron ions. To eliminate any organic contaminants at the surface of silica, the samples were exposed to 10 Torr of O_2 for 30 min at 400 °C before outgassing under high vacuum [Parmaliana et al 2002]. NO was dosed at room temperature. Serial IR spectra have followed the evolution of the spectrum up to the attainment of equilibrium (30 min). The progressive evolution of the system upon reducing the NO pressure was then followed by recording the spectra down to full evacuation of the gas phase. The IR spectrum collected before admitting NO was used as background. The spectra were recorded with a Bruker IFS28 instrument equipped with a MCT detector, using a 4 cm^{-1} and a number of co-added scans of 250 in order to reach an acceptable signal-to-noise ratio.

Determination of "potentially" bioavailable iron

To determine the amount of Fe(II) which could be extracted from the surface by endogenous chelators, quartz samples were incubated in an aqueous solution of ferrozine (a strong chelator specific for Fe(II)) [Stookey 1970]. The total amount of removable iron was determined upon incubation in an aqueous solution of ferrozine in the presence of ascorbic acid, which fully reduces Fe(III) ions to Fe(II). The difference between the two values obtained measures the amount of Fe(III) in the pristine material.

200 mg of dust were incubated in 8 mL of a 3 mM solution of ferrozine in the absence or in the presence of 3 mM ascorbic acid for 9 days. The amount of iron extracted was determined on the supernatant spectrophotometrically (Uvkon 930) by measuring the absorption of the iron-ferrozine complex at 562 nm, following a technique previously described [Lund & Aust 1990].

Generation of free radicals (EPR / Spin Trapping)

The spin trapping technique adopted allows qualitative and quantitative evaluation of free radical generation [Fubini et al 1995, 2001]. The release of radical species was monitored in an aqueous suspension of the particles by means of Electron Paramagnetic Resonance spectroscopy (Miniscope 100 EPR spectrometer, Magnettech) using the spin trapping technique. DMPO (5-5'-dimethyl-1-pirroline-N-oxide) was employed as trapping agent, with a procedure largely described in previous papers [Fubini & Mollo 1995; Fenoglio et al 2000]. All the experiments have been repeated at least twice. The radical yield was progressively measured on an aliquot of 50 µL of the suspension up to one hour.

Hydroxyl radicals (Fenton activity)

150 mg of each powder was suspended in a buffered solution (0.2 M potassium phosphate buffer, pH 7.4) and 0.15 M of DMPO. The reaction was triggered by adding hydrogen peroxide (H_2O_2) as target molecule (0.2 M) to the particle suspension.

$COO^{-\cdot}$ radicals (cleavage of a C-H bond)

150 mg of each dust was suspended in a buffered solution (0.2 M potassium phosphate buffer, pH 7.4) and 0.15 M of DMPO. The reaction was started by adding sodium formate as target molecule to the particle suspension (1.0 M solution in 0.2 M potassium phosphate buffer, pH 7.4). The experiments were also repeated in the presence of 3 mM of ascorbic acid as reducing agent. Instrument setting were: receiver gain 9 x 10^2, microwave power 10 mW, modulation amplitude 1 G, scan time 80 s, 3 scans.

Cell culture, particle preparation and cell treatment

NR8383 rat AMΦ (ATCC, Manassas, USA) were cultured in Kaighn's modified medium (F12-K Nutrient Mixture, Gibco, Eggenstein, Germany) containing 15 % fetal calf serum (FCS), 1 % penicillin/streptomycin and 1 % glutamine (all purchased from Sigma-Aldrich, Taufkirchen, Germany) at 37 °C and 5 % CO_2. Three days before each experiment, cells were seeded in a concentration of 1.25 x 10^5 cells/cm^2 in assay-specific culture dishes. If not otherwise mentioned incubations were done at 37 °C and 5 % CO_2. Prior to experiments particles (DQ12, Qz, QzFe/ll and QzFe/hl) were heat-sterilized at 150 °C for 16 h in order to destroy potential endotoxins. Immediately before the experiments, particle were freshly suspended either in complete cell culture medium (see above) or Hank's Balanced Salt Solution ($HBSS^{(+/+)}$ or $HBSS^{(-/-)}$) (phenol red free, with or without Mg^{2+} and Ca^{2+}; Invitrogen GmbH, Karlsruhe, Germany). Suspensions were sonicated in a water bath for 10 min (Sonorex TK 52, Schaltech, Mörfelden-Walldorf, Germany) and added to AMΦ in concentrations of 5, 10, 20, 40 or 80 µg/cm^2 for 1, 4 or 24 h as indicated.

Particle uptake by alveolar macrophages

Particle uptake was analyzed via flow cytometry (FACSCalibur Becton Dickinson, Heidelberg, Germany) measuring the sideward scatter (SSC) and forward scatter (FSC) of laser light deflected by AMΦ. The SSC is directly related to cell granularity and was used as marker of particle uptake [Palecanda & Kobzik 2000], whereas FSC correlates to the cell size thus being a cofactor. Therefore, NR8383 cells were seeded in 24-well microtiter plates. Cells were treated with particles in concentrations of 10, 20 or 40 µg/cm^2 for 1 h. NR8383 cells were

scraped on ice, centrifuged (200 x g, 10 min, 4 °C) and washed with 300 µL of ice cold $HBSS^{(-/-)}$ and centrifuged again. The pellet was resuspended in 200 µL ice cold $HBSS^{(-/-)}$. In sum 12,000 events were counted. For calculation an electronical gate was set containing AMΦ of all sizes and granularities expressed in a FSC-SSC-histogram. Cell debris and free particles were excluded by the same gate. Univariant histograms of SSC determined the median of cell granularity, indicating the particle uptake by AMΦ. Data were measured with CellQuest 3.3 and analyzed using CellQuest Pro (Becton Dickinson, Heidelberg, Germany).

Cytotoxicity assays

Cell viability was analyzed by WST-1 assay (Roche Diagnostics GmbH, Mannheim, Germany), and apoptosis was evaluated by the detection of hypodiploid DNA-content of AMΦ [Nicoletti et al 1991].

The WST-1 assay is based on the principle of the reduction of stable tetrazolium salt WST-1 to a soluble violet formazan product within mitochondria of viable cells. For this assay, NR8383 cells were seeded in octoplicate in 96-well microtiter plates. After 24 h of particle treatment at concentrations of 5, 10, 20, 40 or 80 µg/cm^2 10 µL WST-1 solution was added to 5 wells per treatment or control and incubated for further 2 h. The remaining three wells were used as controls for the absorption by the particles and therefore measured without WST-1 substrate application. Optical density was detected at 450 nm using the Multiskan ELISA reader (Thermo Fisher Scientific, Dreieich, Germany). For data calculation the mean of the obtained values of the wells without WST-1 was subtracted from the mean of the WST-1 substrate treated samples and expressed as percentage of untreated cells.

The late stage of apoptosis is indicated by DNA-fragmentation into oligonucleosomal units, also termed hypodiploidic cells, because of the reduced DNA-content. The cytotoxicity method according to Nicoletti determines the percentage of apoptotic nuclei after 7-amino-actinomycin D (7-AAD) staining via flow cytometry. For this, NR8383 cells were seeded in 24-well microtiter plates. Particles were applied in concentrations of 10, 20, 40 or 80 µg/cm^2 for 24 h. NR8383 cells were scraped on ice, centrifuged (200 x g, 10 min, 4 °C) and washed with 300 µL of ice cold $HBSS^{(-/-)}$ and centrifuged again. The pellet was resuspended in 200 µL ice cold 7-AAD (Sigma), which is a DNA-binding fluorescence-dye. During 15 min of incubation in hypotonic buffer (0.1 % tri-sodium citrate dihydrate, 0.1 % Triton X-100, 50 µg/mL 7-AAD) cell membrane but not the nucleus membrane is lyzed thus making the DNA accessible to 7-AAD. For measurement and calculation an electronical gate was set containing AMΦ of all sizes. Cell debris and free particles were excluded by a previously defined gate. In sum 10,000 events within this gate were counted. Univariant histograms of

the appropriate fluorescent channel 3 (FL-3) determined the percentage of 7-AAD stained nuclei, in detail the hypodiploidic DNA-content, in relation to the amount of diploidic DNA of non-apoptotic cells. Data were measured by CellQuest 3.3 and analyzed by CellQuest Pro (Becton Dickinson, Heidelberg, Germany).

Gene expression analysis by quantitative RT-PCR

NR8383 cells were seeded in 6-well plates, treated with particles as indicated for 4 h, scraped and centrifuged (200 x g, 5 min, 4 °C). The pellet was resuspended in 0.5 mL Trizol® Reagent (Invitrogen GmbH, Karlsruhe, Germany) and stored at -20 °C until further analysis. The RNeasy® mini kit (Qiagen, Hilden, Germany) coupled to DNAse treatment was used to purify total RNA from salts and residual DNA. Quantity and purity of RNA were evaluated using spectrophotometry at 230, 260, 280, and 320 nm. cDNA was synthesized using the iScript™ cDNA Synthesis kit (BioRad, CA, USA), starting from 0.5 µg of RNA. cDNA was diluted 15 x in water before use. PCR primers for rat HO-1, TNF-α and the housekeeping gene GAPDH were designed using Primer Express software (Applied Biosystems). Primer sequences for HO-1 were 5'-GGG AAG GCC TGG CTT TTTT-3' (forward) and 5'-CAC GAT AGA GCT GTT TGA ACT TGGT-3' (reverse), for TNF-α 5'-GCT GTC GCT ACA TCA CTG AAC CT-3' (forward) and 5'-TGA CCC GTA GGG CGA TTA CA-3' (reverse) and for GAPDH 5'-TGA TTC TAC CCA CGG CAA GTT-3' (forward) and 5'-TGA TGG GTT TCC CAT TGA TGA-3' (reverse). qRT-PCR was performed with a MyiQ Single Color real time PCR detection system (BioRad) using iQ™ SYBR® Green Supermix (Biorad), 5 µL diluted cDNA, and 2.5 µL of 0.3 µM forward and reverse primer in a total volume of 25 µL. PCR was conducted as follows: a denaturation step at 95 ºC for 3 min was followed by 40 cycles at 95 ºC (15 seconds) and 60 ºC (45 seconds). After PCR, a melt curve (60-95 ºC) was generated for product identification and purity. PCR efficiency of all four primer sets, as assessed by the use of cDNA dilution curves, was 90 - 100 %. Data were analyzed using the MyiQ Software system (BioRad) and were expressed as relative gene expression (fold increase) using the $2^{-\Delta\Delta Ct}$ method [Livak & Schmittgen 2001].

Release of the proinflammatory cytokine TNF-α

NR8383 cells were seeded in 24-well microtiter plates. After 24 h of particle treatment cell-free supernatants were collected, centrifuged (200 x g, 10 min, 4 °C) and aliquots were stored at -20 °C. The supernatants were analyzed using a commercial TNF-α ELISA kit (R&D Systems, Wiesbaden, Germany) according to the manufacturer's manual and using a Multiskan ELISA reader (Thermo Fisher Scientific, Dreieich, Germany).

Statistical analysis

All biological assays were performed in at least three independent experiments. Statistical analysis was performed using SPSS 18.0 for Windows. Data are presented mean or median as indicated in the figure legends ± SEM. Results were statistically evaluated by analysis of variance (ANOVA) with post hoc testing Dunnett or LSD as indicated. Differences compared to controls were considered significant at * $p \leq 0.05$, ** $p \leq 0.01$ and *** $p \leq 0.001$. Differences in responses to iron doped quartz samples compared to the native quartz sample were considered significant at # $p \leq 0.05$, ## $p \leq 0.01$ and ### $p \leq 0.001$.

3.3 RESULTS

The main physico-chemical features of the quartz samples examined in the present study are reported in Table 3.1. It is noteworthy that both pristine quartzes - the reference DQ12 and Qz employed here for iron deposition - do contain iron impurities up to about 0.1 %. This quantity, though apparently small, could cover a sizable fraction of the exposed surface if iron ions are mostly associated with the surface.

Upon loading, a significant amount of the iron present in the impregnating solution (first column) is retained at the surface. While the high loading solution had an iron concentration tenfold to that of the low loading one, the amount of iron retained at the surface of QzFe/hl, is only fourfold compared to the retained iron at the QzFe/ll surface (second column), suggesting a limit for iron deposition. Opposite to DQ12 with no aluminum traces on its surface, both pure Qz and the iron loaded samples contain about 1.5 % of aluminum. Again, if mostly located at the surface such amount of aluminum would cover an appreciable part of it. Note that the amount of aluminum present is substantially unchanged by impregnation, so suggesting that no aluminum displacement by iron ever occurred during the deposition procedure.

Table 3.1 Physico-chemical properties of quartz samples

Quartz	Fe loading	Elemental composition [% wt]			Potentially bioavailable iron[b]			ζ-potential [mV] pH = 5.0	Detectable crystalline phases[c]
		SiO_2	FeO	Al_2O_3	Total FeO [% wt]	Fe(II)[d] [% of total]	Fe(III)[d] [% of total]		
DQ12	-	99.9	0.09	-	0.01	61	39	- 42.2	α-quartz
Qz	-	98.2	0.12	1.65	0.01	48	52	- 65.1	α-quartz
QzFe/ll	0.67 %	97.7	0.49	1.76	0.06	10	90	- 64.8	α-quartz
QzFe/hl	6.7 %	96.8	1.69	1.47	0.23	6	94	- 47.5	α-quartz, hematite

[a] evaluated by means of XRF spectroscopy
[b] evaluated by means of DR UV-VIS spectroscopy
[c] evaluated by means of XRD spectroscopy

Surface charge

The ζ-potential measured at pH 5.0 of all samples are reported in Table 3.1. The two non-loaded quartzes, Qz and DQ12, exhibit a large difference in ζ-potential, Qz being at a value about 23 mV lower than Qz. This has to be ascribed to differences in the overall acidity of the surface arising from the presence of associated impurities.

Iron-loading did not significantly modify the value of the Qz ζ-potential at low loading, i.e.

when the total iron was below 0.5 % in weight as FeO [Table 3.1], but markedly reduced the ζ-potential value of about 18 mV at high loading. This confirms an intrinsic surface difference between the two loaded specimens as far as metal ions and acidity is concerned.

Dispersion of iron ions at the surface of the quartz particles

Qualitative evidence of the organization of iron ions at the surface of the two iron loaded quartzes is given by the different colors acquired after impregnation and calcination. QzFe/ll is pink because isolated Fe(III) are only present; QzFe/hl instead exhibits a brownish color, so suggesting the presence of iron oxide particles. Accordingly, DR UV-Vis spectra exhibit differences in both amount and degree of dispersion of iron ions at the surface [Figure 3.1].

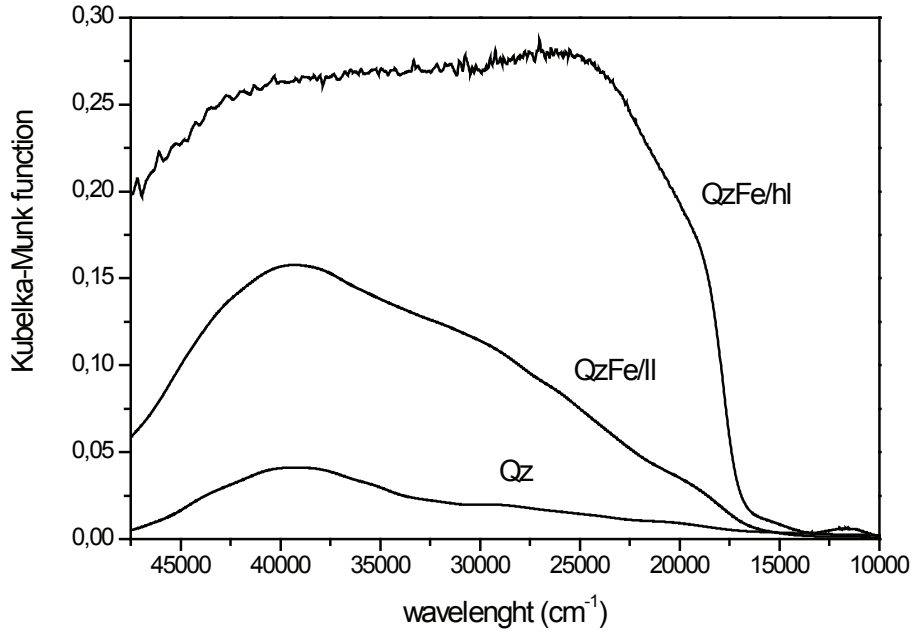

Figure 3.1 Dispersion of iron ions in the quartz samples.
Diffuse Reflectance UV-Vis spectra of the samples recorded in air: untreated quartz (Qz), quartz impregnated with 0.67 % wt Fe(III) (QzFe/ll), and quartz impregnated with 6.7 % wt Fe(III) (QzFe/hl). The intensity of the spectrum QzFe/hl was reduced ten times.

The spectrum of the original quartz dust (Qz) also reveals the presence of iron. It shows two components: a main band at ca. 40000 cm^{-1} due to $O^{2-} \rightarrow Fe^{3+}$ charge transitions involving isolated Fe(III) ions in a (distorted) octahedral symmetry; and a lower frequency broad tail (from 30000 to 15000 cm^{-1}), due to few FeO_x aggregates, ranging from dimeric/oligomeric species to three dimensional nanoparticles [Arena et al 2005]. As the spectrum was recorded in air, the ligand sphere of iron ions comprises both surface oxygen atoms of the quartz and adsorbed water molecules, which saturate the coordinative positions not involved in the interaction with the support. QzFe/ll exhibited a pattern, similar in shape but significantly more intense, with a marked prevalence of supported isolated iron ions with respect to iron

oxide aggregates. Conversely, the spectral profile of QzFe/hl is characterized by a step-like absorption (at about 15000 cm^{-1}), monitoring the overwhelming presence of iron oxide particles.

The presence of iron-oxide nanoparticles in QzFe/hl is confirmed by XRD analysis [Table 3.1]. All samples exhibited the typical XRD spectrum of the α-quartz crystalline polymorph. Only the diffractogram of QzFe/hl shows two new peaks at about 2θ = 35° - 40°, typical of hematite (Fe_2O_3).

Degree of coordination of iron ions at the surface of quartz

Because of its strong affinity toward Fe(II) ions and of the high intensity of the ν_{NO} bands [Franz & Lippard 1999; Spoto et al 2000], the NO probe resulted particularly informative in previous studies on asbestos [Martra et al 1999; Turci et al 2005, 2007]. IR spectra of adsorbed NO reveals the degree of coordination of iron ions at the surface by filling the vacancies resulting from the desorption of water molecules and the condensation of silanols into siloxanes. Note that outgassing of the samples also involves a reduction of supported iron ions from Fe(III) to Fe(II) [Pirngruber et al 2007] without modifications in either location or degree of coordination of the iron ions. By dosing NO on such centers nitrosylic adducts are formed, the IR pattern of which are dependent upon the Fe(II) $(NO)_x$ stoichiometry, where x is the number of coordinative positions not involved in the interaction with the support (the total coordination number of iron being always 6).

Previous studies revealed that a typical spectral pattern of NO adsorbed on an iron containing material is the result of the superposition of five different absorption bands [Turci et al 2007].

- Two bands, one between 1804 - 1808 coupled with a second one at 1900 cm^{-1}, correspond to a trinitrosylic species [$Fe–(NO)_3$]
- Two bands, one between 1730 - 1770 and a second weak component at about 1840 cm^{-1}, correspond to a dinitrosylic species [$Fe–(NO)_2$]
- One band between 1810 - 1818 cm^{-1} corresponds to a mononitrosylic species [Fe–(NO)]

The original quartz (Qz) did not show any detectable adsorption of NO, likely because of the very low amount of iron present at the surface [spectra not reported].

The IR spectra of both impregnated samples are reported in Figure 3.2. At maximum NO coverage, the spectrum of QzFe/ll (dotted line) is dominated by a main band at 1817 cm^{-1},

resulting from the superposition of a component due of mononitrosylic species (adducts formed by one NO molecule adsorbed on a Fe(II) center with 5 bonds to the support) and a low frequency band of trinitrosylic species (adducts formed by three NO molecule adsorbed on a Fe(II) center with 3 bonds to the support), coupled with the minor component at ca. 1900 cm^{-1}. By decreasing NO pressure, trinitrosylic species were converted into dinitrosylic species responsible for enhancing the band at 1755 - 1765 (change in position monitoring heterogeneity among the adsorption sites), coupled with an unresolved component at ca. 1840 cm^{-1}. The presence of centers coordinating up to three NO molecules clearly indicates the presence of iron ions poorly coordinated to the support, i.e. with linked only to three surface oxygen atoms. These are the most reactive centers from which iron is more easily removable.

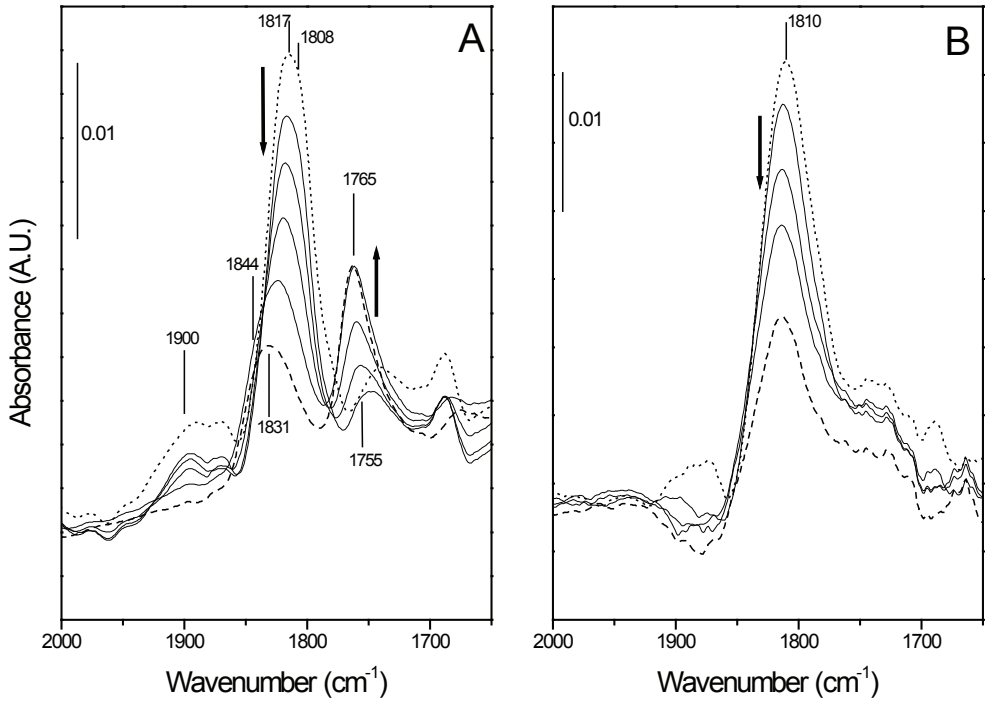

Figure 3.2 Coordinative state of iron ions at the surface of quartz samples.
Evolution of IR spectra of NO adsorbed at room temperature by decreasing P_{NO} on samples (A) QzFe/ll (low Fe loading) and (B) QzFe/hl (high Fe loading), previously degassed at 400 °C for 45 min. NO pressure: from 50 Torr (dotted-line spectrum) to 10^{-3} Torr (dashed-line spectrum).

Conversely, the shape of the spectral pattern of QzFe/hl and its evolution by decreasing NO pressure in equilibrium with the sample indicates that only mononitrosyls were formed. Thus on QzFe/hl mostly highly coordinated iron sites are exposed at the surface.

Mobilization of iron

Chelation experiments were carried out to determine the amount of poorly coordinated Fe(II) and Fe(III) ions exposed at the surface of the quartz samples, which may be extracted by chelators and are available for reaction. Ferrozine, a bidentate N donor chelator (pH 4.0) specific for Fe(II), was used in the presence or absence of ascorbic acid, following a method set up by Hardy and Aust [1995] and successfully applied by some of us to a large variety of particulates, including asbestos, diatomaceous earth [to be published] and volcanic ashes [Horwell et al 2003, 2007]. Since ascorbic acid reduces Fe(III) to Fe(II), the amount of iron measured in the presence and absence of ascorbic acid corresponds to the total iron mobilized [Figure 3.3; Table 3.1]. The amount of Fe(III) is calculated by subtracting the total iron from the amount of Fe(II). As expected, the impregnated samples exhibited higher amounts of removable iron (mainly Fe(III)) which increased with the loading. Upon calcination iron is usually oxidized to Fe(III) [El Malki et al 2000; Berlier et al 2002]. Surprisingly the amount of Fe(II) slightly increases with loading, suggesting the presence of a complex redox equilibrium at the surface. This is not unusual since Fe(II) ions, someway stabilized at the surface, have been found in aged quartz samples [Clouter et al 2001; Fenoglio et al 2001] and also in freshly erupted volcanic ashes which experienced very high temperature [Horwell et al 2003, 2007].

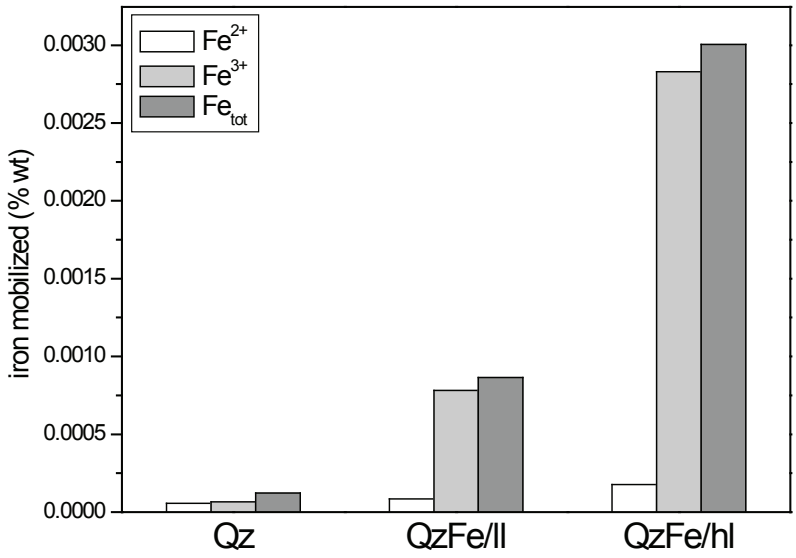

Figure 3.3 Iron mobilization.
Amount of iron ions mobilized surface of quartz dusts by using ferrozine (Fe(II), white column) and the ferrozine-ascorbic acid system (total iron, dark grey column). The amount of Fe(III) (pale grey column) has been obtained from the difference between the amount of total iron and the Fe(II) fraction.

Generation of oxygen and carbon centered free radicals (EPR / Spin Trapping)

All samples were tested by means of the spin trapping technique both for their potential to generate HO· following the reaction with H_2O_2 (Fenton activity) and for their ability to cleave a C-H bond by using sodium formate as a model for organic molecules/biomolecules. The free radical yield recorded during these two tests may be evaluated from the intensity of the EPR spectra, representing DMPO adducts [Figure 3.4]. All samples show a remarkable Fenton activity. Iron impregnation appears to slightly enhance HO· generation with order of activity being QzFe/hl > QzFe/ll > Qz [Figure 3.4 A]. Conversely, impregnation fully inhibits the ability of quartz to cleave C-H bonds. While the pristine Qz sample is definitely active, QzFe/hl and QzFe/ll are fully inactive in this reaction [Figure 3.4 B]. Note, that when the reaction was carried out in presence of ascorbic acid as reducing agent, both impregnated samples exhibited an activity close to that of pristine Qz [data not shown for brevity]. Finally, DQ12 reference quartz exhibits a HO· yield close to Qz but, not carboxyl free radicals, as previously reported [Ghiazza et al 2010].

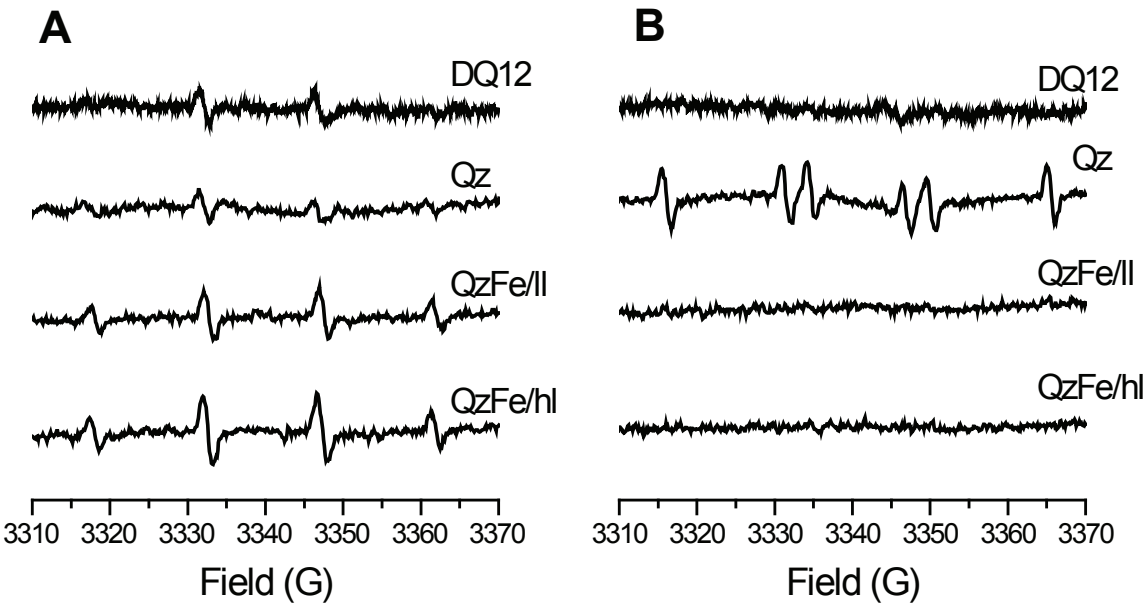

Figure 3.4 Free radical generation from aqueous suspension of samples.
(A) HO· generated by quartz particles from a solution of H_2O_2 (Fenton activity) and (B) COO^-· generated following the cleavage of the C-H bond in sodium formate. Spectra have been collected after 60 min of incubation. Instrument setting: receiver gain 9 x 10^2, microwave power 10 mW modulation amplitude 1G, scan time 80 s, 3 scans.

Particle uptake by alveolar macrophages

In order to investigate whether differences in the iron-loading have an effect on the internalization of particles by AMΦ, uptake was measured by means of flow cytometry. For all four tested particles a concentration-dependent uptake could be observed. Particle size measured by FSC and granularity measured by SSC in the absence of cells showed similar values for the different samples [data not shown]. As such, the uptake pattern of DQ12, native and iron-loaded Qz samples by AMΦ could be directly compared. The results indicated no differences in uptake, although there might be a slight trend for a reduced uptake of both iron-loaded samples at higher concentrations [Figure 3.5].

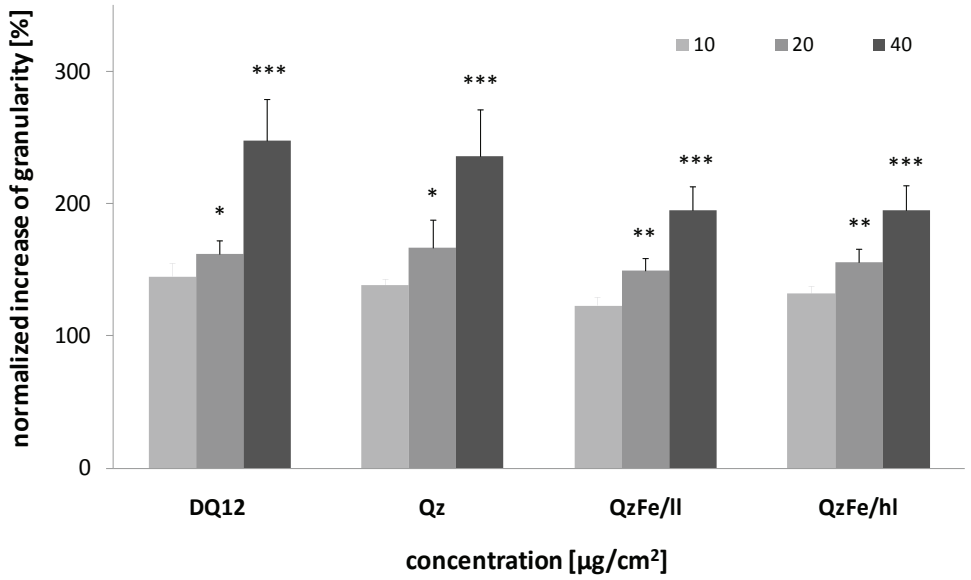

Figure 3.5 Particle uptake by NR838 cells is concentration-dependent.
FACS analysis shows an increase in particle uptake by AMΦ measured by sideward scatter (SSC) of laser light indicating cellular granularity. AMΦ were treated with DQ12, Qz, QzFe/ll and QzFe/hl particles in concentrations of 10, 20 or 40 µg/cm^2 for 1 h. Figure represents medians ± SEM normalized to control cells of four independent experiments, with * $p \leq 0.05$, ** $p \leq 0.01$ and *** $p \leq 0.001$ vs. control (ANOVA with Dunnett post-hoc comparison).

Cytotoxicity

The effect of the iron on the quartz induced cytotoxicity was evaluated by investigation of mitochondrial dehydrogenase activity as an indirect indicator for cell viability [Figure 3.6]. The positive control DQ12 was found by far to be the most toxic sample towards AMΦ. The cytotoxic effects of Qz samples were found to be rather independent of iron-loading. However, at the highest tested concentration of 80 µg/cm^2 both samples QzFe/ll and QzFe/hl were significantly less toxic than the Qz sample. As a second assay to determine cytotoxic particle effects, hypodiploidy of the DNA-content was investigated, being a specific marker of apoptosis. Untreated Qz showed a significant dose-dependent increase in apoptosis of AMΦ.

In contrast, the two iron loaded samples did not reveal any notable induction of apoptosis. However, the DQ12 caused a markedly stronger apoptotic response than Qz [Figure 3.6 B]. Remarkably, at the highest tested concentration (80 µg/cm^2) the effect of DQ12 was found to be similar to the effect of staurosporine (0.1 µM), which is a known positive control for apoptosis induction [data not shown].

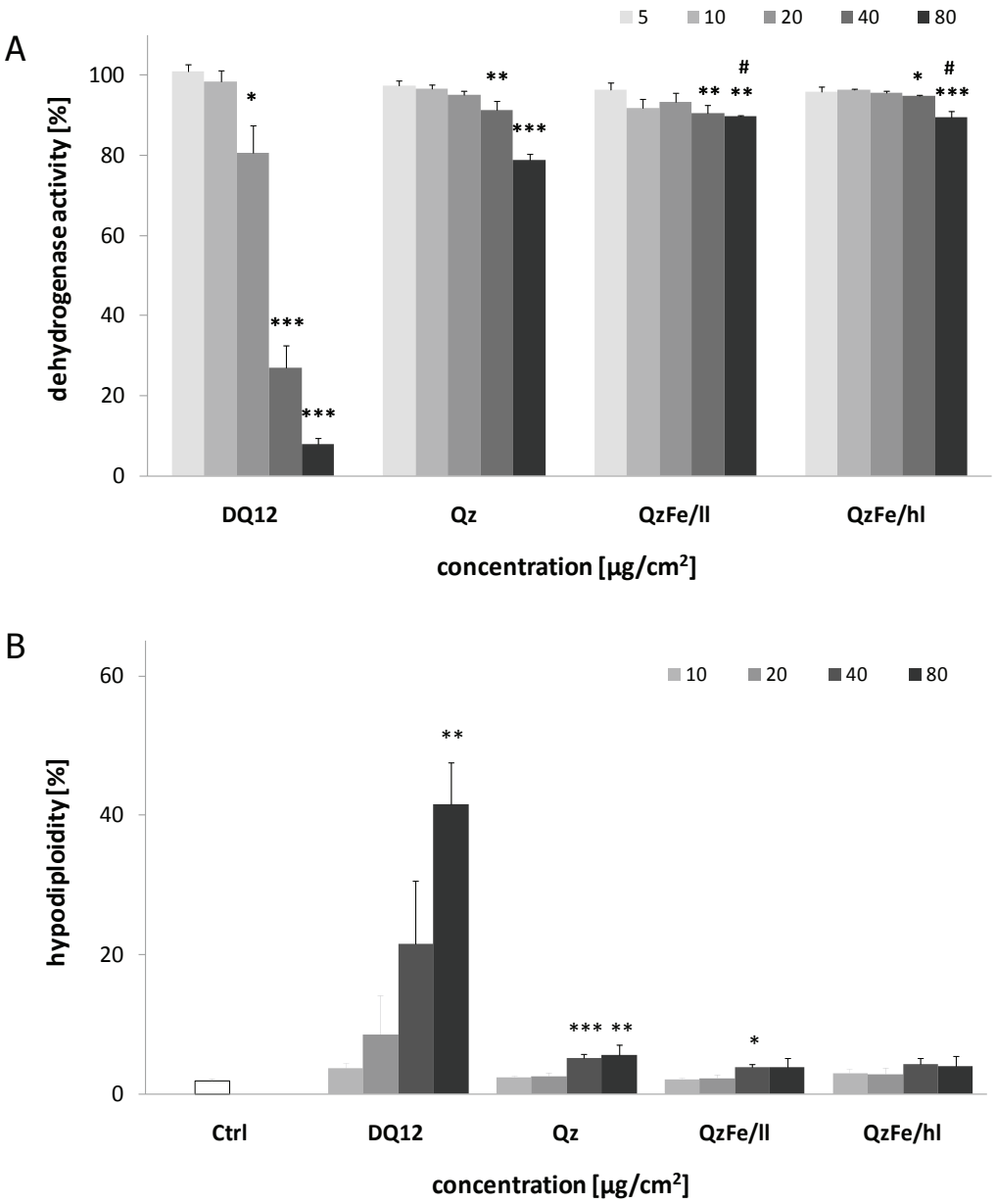

Figure 3.6 Particle-dependent effects on cell viability in NR8383 cells.
(A) AMΦ were treated with DQ12, Qz, QzFe/ll and QzFe/hl particles in concentrations of 5, 10, 20, 40 or 80 µg/cm^2 for 24 h. Mitochondrial activity of particle treated AMΦ reveals only toxicity for DQ12 particles at concentrations of and above 20 µg/cm^2, whereas the other quartz particles showed significant toxicity at 40 and 80 µg/cm^2. Figure represents mean ± SEM of three independent experiments, with * $p \leq 0.05$, ** $p \leq 0.01$ and *** $p \leq 0.001$ vs. control (ANOVA with Dunnett post-hoc comparison). Statistical significance of iron-doped quartz vs. appropriate quartz control with # $p \leq 0.001$ (ANOVA with LSD post-hoc comparison).
(B) AMΦ were treated with DQ12, Qz, QzFe/ll and QzFe/hl particles in concentrations of 10, 20, 40 or 80 µg/cm^2 for 24 h. Apoptotic cells with degraded DNA are detected by their hypodiploid DNA-content. Data represent mean ± SEM of four independent experiments

Induction of oxidative stress

The influence of the iron-loading on quartz-induced oxidative stress in AMΦ was evaluated via mRNA expression analysis of the well-known oxidative stress response gene HO-1 [van Berlo et al 2010]. DQ12 was found to cause an induction of HO-1 gene in a concentration-dependent manner. In contrast, none of the three other samples revealed any notable induction of HO-1 mRNA [Figure 3.7].

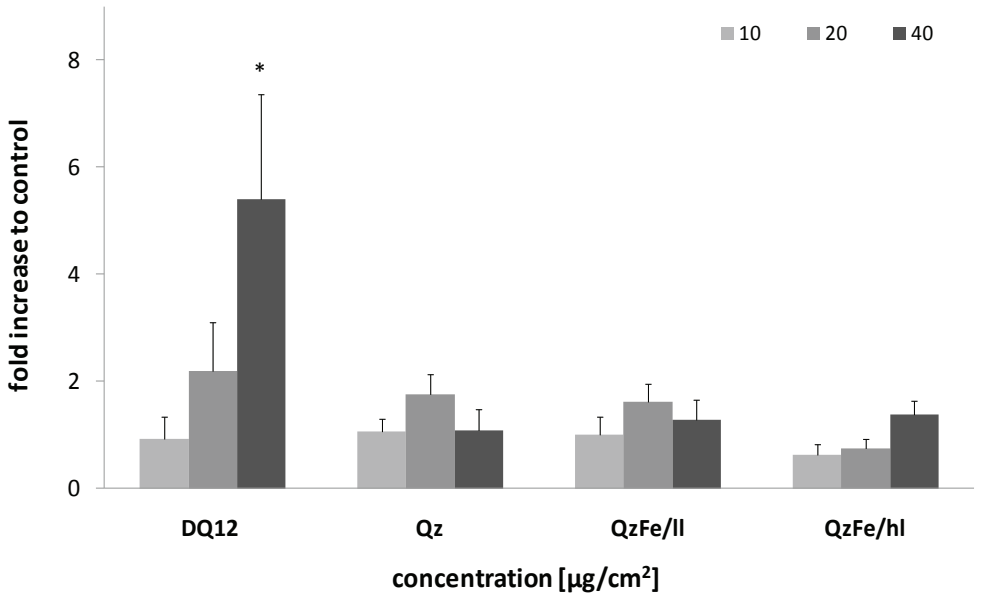

Figure 3.7 Quartz particles have different impact on regulation of oxidative molecules.
NR8383 cells were treated with 10, 20 or 40 µg/cm^2 of indicated particles for 4 h. As indicator for the oxidative stress response HO-1 was investigated. Figure represents means ± SEM of three independent experiments, with * $p \leq 0.05$ vs. medium control (ANOVA with LSD post-hoc comparison).

Induction of the proinflammatory cytokine TNF-α

The inflammogenic effect of the quartz samples was evaluated by investigating the particle-induced increase of the pro-inflammatory cytokine TNF-α, both on the mRNA and the protein level in the AMΦ [Figure 3.8]. None of the three Qz samples caused an increase in mRNA expression. For the DQ12 sample a trend was found, although this did not reach a statistical significance [Figure 3.8 A]. However, a dose response was found on the protein level after treatment of the AMΦ with DQ12 as well as with pristine Qz. In line with the HO-1 expression findings, the strongest effect could be observed with DQ12 [Figure 3.8 B]. Remarkably, the iron impregnated Qz appeared to lead to a significant abrogation of TNF-α release from AMΦ, when compared to the original Qz sample at the treatment concentration of 40 µg/cm^2. A similar, albeit non-significant trend was also observed at the 80 µg/cm^2 concentration, supporting the inflammation inhibiting action of surface-bound iron.

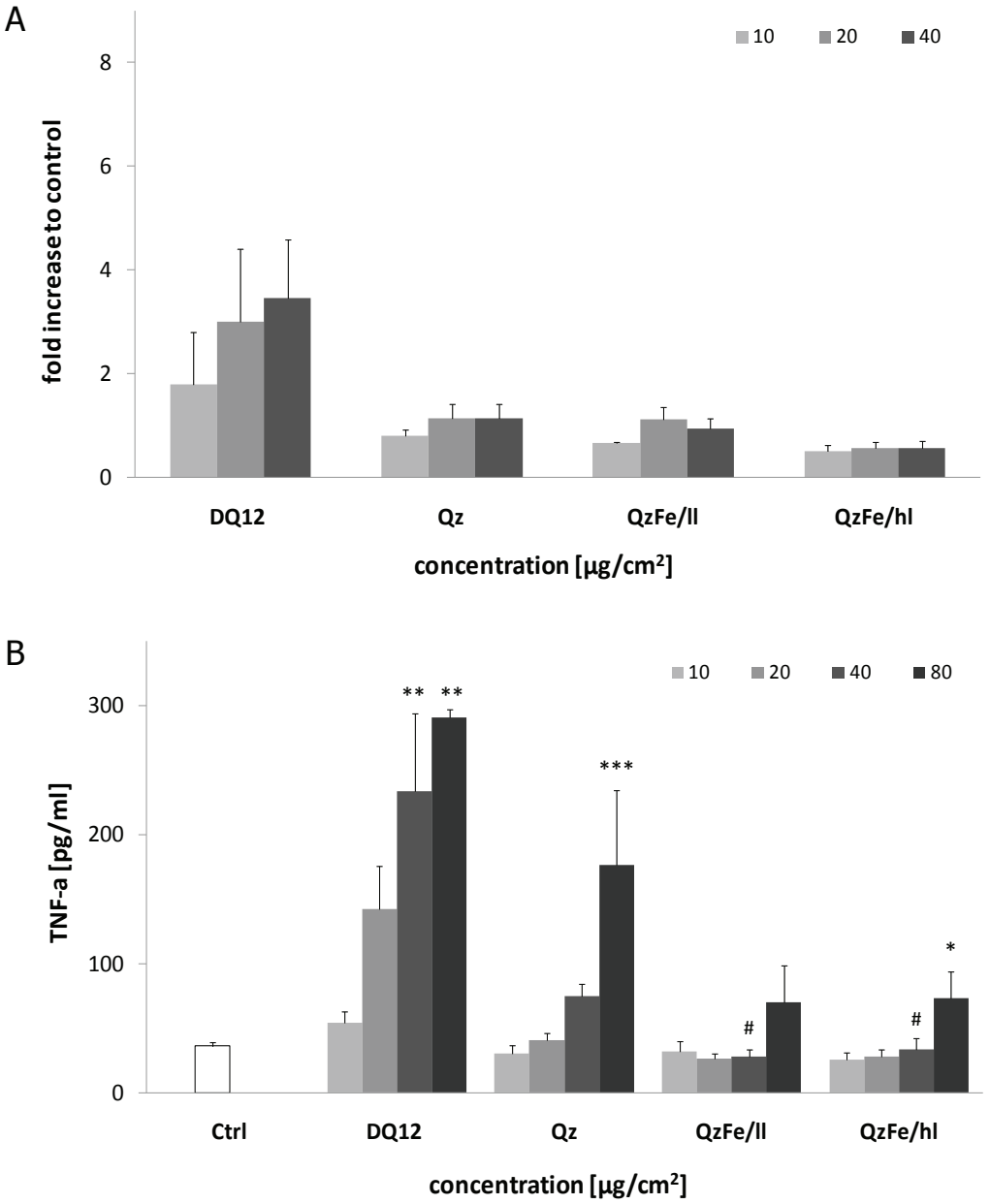

Figure 3.8 Particle-dependent impact on mRNA and protein level of TNF-α.
(A) NR8383 cells were treated with DQ12, Qz, QzFe/ll and QzFe/hl particles in concentrations of 10, 20 or 40 µg/cm^2 for 4 h. Just DQ12 was able to enhance TNF-α mRNA expression. (B) AMΦ were treated with concentrations of 10, 20, 40 or 80 µg/cm^2 of indicated particles for 24 h. DQ12 and Qz particles trigger the release of TNF-α protein by NR8383 cells in a concentration-dependent manner. QzFe/ll and QzFe/hl particles cause the release of TNF-α from that AMΦ only at the highest concentration. Figure represents means ± SEM of four independent experiments, with * $p \leq 0.05$, ** $p \leq 0.01$ and *** $p \leq 0.001$ vs. medium control (ANOVA with Dunnett post-hoc comparison). Statistical significance of iron-doped quartz samples vs. appropriate quartz control # $p \leq 0.01$ (ANOVA with LSD post-hoc comparison).

3.4 DISCUSSION

Results obtained in this study largely confirm the variability in the biological activities of different sources of quartz particles, as well as the involvement of several physico-chemical features in the cellular responses elicited upon contact with quartz.

The pristine Qz employed in this study turned out to differ from the reference quartz DQ12, being in some tests inactive or much less active than DQ12. Note that this commercial sample was chosen on the basis of a study in which Qz turned out to be fibrogenic in a rat model [Corsini et al 2003]. This notwithstanding, its activity appears to be far lower than that of DQ12. It is noteworthy that loading with iron induced modifications in some but not all quartz-induced cellular responses.

The comparison between the two original quartz specimens and the effect of iron-loading on the cellular responses elicited, in the light of their differences in physico-chemical properties, will be discussed separately.

Surface characteristics of the various quartz particles examined

DQ12 contains approximately the same level of iron as Qz, but opposite to it - and to many other commercial quartz dusts - there is no aluminum on the DQ12 surface. This is well-reflected in the ζ-potential value at pH 5.0, much lower than the value of Qz and very close to what is measured, under the same conditions, on a very pure quartz or vitreous silica dust [unpublished results]. DQ12 exhibits a Fenton-like activity but no detectable release of carbon centered radicals arising from a homolytic rupture of a C-H bond. This is consistent with the relative high purity of this specimen. Previous studies by some of us have shown that only Fe(II) containing quartz, with iron in a well-defined surface site, exhibits such reactivity [Fenoglio et al 2001; Ghiazza et al 2010]. Removable iron is about one tenth of the total iron content, probably the few "bioavailable" Fe(II) ions detected are located in a position non apt to react.

The Qz sample contains, beside iron (at a level close to DQ12), more than a tenfold amount of aluminum. This may be either located at the surface of quartz or contained in small alumina aggregates. We discard the presence of alumina aggregates for two reasons. No crystalline phases other than quartz were detected by XRD and the very low ζ-potential suggests surface aluminum substituting for silicon. As known from the chemistry of aluminosilicates in these conditions aluminum increases the acidity of silanols, consequently lowering the ζ-potential value. Qz is active in both Fenton activity and release of carboxylate radicals from the formate ion. In this case, the few Fe(II) present at the surface would be in a reactive position.

Upon iron-loading two different surface situations were attained. With QzFe/ll, iron-loading mainly increased the number of dispersed Fe(III) ions, with no variations in the ζ-potential value. Instead, iron deposition on QzFe/hl, leads to the formation of oxidic dimers/oligomers or small size aggregates of Fe_2O_3 (hematite), visible in the XRD pattern, which could virtually cover a large part of the surface of quartz. The intense absorption observed in the DR UV-Vis spectra of QzFe/hl confirms that Fe_2O_3 particles, even of large size, are present, iron being in excess by respect to the available quartz surface. In this case, the ζ-potential moves to higher values. This may be ascribed to the effect of hematite hindering a large part of the quartz surface. Hematite has a much higher ζ-potential than silica, being less acidic, its value on pure hematite nanoparticles falling is positive at pH 5.0 [Fubini et al 2010] and to a lower abundance of free silanols. This suggests a high degree of coverage of the silica surface.

The identification of poorly coordinated iron ions at the surface by means of NO adsorption is in agreement with the picture given by the DR UV-Vis spectroscopy. QzFe/ll exhibits iron ions with low coordination to the quartz surface, corresponding to isolated iron ions, while QzFe/hl exhibits a much higher coordination of iron ions, corresponding to Fe(III) ions bound to the quartz surface or organized in hematite nanoparticles.

Fenton activity was slightly enhanced upon increasing iron content, which is expected as both iron and silica framework contribute to such reaction [Fubini 1998a; Fubini et al 2001]. Even if mainly present in the Fe(III) oxidative state deposited iron may be reduced to Fe(II) by H_2O_2 which, in turn, may generate HO· via the Fenton reaction as follows:

$$Fe^{3+} + H_2O_2 \rightarrow Fe^{2+} + HO_2^{\cdot} + H^+$$
$$Fe^{2+} + H_2O_2 \rightarrow Fe^{3+} + HO^{\cdot} + HO^-$$

Surprisingly the cleavage of the C-H bond was fully suppressed on both iron-loaded samples in spite of a substantial Fe(II) content, close to that of the pristine Qz. Probably, the radical activity of Fe(II) at the silica framework is suppressed by the presence of increasing amounts of Fe(III), which may hinder the ions inhibiting a direct reaction with the target molecule. In the presence of the reducing agent ascorbic acid, however, some activity was detected [data not shown]. This suggests, that some of the surface-bound iron ions may undergo redox cycling and generate free radicals when in contact with cellular fluids or *in vivo*.

In conclusion we may state that on quartz different chemically not equivalent iron species may coexist, generating a substantial heterogeneity at the surface exposed.

Uptake by alveolar macrophages

In view of the importance of AMΦ activation and particle clearance in particle-exposed lung tissue, the uptake of quartz particles by AMΦ was investigated [Oberdörster 1996; Albrecht et al 2007; Haberzettl et al 2008]. The analysis reveals that iron-loading does not significantly influence the level of uptake of particles by NR8383 cells, as this process occurs nearly equally with all tested samples. Even for DQ12 similar levels of uptake were found, thus its higher activity observed in the other tests can not be ascribed to a more pronounced particle uptake. In the light of the marked differences in iron distribution surface charge and presence of aluminum, we may state that AMΦ uptake is not dependent upon surface composition. It has to be pointed out, that this only applies to phagocyting cells. It might well be that endocytosis/pinocytosis in other cell types could be affected by theses modifications in surface charge and composition.

Cytotoxicity

The Qz sample and the reference DQ12 reduced cell viability and induced apoptosis, whereat DQ12 was much more potent than Qz in both, confirming the exceptionally high activity of this quartz specimen. Iron-loading of Qz, being not critical for particle uptake, was found to be associated with a diminished cytotoxicity of Qz. This beneficial effect was revealed by both measurement of mitochondrial dehydrogenase activity and evaluation of the induction of hypodiploid DNA-content. Interestingly, the latter method suggests that iron may decrease quartz-induced apoptosis in AMΦ, a process which has been linked to the development of fibrosis in experimental models [Iyer et al 1996; Ortiz et al 1998; Borges et al 2001]. To verify the precise role of iron in modulating quartz-induced apoptosis further investigations are needed on the involvement of the known alternative pathways of apoptosis.

Free radical release, oxidative stress and inflammatory response

Since formation of radicals and induction of oxidative stress are considered to be important features in toxic and inflammatory effects of inhaled particles including quartz [Fubini & Hubbard 2003; van Berlo et al 2010], current investigations also focused on this aspect. We recall here that oxidative stress may arise by sustained generation of free radicals at the particle surface and/or by release of reactive oxygen species by phagocyting cells.

The potency to induce an oxidative stress measured as changes in the oxidative stress marker HO-1 and by expression of the inflammatory cytokine TNF-α did not parallel particle generation of free radicals via Fenton like activity, which was somewhat similar with all samples. The mRNA expression of HO-1 indicated that only DQ12 particles induce oxidative

stress significantly. In contrast, none of the three other samples revealed any notable induction of HO-1 mRNA. As such, the potential effect of iron modification on the induction of oxidative stress in AMΦ could not be confirmed by this measurement. The ability of DQ12 to induce HO-1 is in line with former studies found in rat lung tissue after intratracheal instillation as well as in a rat lung epithelial cell line upon *in vitro* treatment [Li et al 2008; van Berlo et al 2010]. In the rat lung epithelial cells the enhanced HO-1 mRNA expression by DQ12 was observed at treatment concentrations that induce oxidative DNA-damages and cell membrane damage as well [Li et al 2008]. In line with this, DQ12 was also found to express the most cytotoxic capacity in the present study. The marked induction of TNF-α on protein level in NR8383 cells by DQ12 is also in line with previous *in vitro* findings [Albrecht et al 2007] as well as *in vivo* studies demonstrating its strong pulmonary toxicity [Huaux et al 1995; Albrecht et al 2004].

Regarding the iron-loading, our most interesting observations were found in TNF-α mRNA and protein expression analyses. The role of this inflammatory cytokine in the development of lung fibrosis by quartz particles has been well-established [Piguet et al 1990; Piguet & Vesin 1994; Ortiz et al 1999]. Between the iron-loaded and the pristine Qz no significant effects in dependence of iron-loading were found on the mRNA expression level. In contrast, we found Qz to be potent in triggering TNF-α production while both iron impregnated samples were less active in AMΦ, suggesting that the presence of more surface iron has an inhibitory effect on this inflammatory response. Interestingly, the responsiveness of both iron loaded samples appeared to be similar. This suggests that even surface bound dispersed iron may diminish the inflammogenic potency of quartz particles, which in turn may impact on fibrogenic responses. In this case the free radical release following rupture of the C-H bond in the formate ion parallels the inflammogenic response elicited. In fact iron deposition on Qz abolished the free radical generating potential, which requires to be restored the presence of ascorbic acid as a reductant. As both loaded samples behave in the same way we may hypothesize that the presence of iron aggregated into small oxidic particles at the surface does not interfere with this beneficial effect. Note that differences in levels of TNF-α production between different quartz samples have also been reported in primary guinea pig MΦ [Bruch et al 2004], but the chemical basis of such differences have not yet been found out.

Possible physico-chemical explanations of the high activity of DQ12 quartz

In the present study DQ12 quartz showed higher cytotoxicity, apoptosis, HO-1 mRNA expression and potency in triggering TNF-α production from AMΦ than Qz. Conversely $HO^{\cdot}$ radicals formation was rather similar for both quartz samples. This does not mean that Fenton activity does not contribute to quartz related toxicity. We are aware that many physico-chemical factors contribute altogether to build up the toxic potency of a given quartz source. Fenton activity will simply contribute equally on all specimens. The point is that the exceptional characteristics of DQ12 have to be associated to physico-chemical features other than free radical release.

Several explanations may be given for the stronger effects elicited by DQ12 when compared to Qz. The absence of aluminum on DQ12 surface, opposite to Qz (and the iron loaded ones derived from it) is likely one of the most obvious explanation of its potency. Elemental analysis revealed aluminum in a range of 1.5 - 1.8 % wt on the surface of the commercially purchased Qz sample and both iron modified Qz samples, but not on DQ12. It has been demonstrated that already very low amounts of aluminum (e.g. 0.16 % wt in studies from our own laboratory) on the surface of DQ12, achieved by aluminum lactate coating procedure, leads to a significant reduction of biological responses in quartz exposed rat lungs [Brown et al 1989; Duffin et al 2001; Albrecht et al 2004, 2005] as well as *in vitro* in both AMΦ [Albrecht et al 2007] and lung epithelial cells [Schins et al 2002].

The presence of aluminum on/into a silica framework is known to increase the acidity of silanols (SiOH), which is reflected by the measure of the ζ-potential. Thus at a given pH-value the number of dissociated silanols will be higher on quartz particles where aluminum is present than on pure ones. This does not much interfere with free radical release but strongly modifies the potency of establishing strong H-bonding which requires a defined number of undissociated silanols. When in appropriate position, silanols may bind to the cell membrane with consequent rupture and cell death [Nolan et al 1981; Fubini & Wallace 1999; Fubini et al 2004]. Indeed cytotoxicity is reported not only for pathogenic quartz dusts but also for most amorphous silicas, which do not release free radicals nor show fibrogenicity, confirming that not always cell death is caused by free radical generation, as hypothesized by some authors [Razzaboni & Bolsaitis 1990]. It is noteworthy that in the present study DQ12 exhibits a stronger activity than the other samples in all tests but its activity is overwhelming in both cytotoxicity assays. Thus, its particular high fibrogenicity could be ascribed to its potency in the disruption of cell membrane as a first step to inflammogenicity. Moreover, it may be recalled that silanols play a crucial role in determining protein adsorption [Fubini et al 2010; Turci et al 2010]. The crucial role of protein adsorption in toxicology, and

particularly in nanotoxicology has been recently stressed out by many authors as reviewed in Nel et al [2009]. Apart from aluminum, differences, e.g. in size distribution as well as in other - yet to be identified - physico-chemical properties may additionally play a role in the differences in toxic potential between DQ12 and Qz.

Effect of iron-loading

Even if the use of DQ12 as reference material shows that the presence and availability of iron and associated radical generating properties may be overruled by other physico-chemical properties, a role of surface bound or leached iron is shown by comparative evaluation of Qz with its two iron-loaded specimens. We confirm here that, when above trace amount, iron has a beneficial effect to AMΦ with regard to their toxic and inflammogenic properties, as previously reported for the toxicity and transformation potency on SHE [Fubini et al 2001; Elias et al 2002b, 2006]. In spite of differences in composition, the two iron-loadings did not yield substantial differences in the biological responses elicited. This may be due either to the inertness of hematite particles or to a role for bioavailable iron. Note that in spite of a different loading, the amount of removable, thus potentially bioavailable iron ions were very close for the two samples.

In conclusion, our current findings indicate that relatively low levels of surface bound and potentially bioavailable iron on quartz may be beneficial in quartz related adverse health effects. The employment of DQ12 quartz as reference materials confirmed the exceptionally high toxic potency of this quartz specimen and also indicated that such potency is not related to a higher free radical release but to other surface features. Most probably undissociated silanols with potential to form strong H-bonds because of the absence of aluminum often present in most quartz dusts will bind and disrupt cell membranes and/or proteins. Finally, we confirm here the importance to employ well-defined samples prepared *ad hoc* for experimental studies in particle toxicology.

ACKNOWLEDGEMENTS

This research was supported by the Italian Ministry of Education, University and Research (MIUR), project title "Study of the mechanisms responsible for cytotoxicity and genotoxicity of silica nanoparticles and nanometric fibrous silicates having strictly controlled size, structure and composition" (PRIN project Prot. 2007498XRF-001).
The DLS and XRF equipments were acquired by the Interdepartmental Center "G. Scansetti" for Studies on Asbestos and Other Toxic Particulates with a grant from Compagnia di San Paolo.

GRANTS

M.G. was recipient of a postdoctoral fellowship from Interdepartimental Centre for Nanostructured Interfaces and Surfaces Università degli Studi di Torino.
A.M.S. participates as a collegiate at the Graduate School GRK1427 funded by the German Research Foundation (DFG). Additionally, this work was financially supported by the Federal Ministry of the Environment (BMU).

3.5 REFERENCES

Albrecht C, Höhr D, Haberzettl P, Becker A, Borm PJ, Schins RP. Surface-dependent quartz uptake by macrophages: potential role in pulmonary inflammation and lung clearance. Inhal Toxicol 2007, 19 Suppl 1:39-48.

Albrecht C, Knaapen AM, Becker A, Höhr D, Haberzettl P, van Schooten FJ, Borm PJ, Schins RP. The crucial role of particle surface reactivity in respirable quartz-induced reactive oxygen/nitrogen species formation and APE/Ref-1 induction in rat lung. Respir Res 2005, 6:129.

Albrecht C, Scherbart AM, van Berlo D, Braunbarth CM, Schins RP, Scheel J. Evaluation of cytotoxic effects and oxidative stress with hydroxyapatite dispersions of different physicochemical properties in rat NR8383 cells and primary macrophages. Toxicol In Vitro 2009, 23(3):520-30.

Albrecht C, Schins RP, Höhr D, Becker A, Shi T, Knaapen AM, Borm PJ. Inflammatory time course after quartz instillation: role of tumor necrosis factor-alpha and particle surface. Am J Respir Cell Mol Biol 2004, 31(3):292-301.

Arena F, Gatti G, Martra G, Coluccia S, Stievano L, Spadaro L, Famulari P, Parmaliana A. Structure and reactivity in the selective oxidation of methane to formaldehyde of low-loaded FeOx/SiO2 catalysts. J Catal 2005, 231(2):365-80.

Azad N, Rojanasakul Y, Vallyathan V. Inflammation and lung cancer: roles of reactive oxygen/nitrogen species. J Toxicol Environ Health B Crit Rev 2008, 11(1):1-15.

Berlier G, Spoto G, Bordiga S, Ricchiardi G, Fisicaro P, Zecchina A, Rossetti I, Selli E, Forni L, Giamello E, C L. Evolution of extraframework iron species in Fe silicalite 1. Effect of Fe content, activation temperature, and interaction with redox agents. J Catal 2002, 208(1):64-82.

Borges VM, Falcao H, Leite-Junior JH, Alvim L, Teixeira GP, Russo M, Nobrega AF, Lopes MF, Rocco PM, Davidson WF, Linden R, Yagita H, Zin WA, DosReis GA. Fas ligand triggers pulmonary silicosis. J Exp Med 2001, 194(2):155-64.

Brown GM, Donaldson K, Brown DM. Bronchoalveolar leukocyte response in experimental silicosis: modulation by a soluble aluminum compound. Toxicol Appl Pharmacol 1989, 101(1):95-105.

Bruch J, Rehn S, Rehn B, Borm PJ, Fubini B. Variation of biological responses to different respirable quartz flours determined by a vector model. Int J Hyg Environ Health 2004, 207(3):203-16.

Cakmak GD, Schins RP, Shi T, Fenoglio I, Fubini B, Borm PJ. In vitro genotoxicity assessment of commercial quartz flours in comparison to standard DQ12 quartz. Int J Hyg Environ Health 2004, 207(2):105-13.

Castranova V, Dalal NS, Vallyathan V. Role of surface free radicals in the pathogenicity of silica. *In:* Silica and Silica-Induced Lung Diseases - Castranova V, Vallyathan V, Wallace, WE, CRC Press 1996a, Boca Raton, USA.

Castranova V, Vallyathan V, Ramsey DM, McLaurin JL, Pack D, Leonard S, Barger MW, Ma JY, Dalal NS, Teass A. Augmentation of pulmonary reactions to quartz inhalation by trace amounts of iron-containing particles. Environ Health Perspect 1997, 105 Suppl 5:1319-24.

Castranova V, Walker W, Vallyathan V. Silica and Silica-Induced Lung Diseases. Informa Healthcare 1996b, Boca Raton, USA.

Clouter A, Brown D, Höhr D, Borm P, Donaldson K. Inflammatory effects of respirable quartz collected in workplaces versus standard DQ12 quartz: particle surface correlates. Toxicol Sci 2001, 63(1):90-8.

Corsini E, Giani A, Lucchi L, Peano S, Viviani B, Galli CL, Marinovich M. Resistance to acute silicosis in senescent rats: role of alveolar macrophages. Chem Res Toxicol 2003, 16(12):1520-7.

Cullen RT, Vallyathan V, Hagen S, Donaldson K. Protection by iron against the toxic effect of quartz. Ann Occup Hyg 1997, 41 Suppl:1420-25.

Donaldson K, Borm PJ. The quartz hazard: a variable entity. Ann Occup Hyg 1998, 42(5):287-94.

Donaldson K, Brown DM, Mitchell C, Dineva M, Beswick PH, Gilmour P, MacNee W. Free radical activity of PM10: iron-mediated generation of hydroxyl radicals. Environ Health Perspect 1997, 105 Suppl 5:1285-9.

Duffin R, Gilmour PS, Schins RP, Clouter A, Guy K, Brown DM, MacNee W, Borm PJ, Donaldson K, Stone V. Aluminium lactate treatment of DQ12 quartz inhibits its ability to cause inflammation, chemokine expression, and nuclear factor-kappaB activation. Toxicol Appl Pharmacol 2001, 176(1):10-7.

El Malki EM, van Santen RA, Sachtler WMH. Active sites in Fe/MFI catalysts for NOx reduction and oscillating N2O decomposition. Journal of Catalysis 2000, 196(2):212-23.

Elias Z, Poirot O, Daniere MC, Terzetti F, Bena F, Fenoglio I, Fubini B. Role of iron and surface free radical activity of silica in the induction of morphological transformation of Syrian hamster embryo (SHE) cells. Ann Occup Hyg 2002a, 46 Suppl 1:53-57.

Elias Z, Poirot O, Daniere MC, Terzetti F, Binet S, Tomatis M, Fubini B. Surface reactivity, cytotoxicity, and transforming potency of iron-covered compared to untreated refractory ceramic fibers. J Toxicol Environ Health A 2002b, 65(23):2007-27.

Elias Z, Poirot O, Fenoglio I, Ghiazza M, Daniere MC, Terzetti F, Darne C, Coulais C, Matekovits I, Fubini B. Surface reactivity, cytotoxic, and morphological transforming effects of diatomaceous Earth products in Syrian hamster embryo cells. Toxicol Sci 2006, 91(2):510-20.

Elias Z, Poirot O, Terzetti F, Daniere MC. Phenotypic and numerical chromosome changes during the neoplastic progression of Syrian hamster embryo cells transformed by silica. Medicina del Lavoro 2002c, 93 Suppl:52.

Fenoglio I, Fonsato S, Fubini B. Reaction of cysteine and glutathione (GSH) at the freshly fractured quartz surface: a possible role in silica-related diseases? Free Radic Biol Med 2003, 35(7):752-62.

Fenoglio I, Martra G, Coluccia S, Fubini B. Possible role of ascorbic acid in the oxidative damage induced by inhaled crystalline silica particles. Chem Res Toxicol 2000, 13(10):971-5.

Fenoglio I, Prandi L, Tomatis M, Fubini B. Free radical generation in the toxicity of inhaled mineral particles: the role of iron speciation at the surface of asbestos and silica. Redox Rep 2001, 6(4):235-41.

Franz KJ, Lippard SJ. NO disproportionation reactivity of Fe tropocoronand complexes. J Am Chem Soc 1999, 121(45):10504-12.

Fubini B. Health effects of silica. *In:* The Surface Properties of Silica - Legrand AP, Wiley and Sons 1998a, Chichester, United Kingdom.

Fubini B. Surface chemistry and quartz hazard. Ann Occup Hyg 1998b, 42(8):521-30.

Fubini B, Fenoglio I, Ceschino R, Ghiazza M, Martra G, Tomatis M, Borm P, Schins R, Bruch J. Relationship between the state of the surface of four commercial quartz flours and their biological activity in vitro and in vivo. Int J Hyg Environ Health 2004, 207(2):89-104.

Fubini B, Fenoglio I, Elias Z, Poirot O. Variability of biological responses to silicas: effect of origin, crystallinity, and state of surface on generation of reactive oxygen species and morphological transformation of mammalian cells. J Environ Pathol Toxicol Oncol 2001, 20 Suppl 1:95-108.

Fubini B, Ghiazza M, Fenoglio I. Physico-chemical Features in the Toxicity of Engineered Nanoparticles. Nanotoxicology 2010.

Fubini B, Hubbard A. Reactive oxygen species (ROS) and reactive nitrogen species (RNS) generation by silica in inflammation and fibrosis. Free Radic Biol Med 2003, 34(12):1507-16.

Fubini B, Mollo L. Role of iron in the reactivity of mineral fibers. Toxicol Lett 1995, 82-83:951-60.

Fubini B, Mollo L, Giamello E. Free radical generation at the solid/liquid interface in iron containing minerals. Free Radic Res 1995, 23(6):593-614.

Fubini B, Otero-Aréan C. Chemical aspects of the toxicity of inhaled mineral dusts. Chem. Soc. Rev. 1999, 28:373-81.

Fubini B, Wallace WE. Modulation of silica pathogenicity by surface processes. *In:* Adsorption Silica Surface (Surfactant Science) - Papirer E, CRC Press 1999, Mulhouse France.

Ghiazza M, Polimeni M, Fenoglio I, Gazzano E, Ghigo D, Fubini B. Does vitreous silica contradict the toxicity of crystalline silica paradigm? Chem. Res. Toxicol. 2010, 23:620-29.

Green FH, Vallyathan V. Pathologic responses to inhaled silica. *In:* Silica and Silica-Induced Lung Diseases - Castranova V, Vallyathan V, Wallace WE, CRC Press 1996, Boca Raton.

Gwinn MR, Vallyathan V. Respiratory burst: role in signal transduction in alveolar macrophages. J Toxicol Environ Health B Crit Rev 2006, 9(1):27-39.

Haberzettl P, Schins RP, Höhr D, Wilhelmi V, Borm PJ, Albrecht C. Impact of the FcgammaII-receptor on quartz uptake and inflammatory response by alveolar macrophages. Am J Physiol Lung Cell Mol Physiol 2008, 294(6):L1137-48.

Hardy JA, Aust AE. The effect of iron binding on the ability of crocidolite asbestos to catalyze DNA single-strand breaks. Carcinogenesis 1995, 16(2):319-25.

Helmke RJ, German VF, Mangos JA. A continuous alveolar macrophage cell line: comparisons with freshly derived alveolar macrophages. In Vitro Cell Dev Biol 1989, 25(1):44-8.

Hetland RB, Schwarze PE, Johansen BV, Myran T, Uthus N, Refsnes M. Silica-induced cytokine release from A549 cells: importance of surface area versus size. Hum Exp Toxicol 2001, 20(1):46-55.

Horwell CJ, Fenoglio I, Fubini B. Iron-induced hydroxyl radical generation from basaltic volcanic ash. Earth Planet Sci Let 2007, 261(3-4):662-69.

Horwell CJ, Fenoglio I, Vala Ragnarsdottir K, Sparks RS, Fubini B. Surface reactivity of volcanic ash from the eruption of Soufriere Hills volcano, Montserrat, West Indies with implications for health hazards. Environ Res 2003, 93(2):202-15.

Huaux F, Lasfargues G, Lauwerys R, Lison D. Lung toxicity of hard metal particles and production of interleukin-1, tumor necrosis factor-alpha, fibronectin, and cystatin-c by lung phagocytes. Toxicol Appl Pharmacol 1995, 132(1):53-62.

Hyun SP, Cho YH, Hahn PS. An electron paramagnetic resonance study of Cu(II) sorbed on quartz. J Colloid Interface Sci 2003, 257(2):179-87.

IARC. Silica, Some Silicates, Coal Dust and Para-Aramid Fibrils. IARC Monogr Eval Carcinog Risks Hum 1997, 68:1-475.

IARC. A review of human carcinogens. Ingested Nitrate and Nitrite and Cyanobacterial Peptide Toxins. IARC Monogr Eval Carcinog Risks Hum 2010, 94.

Iler RK. The chemistry of silica. Wiley and Sons 1979, p; New York.

Iyer R, Hamilton RF, Li L, Holian A. Silica-induced apoptosis mediated via scavenger receptor in human alveolar macrophages. Toxicol Appl Pharmacol 1996, 141(1):84-92.

Kamp DW, Weitzman SA. The molecular basis of asbestos induced lung injury. Thorax 1999, 54(7):638-52.

Kanj RS, Kang JL, Castranova V. Measurement of the release of inflammatory mediators from rat alveolar macrophages and alveolar type II cells following lipopolysaccharide or silica exposure: a comparative study. J Toxicol Environ Health A 2005, 68(3):185-207.

Lane KB, Egan B, Vick S, Abdolrasulnia R, Shepherd VL. Characterization of a rat alveolar macrophage cell line that expresses a functional mannose receptor. J Leukoc Biol 1998, 64(3):345-50.

Li H, van Berlo D, Shi T, Speit G, Knaapen AM, Borm PJ, Albrecht C, Schins RP. Curcumin protects against cytotoxic and inflammatory effects of quartz particles but causes oxidative DNA damage in a rat lung epithelial cell line. Toxicol Appl Pharmacol 2008, 227(1):115-24.

Lison D, Laloy J, Corazzari I, Muller J, Rabolli V, Panin N, Huaux F, Fenoglio I, Fubini B. Sintered indium-tin-oxide (ITO) particles: a new pneumotoxic entity. Toxicol Sci 2009, 108(2):472-81.

Livak KJ, Schmittgen TD. Analysis of relative gene expression data using real-time quantitative PCR and the 2(-Delta Delta C(T)) Method. Methods 2001, 25(4):402-8.

Lund LG, Aust AE. Iron mobilization from asbestos by chelators and ascorbic acid. Arch Biochem Biophys 1990, 278(1):61-4.

Martra G, Chiardola E, Coluccia S, Marchese L, Tomatis M, Fubini B. Reactive sites at the surface of crocidolite asbestos. Langmuir 1999, 15(18):5742-52.

Nel AE, Madler L, Velegol D, Xia T, Hoek EM, Somasundaran P, Klaessig F, Castranova V, Thompson M. Understanding biophysicochemical interactions at the nano-bio interface. Nat Mater 2009, 8(7):543-57.

Nicoletti I, Migliorati G, Pagliacci MC, Grignani F, Riccardi C. A rapid and simple method for measuring thymocyte apoptosis by propidium iodide staining and flow cytometry. J Immunol Methods 1991, 139(2):271-9.

Nolan RP, Langer AM, Harington JS, Oster G, Selikoff IJ. Quartz hemolysis as related to its surface functionalities. Environ Res 1981, 26(2):503-20.

Oberdörster G. Significance of particle parameters in the evaluation of exposure-dose-response relationships of inhaled particles. Inhal Toxicol 1996, 8 Suppl:73-89.

Ortiz LA, Lasky J, Lungarella G, Cavarra E, Martorana P, Banks WA, Peschon JJ, Schmidts HL, Brody AR, Friedman M. Upregulation of the p75 but not the p55 TNF-alpha receptor mRNA after silica and bleomycin exposure and protection from lung injury in double receptor knockout mice. Am J Respir Cell Mol Biol 1999, 20(4):825-33.

Ortiz LA, Moroz K, Liu JY, Hoyle GW, Hammond T, Hamilton RF, Holian A, Banks W, Brody AR, Friedman M. Alveolar macrophage apoptosis and TNF-alpha, but not p53, expression correlate with murine response to bleomycin. Am J Physiol 1998, 275(6 Pt 1):L1208-18.

Palecanda A, Kobzik L. Alveolar macrophage-environmental particle interaction: analysis by flow cytometry. Methods 2000, 21(3):241-7.

Parmaliana A, Arena F, Frusteri F, Martinez-Arias A, Lopez-Granados M, Fierro JLG. Effect of Fe-addition on the catalytic activity of silicas in the partial oxidation of methane to formaldehyde. Appl Catal Gen 2002, 226:163-74.

Piguet PF, Collart MA, Grau GE, Sappino AP, Vassalli P. Requirement of tumour necrosis factor for development of silica-induced pulmonary fibrosis. Nature 1990, 344(6263):245-7.

Piguet PF, Vesin C. Treatment by human recombinant soluble TNF receptor of pulmonary fibrosis induced by bleomycin or silica in mice. Eur Respir J 1994, 7(3):515-8.

Pirngruber GD, Roy PK, Prins R. The role of autoreduction and of oxygen mobility in N2O decomposition over Fe-ZSM-5. J Catal 2007, 246(1):147-57.

Razzaboni BL, Bolsaitis P. Evidence of an oxidative mechanism for the hemolytic activity of silica particles. Environ Health Perspect 1990, 87:337-41.

Schins RP, Duffin R, Höhr D, Knaapen AM, Shi T, Weishaupt C, Stone V, Donaldson K, Borm PJ. Surface modification of quartz inhibits toxicity, particle uptake, and oxidative DNA damage in human lung epithelial cells. Chem Res Toxicol 2002, 15(9):1166-73.

Seiler F, Rehn B, Rehn S, Bruch J. Different toxic, fibrogenic and mutagenic effects of four commercial quartz flours in the rat lung. Int J Hyg Environ Health 2004, 207(2):115-24.

Smith KR, Veranth JM, Hu AA, Lighty JS, Aust AE. Interleukin-8 levels in human lung epithelial cells are increased in response to coal fly ash and vary with the bioavailability of iron, as a function of particle size and source of coal. Chem Res Toxicol 2000, 13(2):118-25.

Smith KR, Veranth JM, Lighty JS, Aust AE. Mobilization of iron from coal fly ash was dependent upon the particle size and the source of coal. Chem Res Toxicol 1998, 11(12):1494-500.

Somorjai GA, McCrea KR, Zhu J. Active sites in heterogeneous catalysis: development of molecular concepts and future challenges. Topics in Catalysis 2002, 18(3-4):157-66.

Spoto G, Zecchina A, Berlier G, Bordiga S, Clerici MG, Basini L. FTIR and UV-Vis characterization of Fe-silicalite. J Mol Catal A 2000, 158(1):107-14.

Stookey LL. Ferrozine - a new spectrophotometric reagent for iron. Anal Chem 1970, 42:779-81.

Turci F, Favero-Longo SE, Tomatis M, Martra G, Castelli D, Piervittori R, Fubini B. A biomimetic approach to the chemical inactivation of chrysotile fibres by lichen metabolites. Chemistry 2007, 13(14):4081-93.

Turci F, Ghibaudi E, Colonna M, Boscolo B, Fenoglio I, Fubini B. An integrated approach to the study of the interaction between proteins and nanoparticles. Langmuir 2010, 26(11):8336-46.

Turci F, Tomatis M, Gazzano E, Riganti C, Martra G, Bosia A, Ghigo D, Fubini B. Potential toxicity of nonregulated asbestiform minerals: balangeroite from the western Alps. Part 2: Oxidant activity of the fibers. J Toxicol Environ Health A 2005, 68(1):21-39.

Vallyathan V. Generation of oxygen radicals by minerals and its correlation to cytotoxicity. Environ Health Perspect 1994, 102 Suppl 10:111-5.

van Berlo D, Haberzettl P, Gerloff K, Li H, Scherbart AM, Albrecht C, Schins RP. Investigation of the cytotoxic and proinflammatory effects of cement dusts in rat alveolar macrophages. Chem Res Toxicol 2009, 22(9):1548-58.

van Berlo D, Knaapen AM, van Schooten FJ, Schins RP, Albrecht C. NF-kappaB dependent and independent mechanisms of quartz-induced proinflammatory activation of lung epithelial cells. Part Fibre Toxicol 2010, 7:13.

van Maanen JM, Borm PJ, Knaapen A, van Herwijnen M, Schilderman PA, Smith KR, Aust AE, Tomatis M, Fubini B. In vitro effects of coal fly ashes: hydroxyl radical generation, iron release, and DNA damage and toxicity in rat lung epithelial cells. Inhal Toxicol 1999, 11(12):1123-41.

CHAPTER IV

EVALUATION OF CYTOTOXIC EFFECTS AND OXIDATIVE STRESS WITH HYDROXYAPATITE DISPERSIONS OF DIFFERENT PHYSICOCHEMICAL PROPERTIES IN RAT NR8383 CELLS AND PRIMARY MACROPHAGES

Catrin Albrecht, Agnes M. Scherbart, Damiën van Berlo, Carola M. Braunbarth, Roel P.F. Schins, Julia Scheel

Toxicology in Vitro, 2009 Apr;23(3):520-30

DECLARATION - STUDY 3

Evaluation of cytotoxic effects and oxidative stress with hydroxyapatite dispersions of different physicochemical properties in rat NR8383 cells and primary macrophages

Declaration:
The manuscript is submitted to a peer-review journal.
Most experimental work presented, was done by Agnes M. Scherbart.
The impact on authoring this paper can be estimated to 40 %.

Toxicology in Vitro 23 (2009) 520–530

Contents lists available at ScienceDirect

Toxicology in Vitro

journal homepage: www.elsevier.com/locate/toxinvit

Evaluation of cytotoxic effects and oxidative stress with hydroxyapatite dispersions of different physicochemical properties in rat NR8383 cells and primary macrophages

Catrin Albrecht [a], Agnes M. Scherbart [a], Damien van Berlo [a], Carola M. Braunbarth [b], Roel P.F. Schins [a], Julia Scheel [c,*]

[a] Particle Research, Institut für Umweltmedizinische Forschung (IUF) at the Heinrich-Heine University gGmbH, Düsseldorf, Germany
[b] Sustech GmbH & Co. KG, Darmstadt, Germany
[c] Corporate Product Safety, Department of Human Safety Assessment, Henkel AG & Co. KGaA, Henkelstr. 67, Düsseldorf 40191, Germany

ARTICLE INFO

Article history:
Received 19 September 2008
Accepted 9 January 2009
Available online 18 January 2009

Keywords:
Nanomaterials
Hydroxyapatite
Cytotoxicity
Oxidative stress
Biocompatibility
Macrophages
Rat

ABSTRACT

Enhanced cytotoxicity and oxidative stress through reactive oxygen species (ROS) formation are discussed as relevant parameters regarding potential hazardous properties of nanomaterials. In this study, the biocompatibility of five hydroxyapatite materials of different size and morphology, i.e., nano/needle-shaped (HA-NN), nano/rod-like (HA-NR), nano/plate-like (HA-NP), fine/dull needle-shaped (HA-FN), and a hydroxyapatite–protein-composite (HPC), was investigated in rat NR8383 and primary alveolar macrophages. Lipopolysaccharide (LPS) and DQ12 quartz served as positive controls. In the water-soluble tetrazolium salt 1 (WST-1) and lactate dehydrogenase (LDH) assays with NR8383 cells, no cytotoxicity was observed for HPC and the pure hydroxyapatite samples up to 3000 μg/ml, while HA-FN showed a significant effect at the highest dose in the LDH assay. In primary cells, no cytotoxicity was observed with all samples up to 300 μg/ml. ROS generation measured by electron paramagnetic resonance (EPR) technique was significantly enhanced with HA-NN and HPC in NR8383 cells. No effect was detected in primary cells, which are considered more relevant to physiological conditions. All hydroxyapatites elicited TNF-α release from the NR8383 cells, but with significantly lower potency than DQ12 quartz and LPS. In conclusion, combined findings in both cell types support a good biocompatibility of the pure hydroxyapatite samples as well as of the hydroxyapatite–protein-composite.

1. Introduction

Cytotoxicity, inflammation and increased oxidative stress through reactive oxygen species (ROS) formation are prominently discussed to be relevant factors regarding the safety of small particles down to the nano-range (Brown et al., 2001; Donaldson et al., 2005; Brunner et al., 2006; Aam and Fonnum, 2007; Pan et al., 2007; Unfried et al., 2007; Lewinski et al., 2008). A complex process involving a plethora of factors needs to be considered when assessing these effects in macrophages, which in different organ systems represent a highly efficient barrier in engulfing and clearing pathogens as well as small particles. Thus, survival of macrophages is one of the key prerequisites for an effective elimination of potentially harmful particles.

Cellular oxidative stress is a fundamental mechanism whereby toxic particles like quartz exert their pathogenicity following inhalation (Donaldson and Tran, 2002; Knaapen et al., 2004). The phagocytic process of such particles has been shown to result in cellular activation (Albrecht et al., 2007), leading to the release of a wide range of inflammogenic and cytotoxic mediators, specifically cytokines, eicosanoids, chemokines and ROS (Schins and Borm, 1999; Donaldson and Tran, 2002), which may in turn exert an adverse effect on the viability and functionality of macrophages themselves, as well as on the surrounding tissue. The release of such inflammatory mediators is considered to be driven by the induction of cellular oxidative stress and associated activation of redox-sensitive

Abbreviations: BAL, broncho-alveolar lavage; BET, Brunauer–Emmett–Teller method; DMPO, 5,5-dimethyl-1-pyrroline-*N*-oxide; ELISA, enzyme-linked immunoabsorbent assay; EPR, electron paramagnetic resonance; ESEM, environmental scanning electron microscopy; FCS, fetal calf serum; HA-FN, hydroxyapatite-fine/dull needles; HA-NN, hydroxyapatite-nano, needles; HA-NP, hydroxyapatite-nano, plate-like; HA-NR, hydroxyapatite-nano, rods; HBSS, Hank's balanced salt solution; HPC, hydroxyapatite–protein-composite; ICP, inductively coupled plasma; LDH, lactate dehydrogenase; LPS, lipopolysaccharide; NF-κB, nuclear factor-kappaB; PBS, phosphate buffered saline; SEM, scanning electron microscopy; TEM, transmission electron microscopy; TNF-α, tumor necrosis factor alpha; ROS, reactive oxygen species; WST-1, water-soluble tetrazolium salt 1.

* Corresponding author. Tel.: +49 211 7972413; fax: +49 211 79812413.
E-mail address: julia.scheel@henkel.com (J. Scheel).

0887-2333/$ - see front matter © 2009 Elsevier Ltd. All rights reserved.
doi:10.1016/j.tiv.2009.01.005

transcription factors (Duffin et al., 2001; Albrecht et al., 2004). Whereas the release of cytokines and chemokines trigger the inflammatory axis via recruitment and activation of additional inflammatory cells, production of ROS is additionally implicated as a major factor in oxidative tissue damage, e.g., to membrane constituents, intracellular proteins and genomic DNA (Knaapen et al., 2004; Donaldson et al., 2005).

On a cellular level the principal mode of particle–macrophage-interactions and their associated response mechanisms are anticipated to be highly similar. Alveolar macrophages are therefore considered as a surrogate to assess the effects on macrophages in various tissues.

It has been reported that different sizes and morphologies of particles, including hydroxyapatite, have the potential to influence the interaction with biological systems (Evans, 1991; Laquerriere et al., 2003; Grandjean-Laquerriere et al., 2004, 2005; Ramesh et al., 2007). In the present study, the biocompatibility of different hydroxyapatite samples in the nano (<100 nm) and fine (0.1–2.5 μm) range, including one hydroxyapatite–protein-composite, was investigated. Engineered hydroxyapatite materials and composites thereof, featuring small particle sizes down to the nano-range, are intended for a variety of biomedical applications (Arts et al., 2006; Huber et al., 2007). Although NR8383 cells potentially represent the best currently available macrophage cell line for studying macrophage function (Lane et al., 1998) studies comparing NR8383 and other cell lines (e.g., RAW264.7 macrophages) to primary macrophages emphasize the need to exercise caution in extrapolating data from cell lines to primary cells (Rao et al., 2002; Maurya et al., 2007). Since this is considered to be of particular importance for the investigation of mechanisms of ROS formation and oxidative stress (Yang et al., 2008), specific measurements were also performed in primary rat macrophages. All samples were evaluated for their ability to cause cytotoxicity and ROS generation in both cellular systems, with primary macrophages being used to verify the results obtained with NR8383 cells. Fine crystalline silica (DQ12 quartz) and lipopolysaccharide (LPS) were used as particulate and ROS-inducing positive controls, respectively. Cytotoxicity was determined using two complementary approaches, the LDH assay as a marker of cell membrane integrity and the WST-1 assay as an indicator of the metabolic competence of the cells. Release of ROS was determined by electron paramagnetic resonance (EPR) coupled to spin trapping. In addition, the release of TNF-α from NR8383 cells was measured by enzyme-linked immunoabsorbent assay (ELISA). The combined results should serve as screening elements for the potential hazard of the materials in a weight-of-evidence approach.

2. Materials and methods

2.1. Particle preparation

The test samples used in this study are listed in Table 1 together with their abbreviations used in the following. HA-NR, HA-NP and HPC were synthesized by precipitation in aqueous solution at constant pH value. Chemical composition and morphology of the particles were determined by pH during precipitation and the absence or presence of protein. An amount of 44.10 g (0.30 mol) calcium chloride dihydrate (p.a., Fisher Scientific GmbH, Schwerte, Germany) was dissolved in 2 l deionized water at room temperature in a precipitation vessel. In case of HPC preparation 35 g denatured collagen (Gelatine, Gelita AG, Eberbach, Germany), was dissolved in 350 ml deionized water at ca 50 °C and added to the calcium solution under stirring. In a second vessel 0.6 mol ammonium phosphate (Sigma–Aldrich, Taufkirchen, Germany) was dissolved in 300 ml deionized water at room temperature. Solutions were adjusted to pH 7 for HPC and HA-NP and pH 9 for HA-NR. The phosphate solution was then pumped into the calcium solution, which was stirred during the whole reaction period. pH was kept constant by adding base with a pH-controlled pump. The precipitate was separated, washed, portioned and gamma-sterilized. HPC, HA-NR and HA-NP were not dried prior to testing.

HA-FN was synthesized by precipitation in aqueous solution using calcium hydroxide (Schaefer Precal 72, Schäfer Kalk, Diez, Germany) and phosphoric acid (Sigma–Aldrich, Taufkirchen, Germany). A volume of 3 l of deionized water was heated to 80 °C in a 10 l precipitation vessel. A volume of 0.6 l calcium hydroxide slurry (20% w/v suspended in water) was added while stirring at constant flow rate. Phosphoric acid (5 M) was added with a pH-controlled pump to maintain a pH of 10 during precipitation. The controlled pump stops the addition of phosphoric acid if all calcium is transformed into calcium phosphate. After 2 h of stirring at 80 °C, the product was separated by decantation and subsequent filtration. The precipitate was separated and dried under vacuum. The resulting powder was portioned and gamma-sterilized.

HA-NN (trade name Ostim®), was purchased from Heraeus Kulzer, Hanau, Germany.

DQ12 quartz (Dörentruper quartz, grinding 12) was provided by IUF (batch 6) as dry material.

2.2. Particle characterization

2.2.1. Water and apatite content

The water content of the wet sediments of HPC, HA-NP and HA-NR as well as of the powder HA-FN was analyzed using a Sartorius MA 100 Moisture Analyzer. Approximate 5 g of the wet sediment was weighed in a flat aluminum plate, homogeneously distributed and immediately heated to 125 °C until the balance stops the program by itself (weight loss below approximate 3 mg/30 s). The protein used for HPC is stable at a temperature of 125 °C. The measured weight loss therefore corresponds to water only. In case of the pure hydroxyapatites HA-NP, HA-NR and HA-FN the residue corresponds to the apatite content. Each analysis was done in duplicate.

2.2.2. Apatite and protein content of HPC

The sediment of HPC consists of water, hydroxyapatite and protein. The content of hydroxyapatite was analyzed by calcination. A dry crucible was filled with approximately 2 g of the wet HPC sediment, heated gradually to 800 °C during 1 h, kept at high temperature for further 30 min and then cooled down to room temperature. The residue after calcination corresponds to the hydroxyapatite content of HPC. The weight difference prior to and after calcination corresponds to water and protein. The water

Table 1
Overview of test samples used in this study.

Test sample	Abbreviation	Source
Hydroxyapatite–protein-composite	HPC	Synthesized at Sustech Darmstadt
Nano-hydroxyapatite, plate-like	HA-NP	Synthesized at Sustech Darmstadt
Nano-hydroxyapatite, rod-like	HA-NR	Synthesized at Sustech Darmstadt
Nano-hydroxyapatite, needle-shaped	HA-NN	Purchased from Heraeus
Fine hydroxyapatite, blunt-ended needles	HA-FN	Synthesized at Sustech Darmstadt

content was determined with the Moisture Analyzer (see Section 2.2.1). The protein content was calculated based on both analyses. Each sample was analyzed in duplicate.

2.2.3. Calcium/phosphorus ratio

The ratio of calcium and phosphorus of HPC, HA-NP, HA-NR and HA-FN was analyzed with inductively coupled plasma (ICP) spectroscopy using a Perkin Elmer Optima 3000 spectroscope. The samples were dissolved in 6 wt% hydrochloric acid and diluted 1:100 with deionized water. Calcium was measured at 316, 318, 397 and 423 nm wavelength. Phosphorus was measured at 213 and 214 nm wavelength. Each analysis was done in duplicate.

2.2.4. Specific surface

Specific surfaces of HPC, HA-NP, HA-NR and HA-FN were analyzed by the Brunauer–Emmet–Teller (BET) method (Brunauer et al., 1938). The wet sediments of HPC, HA-NP and HA-NR were snap frozen with liquid nitrogen, freeze-dried and ground manually thereafter. The specific surface was determined with a Quantachrome Autosorb-3B. Prior to nitrogen adsorption the dried samples were heated at 100 °C for 24 h. The measurement was based on five points.

2.2.5. Particle size and morphology

Particle morphology and size were analyzed by transmission electron microscopy (TEM) with a Philips CM12 transmission electron microscope. Wet sediments (HPC, HA-NP and HA-NR) and powder (HA-FN) were dispersed in ethanol, sprayed onto a copper grid and investigated at 120 kV acceleration voltage.

Environmental scanning electron microscopy (ESEM) was performed using a FEI Quanta FEG 200 device. Samples were mounted on a carbon-taped sample holder, vaporized with gold and scanned with 15 kV acceleration voltage in an atmosphere of 1 mbar water vapor.

Particle size distribution of DQ12 quartz (batch 6, IUF, Düsseldorf, Germany) was determined by scanning electron microscopy (SEM), as described previously (Albrecht et al., 2002, 2004).

2.3. Preparation of particle suspensions

All particle suspensions were freshly prepared before each experiment. Depending on the method, particles were suspended either in Kaighn's modified medium containing 15% fetal calf serum (FCS), 1% penicillin/streptomycin and 1% glutamine (all purchased from Sigma–Aldrich, Taufkirchen, Germany) for the toxicity and cytokine assays or in Hank's balanced salt solution ($HBSS^{(+/+)}$) (phenol red free, $+Mg^{2+}$ and Ca^{2+}) for ROS detection. The $HBSS^{(+/+)}$ was used to avoid radical scavenging by serum constituents in the ROS assay, while complete culture medium was required for all other assays to maintain appropriate cell viability for 24 h. Following overnight stirring at a frequency of 300 rpm (IKA-MAG® RET-GS), all hydroxyapatite samples were added to the NR8383 cells at final concentrations of 30, 100, 300, 1000 and 3000 μg/ml. Particle concentrations were calculated in respect to the solids content of the synthetic products. DQ12 quartz, which was used as positive control particle, was added at final concentrations of 3, 10, 30, 100 and 300 μg/ml. Experiments with primary macrophages were carried out using particle concentrations of 30 and 300 μg/ml.

2.4. Macrophage cell culture

NR8383 rat alveolar macrophages (ATCC, Manassas, USA) as well as primary rat macrophages were cultured in Kaighn's modified medium (F12-K Nutrient Mixture, Gibco, Eggenstein, Germany) containing 15% FCS, 1% penicillin/streptomycin and 1% glutamine (all purchased from Sigma–Aldrich, Taufkirchen, Germany) and incubated in a humified incubator (Heraeus, BB 6060 CU) at 37 °C and 5% CO_2.

2.5. Isolation and cultivation of primary rat macrophages

For preparation of primary macrophages 11-week-old female Wistar rats (Janvier, France) were sacrificed by bleeding via Aorta *abdominalis* following deep anesthetization with Pentobarbital (Narcoren®, 50 mg/kg body weight). Primary cells were obtained by broncho-alveolar lavage (BAL) with four times 5 ml phosphate buffered saline (PBS; Sigma–Aldrich, Taufkirchen, Germany) containing 1% penicillin/streptomycin. Cells were pooled, counted and seeded into 96-well microtiter plates. After 2 h of incubation at 37 °C and 5% CO_2, cells were gently rinsed with medium to remove non-adherent cells. The adherent macrophage fraction was cultivated for further 24 h (37 °C, 5% CO_2) prior to treatment. Cytospins of each preparation were used to determine cell yield and purity. Therefore, 100 μl of cell suspension was mixed with 100 μl PBS and spun onto glass slides (600 rpm, 5 min) using a cytospin 3 (Shandon GmbH, Frankfurt, Germany), dried and stained by May-Gruenwald (Sigma–Aldrich, Taufkirchen, Germany) and Giemsa (Merck, Darmstadt, Germany). Analysis of the cytospin preparations using a BX Microscope (Olympus, Hamburg, Germany) revealed a macrophage purity of $\geqslant$98%.

2.6. Cytotoxicity

The effects of the particles on cell viability were determined using two independent approaches, i.e., the WST-1 assay and the LDH assay. The WST-1 assay (Roche, Mannheim, Germany) is based on the principle of reduction of the stable tetrazolium salt WST-1 to a soluble violet formazan product by viable cells. For this assay, cells (10.000/50 μl/well) were seeded in octoplicate into wells of 96-well microtiter plates. Treatment was performed by adding 50 μl of the different particle dilutions to the cells or 50 μl medium (controls). After 24 h of particle treatment 10 μl WST-1 solution (Roche, Mannheim, Germany) was added to five wells per treatment or control, and cells were incubated for a further 4 h (37 °C, 5% CO_2). The other three wells were used to control for absorption by the particles and were, therefore, measured without WST-1 substrate application. Optical density was then measured at 450 nm using a Multiskan ELISA reader (Thermo Fisher Scientific, Dreieich, Germany). For data calculation the mean of the obtained values of the wells without WST-1 was then subtracted from the mean of the values with WST-1 substrate and expressed as percentage of control cells.

The LDH assay (Roche, Mannheim, Germany) is based on the measurement of the leakage of the cytosolic, cell impermeable enzyme LDH through damaged cell membranes. For this assay, cells (10.000/50 μl/well) were seeded into wells of 96-well microtiter plates and treated as described for the WST-1 assay, after which the assay was performed and data were calculated according to manufacturer's instructions (LDH kit, Roche, Mannheim, Germany).

2.7. TNF-α release

Cells (50.000/50 μl/well) were seeded into wells of 96-well microtiter plates and treated as described for the cytotoxicity assays. After 24 h treatment cell-free supernatants were collected, centrifuged at 1000*g* for 10 min at 4 °C and aliquots were frozen at −20 °C until measurement. Supernatants were analyzed using a commercial TNF-α kit (R&D Systems, Wiesbaden, Germany) according to the manufacturer's manual using a Multiskan ELISA reader (Thermo Fisher Scientific, Dreieich, Germany).

2.8. Electron paramagnetic resonance (EPR)

Cells were seeded in complete culture medium in 96-well plates for 3 days (NR8383 cells) or 24 h (primary macrophages). Medium was then replaced with $HBSS^{(+/+)}$ 30 min prior to treatment. Cells were treated with particle suspensions at the indicated concentrations in the presence of the spin trapping agent 5,5-dimethyl-1-pyrroline-*N*-oxide (DMPO, 0.11 M, Sigma–Aldrich, Taufkirchen, Germany). Since pilot experiments revealed a gradual increase of the DMPO-signal measured 0.5, 1, 2, and 3 h after cell treatment with HPC, DQ12 or LPS, radical formation was measured at the latter time point in the cell-free supernatants using a MiniScope MS200 Spectrometer (Magnettech, Berlin, Germany) with the following instrumental settings: room temperature, microwave frequency = 9.39 GHz, magnetic field = 3360 G, sweep width = 100 G, scan time = 30 s, number of scans = 3, modulation amplitude = 2 G, and receiver gain = 900. Quantification was carried out on first derivation of EPR signal generated as a characteristic DMPO–OH quartet, as the mean of amplitudes, and outcomes are expressed in arbitrary units (a.u.).

2.9. Statistical analysis

All biological assays were performed in three independent experiments. Statistical analysis was performed using SPSS 14.0 for Windows. For all assays, concentration-dependent effects of the various treatments were evaluated using ANOVA testing followed by Dunett *t* post hoc comparison. LPS effects were evaluated by the Student's *t*-test. Statistically significant effects are indicated in the figures with *, **, and *** and represent significance at cut off levels of $p < 0.05$, $p < 0.01$, and $p < 0.001$, respectively.

3. Results

3.1. Particle characteristics

Test samples were characterized through a variety of parameters, from thorough chemical description to surface characteristics, morphology and size.

The Ca/P-ratio of the synthesized hydroxyapatites (HA-NR, HA-NP, HA-FN) as well as of the composite material HPC are shown in Table 2. Stoichiometric hydroxyapatite $Ca_{10}(PO_4)_6(OH)_2$ has a Ca/P-ratio of 1.67. This value only applies to the purchased needle-shaped nano-hydroxyapatite (HA-NN) (Huber et al., 2006). All other synthesized hydroxyapatites (HA-NR, HA-NP, HA-FN) as well as the composite material HPC show a higher Ca/P-ratio, indicating a higher Ca-content. HPC and HA-NP, which are synthesized under similar conditions (with the only difference in the presence (HPC) or absence (HA-NP) of protein), have an identical Ca/P-ratio of 1.95. Hydroxyapatites synthesized at higher pH, i.e., HA-NR at pH 9 and HA-FN at pH 10, revealed an even higher Ca/P-ratio of approximate 2.1. The protein content of HPC was determined to 36.2 wt%.

Specific surface values analyzed by BET are also displayed in Table 2. The specific surfaces of the nano-sized hydroxyapatites HA-NR (166 m^2/g) and HA-NP (154 m^2/g) are highly similar. The specific surface of HA-NN (106 m^2/g, Huber et al., 2006) is slightly lower, but still comparable with HA-NR and HA-NP. These results are in good agreement with the particle size data of all three nano-sized hydroxyapatites (Table 3). HA-FN is approximately ten times larger than the nano-sized hydroxyapatites and in correlation with its larger size possesses a specific surface of only 27 m^2/g. The BET value of HPC was found to lie in between those of the nano-sized and the larger hydroxyapatites. It cannot be excluded that the protein content might also influence nitrogen adsorption, which is the basic principle of BET. The drying necessary for BET inevitably leads to an altering of the test samples. Thus, results of BET provide relative values which might be considered on their own, but are not direct characteristics of the dispersed samples as they have been used in the macrophage assays.

Table 2
Chemical composition and specific surface of the test samples.

Test sample	Ca/P-ratio	Protein content (wt%)	Specific surface (m^2/g)
HPC	1.95 ± 0.28	36.2	67
HA-NP	1.95 ± 0.07	–	154
HA-NR	2.02 ± 0.20	–	166
HA-NN	1.67 (Huber et al., 2006)	–	106 (Huber et al., 2006)
HA-FN	2.12 ± 0.13	–	27

Particle size and morphology were analyzed by TEM and in case of HPC and HA-NP additionally by ESEM. The results are listed in Table 3 and shown in Figs. 1 and 2. Statements regarding particle morphology and particle size are limited by the method of electron microscopy, i.e., very big particles or agglomerates cannot be detected by electron microscopy, since the electron beam will not pass through. Also, the size of very small particles may not be measurable. In addition, the analyzed particles represent only a tiny fragment of the whole sample. Therefore, it is not feasible to provide statistically valid information about the size distribution. The results listed in Table 3 indicate the main fraction of the imaged particles.

Although HPC and HA-NP were synthesized under almost identical conditions, the only difference being that protein was present (HPC) or absent (HA-NP), their resulting particle size and morphology were found to be extremely different (Figs. 1a and b). Whereas HA-NP forms nano-sized plate-like particles, HPC consists of micro-sized particles of irregular shape. This clear difference was confirmed by ESEM as shown in Fig. 2. While TEM was performed using non-dried sediments, thus preserving the original particle morphology, the freeze-drying and grinding procedures used for ESEM samples led to an agglomeration of particles. HA-NP showed a rough surface, formed by single plate-like nanoparticles. In contrast, HPC exhibited a smooth surface with no fine structure, due to the protein content of approximately 36%.

Specific surface (9.4 m^2/g), particle size (average 960 μm) and morphology of DQ12 quartz are described elsewhere (Albrecht et al., 2002, 2004), as well as the characteristics of HA-NN (Huber et al., 2006), which are referenced in Tables 2 and 3.

3.2. Macrophage assays

3.2.1. WST-1 assay in NR8383 cells

No cytotoxic effects were observed with any of the test samples either in the fine or in the nano-size range (Fig. 3). HA-FN showed a tendency for a concentration-dependent decrease of formazan formation, indicating lower viability, however this did not reach statistical significance in the concentration range tested. In contrast, the positive control DQ12 quartz showed clear concentration-dependent effects in the WST-1 assay. A significant effect was observed with 30 μg/ml, and the highest concentration (300 μg/ml) resulted in a nearly complete (>90%) viability loss. An amount of 10 μg/ml LPS resulted in a viability reduction of about 50%.

3.2.2. LDH release from NR8383 cells

No significantly enhanced LDH release was detected after 24 h following treatment with the nano-hydroxyapatites (Fig. 4). The LDH release at 100 μg/ml of HPC, HA-NN, HA-NR and HA-FN was very similar, i.e., around 10%, whereas DQ12 quartz-induced LDH release was approximately five times higher (50%). Although HPC elicited a significant LDH release at this concentration, a cytotoxic

Table 3
Particle size and morphology of the test samples.

Test sample	Morphology	Average particle size (nm)	Figure
HPC	Irregular shaped	1200 × 2100	1a
HA-NP	Mainly nano-sized plates	3 × 20 × 45	1b
HA-NR	Mainly nano-sized rods	5 × 90	1c
HA-NN	Needles (Huber et al., 2006)	3 × 20 × 100 (Huber et al., 2006)	Huber et al. (2006)
HA-FN	Intermediate morphology between rods and needles (“blunt-ended needles”)	95 × 740	1d

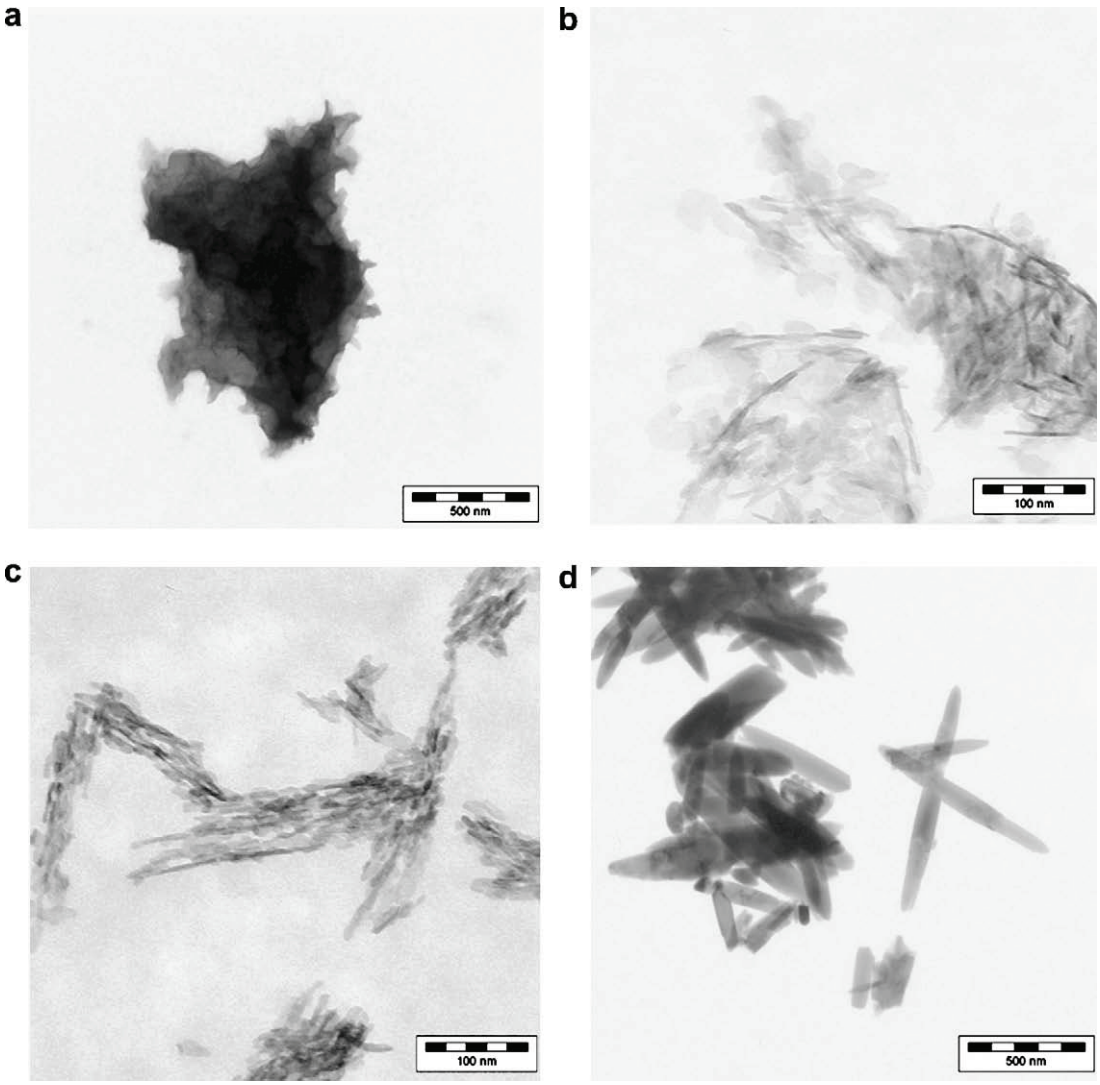

Fig. 1. Effect of the synthesis conditions on the particle size and morphology investigated by TEM. Particles were dispersed in wet form (no prior drying) in ethanol, sprayed onto a copper grid and investigated at 120 kV acceleration voltage. (a) The protein in HPC is contrasted with uranyl acetate and analyzed at a magnification of 10000, (b) HA-NP at a magnification of 45000, (c) HA-NR at a magnification of 45000 and (d) HA-FN at a magnification of 10000.

effect is not supported since concentration-dependency was not observed. In contrast, a clear dose-dependent increase of LDH was detected in the culture supernatants of HA-FN treated NR8383 cells. A significant effect was also observed with DQ12 quartz in a dose-dependent manner and with LPS, tested at a single dose of 10 μg/ml. Detailed results are shown in Fig. 4.

3.2.3. TNF-α release from NR8383 cells

All treatments were found to elicit significant release of TNF-α after 24 h (Fig. 5). When comparing the different particle treatments DQ12 quartz appeared to be the most potent one causing a significant TNF-α release already at 30 μg/ml. HPC, HA-NR and HA-NP were found to be effective at 100 μg/ml, whereas HA-NN and HA-FN induced a significant TNF-α release starting at 300 μg/ml. Notably, at the latter concentration the release of TNF-α by DQ12 quartz was found to be impaired. Similarly, most other compounds also showed a tendency for reduced cytokine values at the highest concentrations. LPS was found to be by far the most potent activator of NR8383 cells, inducing 300 times higher TNF-α levels than the negative control.

3.2.4. ROS generation by NR8383 cells

Significant increases in ROS generation were observed for HPC, HA-NN, HA-FN and DQ12 quartz (Fig. 6). HPC induces significant

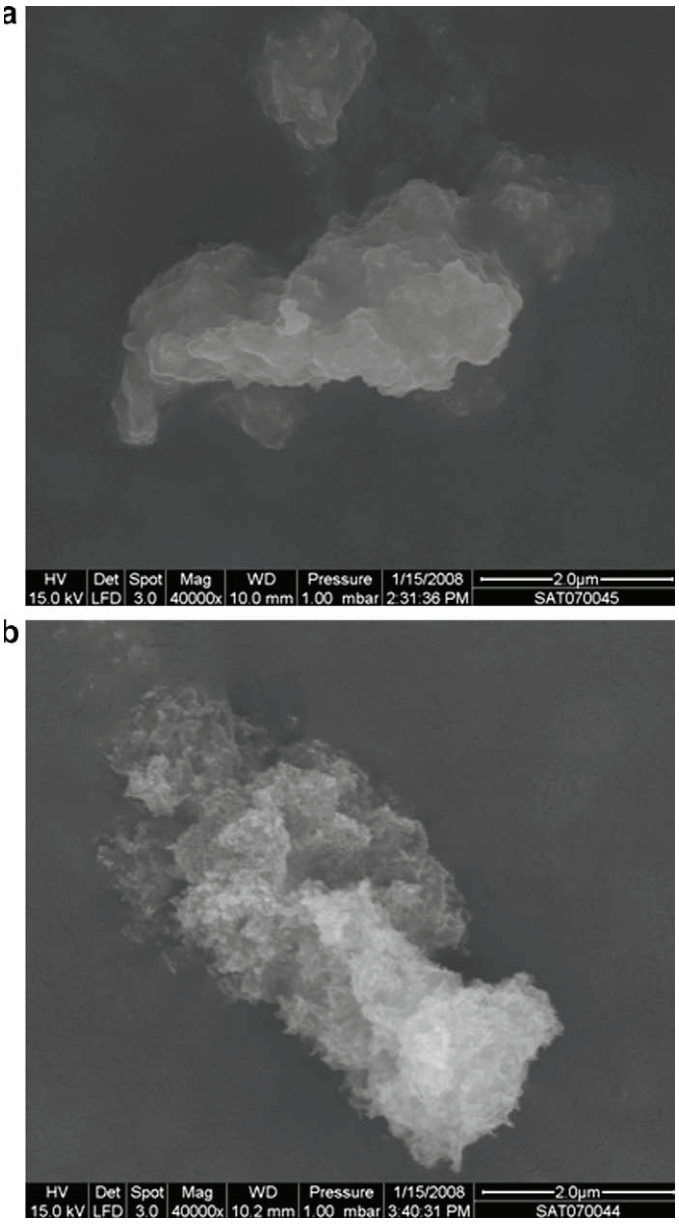

Fig. 2. Effect of the synthesis conditions on the morphology, investigated by ESEM. The freeze-dried, grinded samples were mounted on a carbon-taped sample holder, vaporized with gold and scanned at 15 kV acceleration voltage in an atmosphere of 1 mbar water vapor. Both samples are scanned at a magnification of 40000; (a) shows HPC and (b) HA-NP.

ROS generation starting at a concentration of 100 µg/ml in contrast to DQ12 quartz and HA-FN, which were only effective at 300 µg/ml. For HA-NN, a significant increase in ROS generation was only found at the highest concentration, i.e., 3000 µg/ml. Although LPS elicited increased ROS generation, this did not reach statistical significance when compared to the control.

3.2.5. LDH release from primary alveolar macrophages

Results of the LDH assay in the primary macrophages following 24 h treatment with the particles as well as LPS are shown in Fig. 7. Effects of the various particles were evaluated at two concentrations, 30 and 300 µg/ml. Treatment of the primary cells with DQ12 quartz resulted in a significant and concentration-dependent increase in LDH release. None of the other treatments (particles, LPS) were found to cause significant cytotoxicity towards the primary macrophages at the tested concentrations.

3.2.6. ROS formation by primary alveolar macrophages

Results of the analysis of the ROS generation by the primary macrophages upon the different treatments are shown in Fig. 8. Neither HPC nor any of the hydoxyapatite samples did show increased ROS production. Significant effects were observed with LPS, which was tested at a concentration of 10 µg/ml as well as with DQ12 quartz at the concentration of 300 µg/ml.

4. Discussion

The main focus of this study was to evaluate ROS generation by macrophages in response to different hydroxyapatite dispersions, while cytotoxicity and, for NR8383 cells, the production of TNF-α were also determined to obtain an overall picture of macrophage responsiveness. This approach is in agreement with observations that a combination of *in vitro* parameters of cytotoxicity and macrophage activation (i.e., TNF-α, ROS) has been a better predictor of the *in vivo* biocompatibility of particles after intratracheal instillation in rat lungs than a single parameter (Bruch et al., 2004). Thorough chemical and morphological characterization should provide the basis to investigate possible relations between physicochemical properties of the particles and the biological response. Inherent limitations of the available analytical methods must also be considered. In particular, electron microscopy does not allow for statistical evaluation of particle sizes and size distributions, and BET generates relative values that may correlate to the particle sizes, but should not be used to interpret the results of *in vitro* macrophage experiments using dispersed materials. It also needs to be considered that the presence of particulate material may affect readouts in *in vitro* assays, for instance enhanced absorption or interaction with specific testing reagents. This was addressed in this study by taking the particle background into account when evaluating the readouts of LDH and WST-1 assays. Moreover, the specific composition of the suspension fluid is likely to affect the reactivity of particles towards the macrophages due to changes in their agglomeration status and/or coating of surfaces by specific components. For instance, serum could act as a dispersion stabilizer for titanium dioxide and decreases the size distribution of dispersed nanoparticles compared to buffer (Bihari et al., 2008), and medium composition was demonstrated to influence nanoparticle agglomeration and associated ROS production in a human monocyte cell line (Foucaud et al., 2007). Such effects may also have influenced the results in the present study, where experiments were performed using complete cell culture medium except for ROS measurements which require $HBSS^{(+/+)}$ to avoid ROS scavenging effects by medium components (data not shown).

Trends in cytotoxicity as observed for the various treatments were overall highly similar using the two independent assays in NR8383 cells. A particular contrast was observed for HA-FN which induced a pronounced LDH release at the highest concentration, however clearly below the DQ12 quartz effect, but no significant effect in the WST-1 assay. Potential size-specific effects on cytotoxicity as observed with HA-FN have been shown for various types of particles (Choi et al., 2005; Yin et al., 2005; Schwarze et al., 2007). The size of primary particles or their aggregates can be considered a potential determinant for uptake and subsequent macrophage responses which could explain for the observed differences, since particles in the fine size range may induce more pronounced responses than in the nano-range (Rothen-Rutishauser et al., 2007), and the "ultrafine hypothesis" has been challenged previously by experimental studies (Schins et al., 2004).

In primary macrophages, no cytotoxic effects were observed with any test sample in the LDH assay, except for the positive control DQ12 quartz. Since the survival of macrophages is one of the key prerequisites for an effective elimination of particles, the

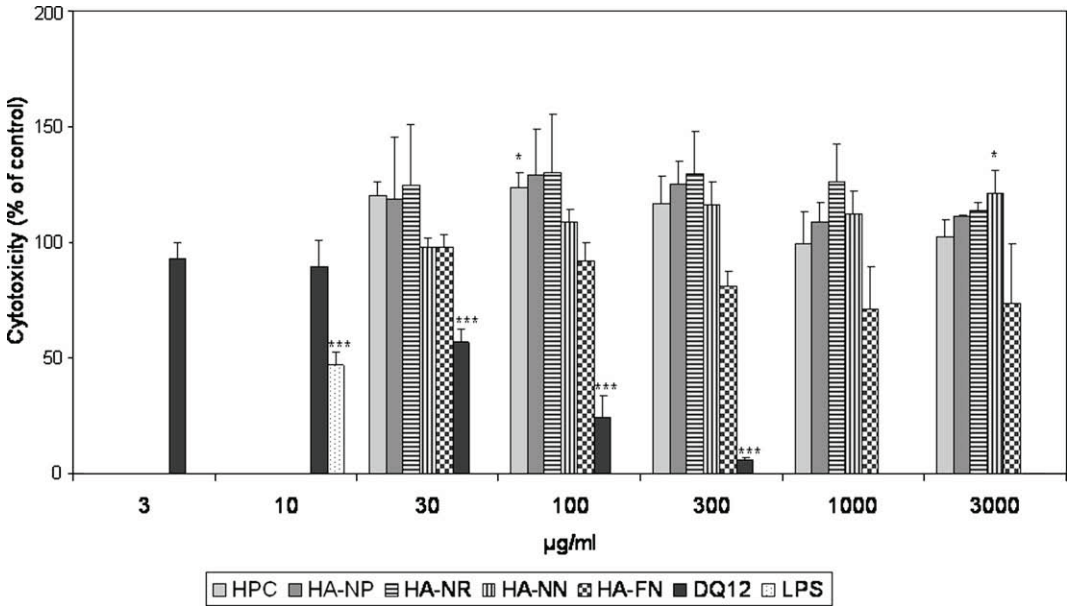

Fig. 3. Cytotoxicity in NR8383 macrophages after treatment with HPC, HA-NP, HA-NR, HA-NN, HA-FN, DQ12 quartz and LPS was investigated by WST-1 assay. Data are presented as mean ± SD ($n = 3$). Statistical significance of concentration-dependent particle effects was tested by Anova post hoc Dunett *t*. LPS effect was examined by Student's *t*-test ($^{*}p < 0.05$; $^{***}p < 0.001$).

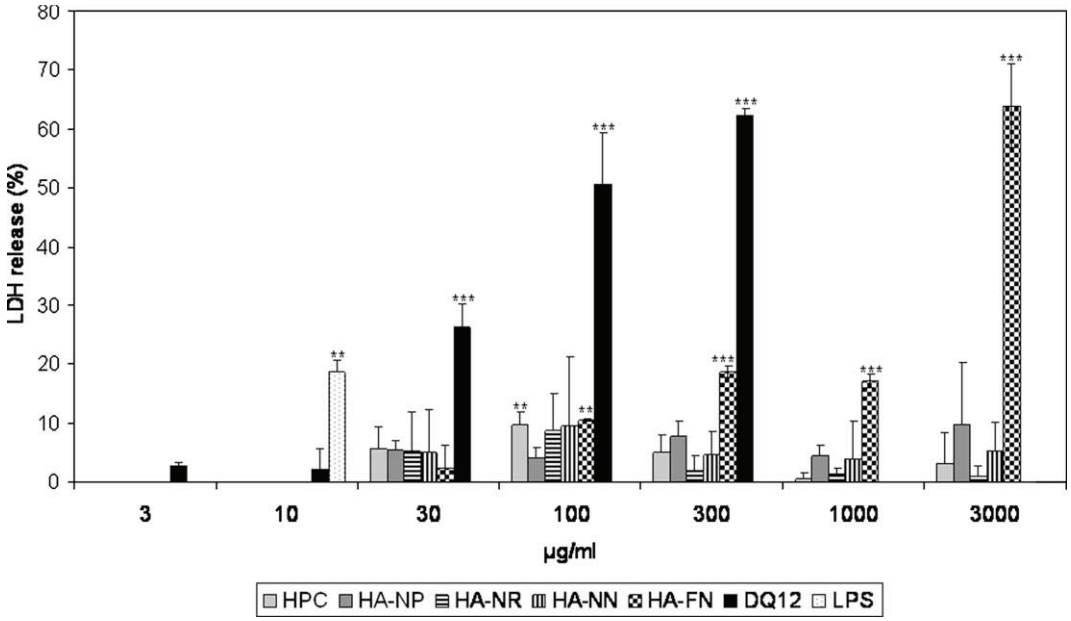

Fig. 4. Cytotoxicity in NR8383 macrophages treated with HPC, HA-NP, HA-NR, HA-NN, HA-FN, DQ12 quartz and LPS was tested by LDH assay. Data are demonstrated as mean ± SD ($n = 3$). Statistical significance of concentration-dependent particle effects was tested by Anova post hoc Dunett *t*. LPS effects were tested by Student's *t*-test ($^{**}p < 0.01$; $^{***}p < 0.001$).

observed low cytotoxicity provides evidence for a good biocompatibility of the tested materials.

TNF-α release, measured in NR8383 cells, showed significant effects for all materials albeit with different potency. Most notably, the effects of all particle samples on TNF-α production were approximately 35- to 50-fold lower than those induced by LPS, for which TNF-α is considered as a dominant mediator of its patho-physiological effects (Bauss et al., 1987; Tracey et al., 1988). DQ12 quartz was also found to be more potent than all hydroxyapatites as shown by a significant induction of TNF-α release after treatment with 30 µg/ml. Importantly, although quartz is known for its inflammatory properties (Bruch et al., 2004; Albrecht et al., 2007) and pathogenicity after high or chronic exposures (Porter et al., 2004), TNF-α is shown not to be the main mediator of these inflammatory effects (Albrecht et al., 2004, 2007). In fact, adverse quartz effects have been associated with its surface reactivity (Fubini, 1998; Albrecht et al., 2004) which is considered to drive the chronic, persistent inflammatory response by orchestrating the activation of multiple mediators. These, apart from TNF-α, include interleukin 1 and 10, macrophage inflammatory protein 2/interleukin 8, interferon-γ, as well as inflammatory cell-derived ROS (Driscoll et al., 1998; Porter et al., 2002; Srivastava et al., 2002; Knaapen et al., 2004). Previous investigations in our laboratory with surface-modified DQ12 quartz particles confirmed that

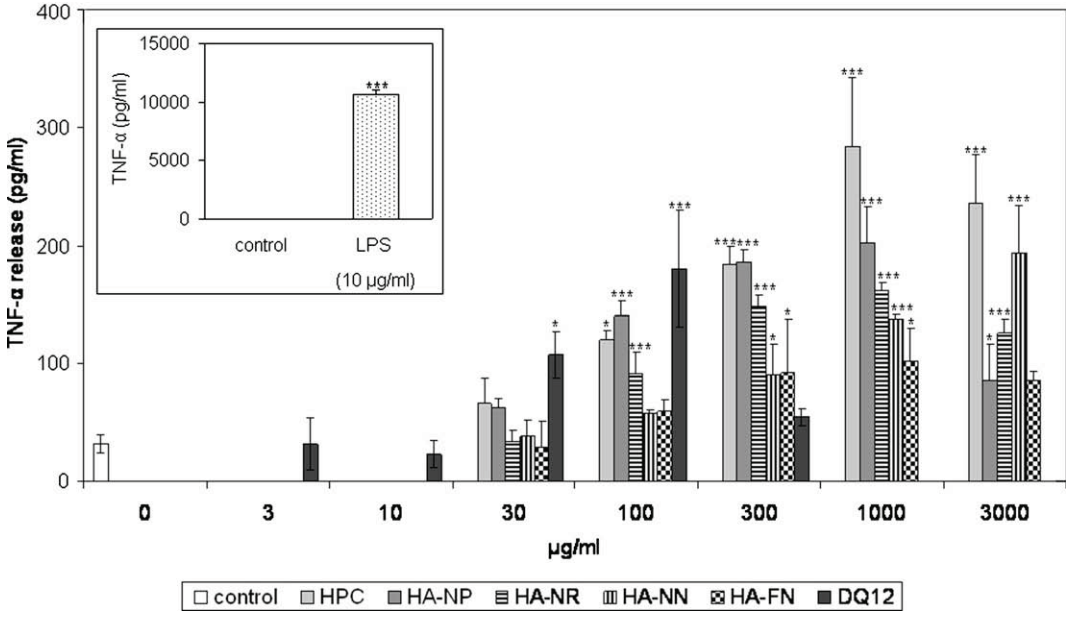

Fig. 5. TNF-α release from NR8383 macrophages after treatment with HPC, HA-NP, HA-NR, HA-NN, HA-FN, DQ12 quartz and LPS was investigated by ELISA. Data are shown as mean ± SD ($n = 3$). Statistical significance of concentration-dependent particle effects was tested by Anova post hoc Dunett *t*. LPS effect was tested by Student's *t*-test (*$p < 0.05$; ***$p < 0.001$).

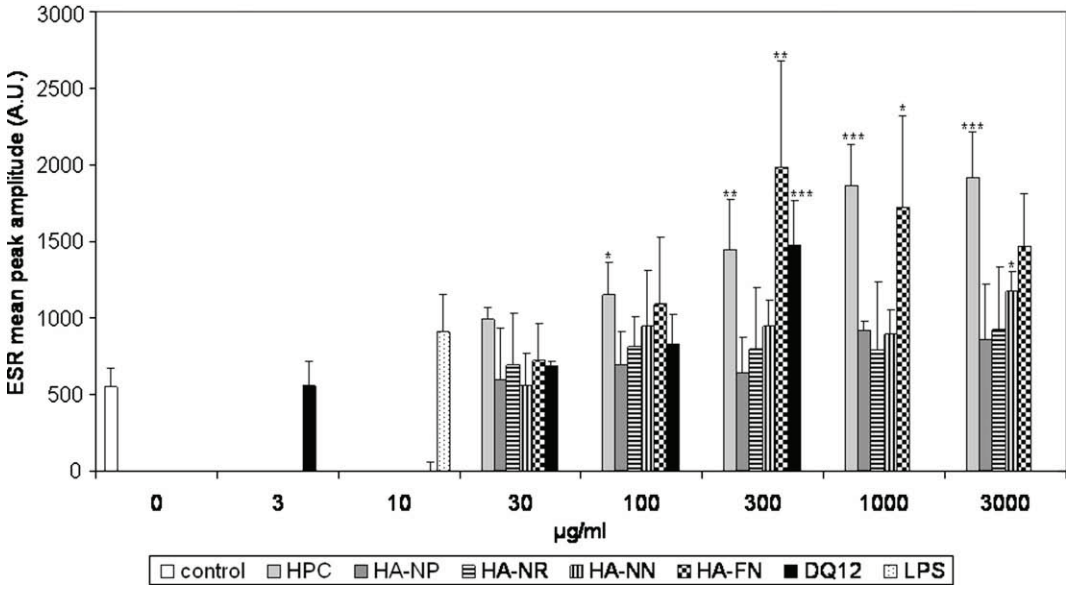

Fig. 6. Measurement of ROS generation by NR8383 macrophages upon treatment with HPC, HA-NP, HA-NR, HA-NN, HA-FN, DQ12 quartz and LPS was investigated by EPR. Data are demonstrated as mean ± SD ($n = 3$). Statistical significance of concentration-dependent particle effects was tested by Anova post hoc Dunett *t*. LPS effect was tested by Student's *t*-test (*$p < 0.05$; **$p < 0.01$; ***$p < 0.001$).

particles can elicit significant TNF-α release from macrophages *in vitro* without causing significant inflammation *in vivo* (Albrecht et al., 2007). Thus, TNF-α induction *per se* does not represent a determinant for an adverse effect, but inflammatory reactions can be regarded as critical when they persist over a longer period of time. In an independent study with the same HA samples (excluding HA-FN) in murine macrophages (Scheel et al., 2009), which focused on toxicity and cytokine production, a significant but transient TNF-α induction was observed for HPC, HA-NP and HA-NR. HA-NN which still showed a significant induction after 42 h in the macrophages was demonstrated to be safe and biocompatible in preclinical and clinical studies (Huber et al., 2006, 2007). Reduced TNF-α release as observed with the majority of the compounds at the higher treatment concentrations may be explained by TNF-α absorption on the relatively large particle surfaces, as has been reported for specific particles and cytokines (Woerle-Knirsch et al., 2006; Veranth et al., 2007), or by enhanced cytotoxicity affecting synthesis and secretion of TNF-α.

A major goal of this study was to investigate the production of ROS, for which EPR has been proved to be a suitable method. Two other methods, DHR (dihydrorhodamine 123) oxidation combined with flow cytometry (FACS analysis) and lucigenin-enhanced chemiluminescence were also evaluated. However these methods could not be validated for the tested materials. In the FACS analy-

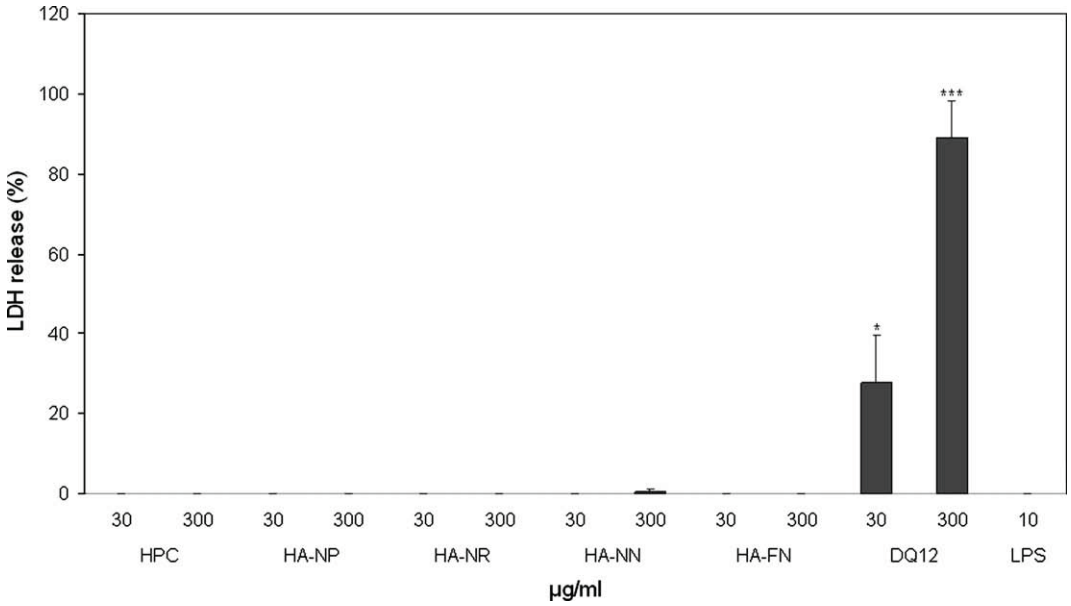

Fig. 7. Cytotoxicity in primary macrophages after treatment with HPC, HA-NP, HA-NR, HA-NN, HA-FN, DQ12 quartz and LPS tested by LDH assay. Data are presented as mean ± SD ($n = 3$). Statistical significance of concentration-dependent particle effects was tested by Anova post hoc Dunett *t*. LPS effects were tested by Student's *t*-test ($^{*}p < 0.05$; $^{***}p < 0.001$).

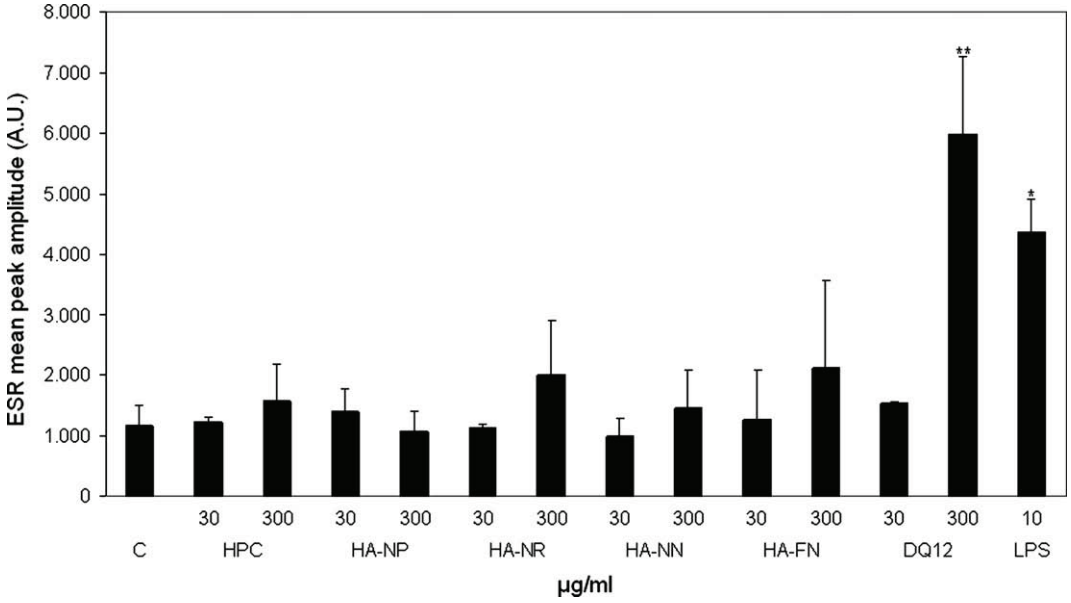

Fig. 8. Reactive oxygen species (ROS) generation of primary macrophages after treatment with HPC, HA-NP, HA-NR, HA-NN, HA-FN, DQ12 quartz and LPS was investigated by EPR. Data are presented as mean ± SD ($n = 3$). Statistical significance of concentration-dependent particle effects was examined by Anova post hoc Dunett *t*. LPS effects were tested by Student's *t*-test ($^{*}p < 0.05$; $^{**}p < 0.01$).

sis, particle events resulting from HPC, HA-NR and HA-NP mostly overlapped with cell events, thus impairing the necessary discrimination, while in the chemiluminescence assay particles interfered by quenching the signal (data not shown). Such artefacts were not observed with the EPR method.

Using this assay, the lack of ROS production by primary macrophages observed for all test samples did not confirm the initial findings with NR8383 cells, where significant ROS generation could be seen upon treatment with various materials, particularly HA-FN and HPC. As discussed before, particle size can modify the macrophage response. However, the overall trends in LDH effects were found to be rather similar at the tested concentrations, as noted above. Despite the partial tendency of HA-FN and HPC for a more pronounced activation of NR8383 macrophages compared to the nano-sized HA samples, overall no clear correlation between biological response and the specific physicochemical properties of the different test samples could be detected.

The NR8383 cell line is derived from rat macrophages, and has been used routinely in many investigations (Chen et al., 1997; Gao et al., 2001; Diabate et al., 2002; Biggs et al., 2003; Albrecht et al., 2007; Pulskamp et al., 2007; Wagner et al., 2007). The contrasting observations in NR8383 cells and primary macrophages may be explained by the modified characteristics (immortalization, antioxidant status, differentiation, surface receptor expression, etc.) of

the cell line compared to primary cells, which obviously resemble more closely the *in vivo* situation (Welborn et al., 1993; Fisher et al., 2000; Valles et al., 2006; Haberzettl et al., 2007). In this regard, both LPS and DQ12 quartz caused a stronger ROS generation by primary macrophages compared to NR8383 cells. These findings support the consensus that preferably, primary cells should be used for such measurements (Rao et al., 2002; Maurya et al., 2007; Yang et al., 2008). In general, *in vitro* cellular systems will need to be further developed, standardized and validated (relative to *in vivo* effects) in order to provide increasingly useful screening data on the relative toxicity of particulate materials (Sayes et al., 2007) and to potentially gain official regulatory acceptance.

5. Conclusions

Various tested hydroxyapatite materials in NR8383 cells and primary macrophages demonstrated an overall low toxicity. Differences could be observed within these cell types regarding the production of ROS, pointing out to inherent differences in both test systems, with primary macrophages being considered more relevant for assessing the physiological situation. Present findings support a good biocompatibility of the various pure hydroxyapatite materials as well as the hydroxyapatite–protein-composite. The usefulness of *in vitro* methods as screening tools to assess the potential hazard of small particles has been demonstrated. Obviously however, future work needs to focus on further development and standardization of the testing of nanomaterials using *in vitro* systems.

Acknowledgements

We thank Christel Weishaupt for technical assistance (IUF, Düsseldorf), Burkhardt Eschen for TEM analyses (Henkel AG & Co. KGaA, Düsseldorf), and Elke Mertens for editorial assistance (Henkel AG & Co. KGaA, Düsseldorf).

References

Aam, B.B., Fonnum, F., 2007. Carbon black particles increase reactive oxygen species formation in rat alveolar macrophages in vitro. Archives of Toxicology 81, 441–446.

Albrecht, C., Borm, P.J., Adolf, B., Timblin, C.R., Mossman, B.T., 2002. In vitro and in vivo activation of extracellular signal-regulated kinases by coal dusts and quartz silica. Toxicology and Applied Pharmacology 184, 37–45.

Albrecht, C., Schins, R.P., Hohr, D., Becker, A., Shi, T., Knaapen, A.M., Borm, P.J., 2004. Inflammatory time course after quartz instillation: role of tumor necrosis factor-alpha and particle surface. American Journal of Respiratory Cell and Molecular Biology 31, 292–301.

Albrecht, C., Hohr, D., Haberzettl, P., Becker, A., Borm, P.J., Schins, R.P., 2007. Surface-dependent quartz uptake by macrophages: potential role in pulmonary inflammation and lung clearance. Inhalation Toxicology 19 (Suppl. 1), 39–48.

Arts, C.J.J., Verdonschot, N., Schreurs, B.W., Buma, P., 2006. The use of a bioresorbable nano-crystalline hydroxyapatite paste in acetabular bone impaction grafting. Biomaterials 27, 1110–1118.

Bauss, F., Droge, W., Mannel, D.N., 1987. Tumor necrosis factor mediates endotoxic effects in mice. Infection and Immunity 55, 1622–1625.

Biggs, D.L., Lengsfeld, C.S., Hybertson, B.M., Ng, K.Y., Manning, M.C., Randolph, T.W., 2003. In vitro and in vivo evaluation of the effects of PLA microparticle crystallinity on cellular response. Journal of Control Release 92, 147–161.

Bihari, P., Vippola, M., Schultes, S., Praetner, M., Khandoga, A.G., Reichel, C.A., Coester, C., Tuomi, T., Rehberg, M., Krombach, F., 2008. Optimized dispersion of nanoparticles for biological in vitro and in vivo studies. Particle and Fibre Toxicology 5.

Brown, D.M., Wilson, M.R., MacNee, W., Stone, V., Donaldson, K., 2001. Size-dependent proinflammatory effects of ultrafine polystyrene particles: a role for surface area and oxidative stress in the enhanced activity of ultrafines. Toxicology and Applied Pharmacology 175, 191–199.

Bruch, J., Rehn, S., Rehn, B., Borm, P.J., Fubini, B., 2004. Variation of biological responses to different respirable quartz flours determined by a vector model. International Journal of Hygiene and Environmental Health 207, 203–216.

Brunauer, S., Emmett, P.H., Teller, E., 1938. Adsorption of gases in multimolecular layers. Journal of the American Chemical Society 60, 309–319.

Brunner, T.J., Wick, P., Manser, P., Spohn, P., Grass, R.N., Limbach, L.K., Bruinink, A., Stark, W.J., 2006. In vitro cytotoxicity of oxide nanoparticles: comparison to asbestos, silica, and the effect of particle solubility. Environmental Science and Technology 40, 4374–4381.

Chen, F., Sun, S., Kuhn, D.C., Gaydos, L.J., Shi, X., Lu, Y., Demers, L.M., 1997. Involvement of NF-kappaB in silica-induced cyclooxygenase II gene expression in rat alveolar macrophages. The American Journal of Physiology 272, L779–L786.

Choi, M.G., Koh, H.S., Kluess, D., O'Connor, D., Mathur, A., Truskey, G.A., Rubin, J., Zhou, D.X., Sung, K.L., 2005. Effects of titanium particle size on osteoblast functions in vitro and in vivo. Proceedings of the National Academy of Science USA 102, 4578–4583.

Diabate, S., Mulhopt, S., Paur, H.R., Wottrich, R., Krug, H.F., 2002. In vitro effects of incinerator fly ash on pulmonary macrophages and epithelial cells. International Journal of Hygiene and Environmental Health 204, 323–326.

Donaldson, K., Tran, C.L., 2002. Inflammation caused by particles and fibers. Inhalation Toxicology 14, 5–27.

Donaldson, K., Tran, L., Jimenez, L.A., Duffin, R., Newby, D.E., Mills, N., MacNee, W., Stone, V., 2005. Combustion-derived nanoparticles: a review of their toxicology following inhalation exposure. Particle and Fibre Toxicology 2, 10.

Driscoll, K.E., Carter, J.M., Howard, B.W., Hassenbein, D., Burdick, M., Kunkel, S.L., Strieter, R.M., 1998. Interleukin-10 regulates quartz-induced pulmonary inflammation in rats. The American Journal of Physiology 275, L887–L894.

Duffin, R., Gilmour, P.S., Schins, R.P., Clouter, A., Guy, K., Brown, D.M., MacNee, W., Borm, P.J., Donaldson, K., Stone, V., 2001. Aluminium lactate treatment of DQ12 quartz inhibits its ability to cause inflammation, chemokine expression, and nuclear factor-kappaB activation. Toxicology and Applied Pharmacology 176, 10–17.

Evans, E.J., 1991. Toxicity of hydroxyapatite in vitro: the effect of particle size. Biomaterials 12, 574–576.

Fisher, C.E., Rossi, A.G., Shaw, J., Beswick, P.H., Donaldson, K., 2000. Release of TNFalpha in response to SiC fibres: differential effects in rodent and human primary macrophages, and in macrophage-like cell lines. Toxicology in Vitro 14, 25–31.

Foucaud, L., Wilson, M.R., Brown, D.M., Stone, V., 2007. Measurement of reactive species production by nanoparticles prepared in biologically relevant media. Toxicology Letters 174, 1–9.

Fubini, B., 1998. Surface chemistry and quartz hazard. The Annals of Occupational Hygiene 42, 521–530.

Gao, N., Keane, M.J., Ong, T., Ye, J., Miller, W.E., Wallace, W.E., 2001. Effects of phospholipid surfactant on apoptosis induction by respirable quartz and kaolin in NR8383 rat pulmonary macrophages. Toxicology and Applied Pharmacology 175, 217–225.

Grandjean-Laquerriere, A., Laquerriere, P., Laurent-Maquin, D., Guenounou, M., Phillips, T.M., 2004. The effect of the physical characteristics of hydroxyapatite particles on human monocytes IL-18 production in vitro. Biomaterials 25, 5921–5927.

Grandjean-Laquerriere, A., Laquerriere, P., Guenounou, M., Laurent-Maquin, D., Phillips, T.M., 2005. Importance of the surface area ratio on cytokines production by human monocytes in vitro induced by various hydroxyapatite particles. Biomaterials 26, 2361–2369.

Haberzettl, P., Duffin, R., Kramer, U., Hohr, D., Schins, R.P., Borm, P.J., Albrecht, C., 2007. Actin plays a crucial role in the phagocytosis and biological response to respirable quartz particles in macrophages. Archives of Toxicology 81, 459–470.

Huber, F.X., Belyaev, O., Hillmeier, J., Kock, H.J., Huber, C., Meeder, P.J., Berger, I., 2006. First histological observations on the incorporation of a novel nanocrystalline hydroxyapatite paste OSTIM in human cancellous bone. BMC Musculoskeletal Disorders 7, 50.

Huber, F.X., Berger, I., McArthur, N., Huber, C., Kock, H.P., Hillmeier, J., Meeder, P.J., 2007. Evaluation of a novel nanocrystalline hydroxyapatite paste and a solid hydroxyapatite ceramic for the treatment of critical size bone defects (CSD) in rabbits. Journal of Materials Science: Materials in Medicine.

Knaapen, A.M., Borm, P.J., Albrecht, C., Schins, R.P., 2004. Inhaled particles and lung cancer. Part A: Mechanisms. International Journal of Cancer 109, 799–809.

Lane, K.B., Egan, B., Vick, S., Abdolrasulnia, R., Shepherd, V.L., 1998. Characterization of a rat alveolar macrophage cell line that expresses a functional mannose receptor. Journal of Leukocyte Biology 64, 345–350.

Laquerriere, P., Grandjean-Laquerriere, A., Jallot, E., Balossier, G., Frayssinet, P., Guenounou, M., 2003. Importance of hydroxyapatite particles characteristics on cytokines production by human monocytes in vitro. Biomaterials 24, 2739–2747.

Lewinski, N., Colvin, V., Drezek, R., 2008. Cytotoxicity of nanoparticles. Small (Weinheim an der Bergstrasse, Germany) 4, 26–49.

Maurya, M.R., Benner, C., Pradervand, S., Glass, C., Subramaniam, S., 2007. Systems biology of macrophages. Advances in Experimental Medicine and Biology 598, 62–79.

Pan, Y., Neuss, S., Leifert, A., Fischler, M., Wen, F., Simon, U., Schmid, G., Brandau, W., Jahnen-Dechent, W., 2007. Size-dependent cytotoxicity of gold nanoparticles. Small (Weinheim an der Bergstrasse, Germany) 3, 1941–1949.

Porter, D.W., Millecchia, L., Robinson, V.A., Hubbs, A., Willard, P., Pack, D., Ramsey, D., McLaurin, J., Khan, A., Landsittel, D., Teass, A., Castranova, V., 2002. Enhanced nitric oxide and reactive oxygen species production and damage after inhalation of silica. American Journal of Physiology 283, L485–L493.

Porter, D.W., Hubbs, A.F., Mercer, R., Robinson, V.A., Ramsey, D., McLaurin, J., Khan, A., Battelli, L., Brumbaugh, K., Teass, A., Castranova, V., 2004. Progression of lung inflammation and damage in rats after cessation of silica inhalation. Toxicological Sciences 79, 370–380.

Pulskamp, K., Diabate, S., Krug, H.F., 2007. Carbon nanotubes show no sign of acute toxicity but induce intracellular reactive oxygen species in dependence on contaminants. Toxicology Letters 168, 58–74.

Ramesh, M., Turner, L.F., Yadav, R., Rajan, T.V., Vella, A.T., Kuhn, L.T., 2007. Effects of the physico-chemical nature of two biomimetic crystals on the innate immune response. International Immunopharmacology 7, 1617–1629.

Rao, K.M., Meighan, T., Bowman, L., 2002. Role of mitogen-activated protein kinase activation in the production of inflammatory mediators: differences between primary rat alveolar macrophages and macrophage cell lines. Journal of Toxicology and Environmental Health 65, 757–768.

Rothen-Rutishauser, B., Muhlfeld, C., Blank, F., Musso, C., Gehr, P., 2007. Translocation of particles and inflammatory responses after exposure to fine particles and nanoparticles in an epithelial airway model. Particle and Fibre Toxicology 4, 9.

Sayes, C.M., Reed, K.L., Warheit, D.B., 2007. Assessing toxicity of fine and nanoparticles: comparing in vitro measurements to in vivo pulmonary toxicity profiles. Toxicological Sciences 97, 163–180.

Scheel, J., Weimans, S., Thiemann, A., Heisler, E., Hermann, M., 2009. Exposure of the murine RAW 264.7 macrophage cell line to hydroxyapatite dispersions of various composition and morphology: assessment of cytotoxicity, activation and stress response. Toxicology in Vitro 23, 531–538.

Schins, R.P., Borm, P.J., 1999. Mechanisms and mediators in coal dust induced toxicity: a review. The Annals of Occupational Hygiene 43, 7–33.

Schins, R.P., Lightbody, J.H., Borm, P.J., Shi, T., Donaldson, K., Stone, V., 2004. Inflammatory effects of coarse and fine particulate matter in relation to chemical and biological constituents. Toxicology and Applied Pharmacology 195, 1–11.

Schwarze, P.E., Ovrevik, J., Hetland, R.B., Becher, R., Cassee, F.R., Lag, M., Lovik, M., Dybing, E., Refsnes, M., 2007. Importance of size and composition of particles for effects on cells in vitro. Inhalation Toxicology 19 (Suppl. 1), 17–22.

Srivastava, K.D., Rom, W.N., Jagirdar, J., Yie, T.A., Gordon, T., Tchou-Wong, K.M., 2002. Crucial role of interleukin-1beta and nitric oxide synthase in silica-induced inflammation and apoptosis in mice. American Journal of Respiratory and Critical Care Medicine 165, 527–533.

Tracey, K.J., Lowry, S.F., Cerami, A., 1988. Cachectin/TNF mediates the pathophysiological effects of bacterial endotoxin/lipopolysaccharide, (LPS). Progress in Clinical and Biological Research 272, 77–88.

Unfried, K., Albrecht, C., Klotz, L.-O., Mikecz von, A., Grether-Beck, S., Schins, R.P.F., 2007. Cellular responses to nanoparticles: target structures and mechanisms. Nanotoxicology 1, 52–71.

Valles, G., Gonzalez-Melendi, P., Gonzalez-Carrasco, J.L., Saldana, L., Sanchez-Sabate, E., Munuera, L., Vilaboa, N., 2006. Differential inflammatory macrophage response to rutile and titanium particles. Biomaterials 27, 5199–5211.

Veranth, J.M., Kaser, E.G., Veranth, M.M., Koch, M., Yost, G.S., 2007. Cytokine responses of human lung cells, (BEAS-2B) treated with micron-sized and nanoparticles of metal oxides compared to soil dusts. Particle and Fibre Toxicology 4, 2.

Wagner, A.J., Bleckmann, C.A., Murdock, R.C., Schrand, A.M., Schlager, J.J., Hussain, S.M., 2007. Cellular interaction of different forms of aluminum nanoparticles in rat alveolar macrophages. The Journal of Physical Chemistry 111, 7353–7359.

Welborn, M.B., Christman, J.W., Shepherd, V.L., 1993. Regulation of tumor necrosis factor-alpha receptors on macrophages: differences between primary macrophages and transformed macrophage cell lines. Regional Immunology 5, 158–164.

Woerle-Knirsch, J.M., Pulskamp, K., Krug, H.F., 2006. Oops they did it again! Carbon nanotubes hoax scientists in viability assays. Nano Letters 6, 1261–1268.

Yang, C.S., Shin, D.M., Lee, H.M., Son, J.W., Lee, S.J., Akira, S., Gougerot-Pocidalo, M.A., El-Benna, J., Ichijo, H., Jo, E.K., 2008. ASK1-p38 MAPK-p47phox activation is essential for inflammatory responses during tuberculosis via TLR2-ROS signalling. Cellular Microbiology 10, 741–754.

Yin, H., Too, H.P., Chow, G.M., 2005. The effects of particle size and surface coating on the cytotoxicity of nickel ferrite. Biomaterials 26, 5818–5826.

CHAPTER V

SUMMARY & GENERAL DISCUSSION

5.1 SUMMARY & GENERAL DISCUSSION

The lung is a susceptible organ to diseases, since it is permanently exposed to the outside environment by breathing. Among all types of professional phagocytes, AMΦ represent those with the most frequent contact to environmental pathogens and particles. AMΦ are equipped with an array of defence mechanisms allowing them to release inflammatory cytokines and growth factors as well as ROS [Castranova & Vallyathan 2000]. The phagocytosis of pathogens can lead to activation of these cells and subsequently to the respiratory burst: In association with the release of inflammatory mediators this has been implicated as a critical factor in the development and progression of occupational lung diseases [Rao 2000; Zhang et al 2000]. Moreover, sustained or chronic generation of oxidants has been associated with induction of DNA-damage and proliferation in lung tissues. Hence this process is also implicated in the mutagenic and carcinogenic effects of inhaled particles [Schins & Hei 2006; Schins & Knaapen 2007].

The adverse health effects associated with exposure to particles in both occupational (e.g. silica-containing dusts, metal oxides) and environmental settings ($PM_{2.5}$, PM_{10}) are nowadays well recognised [Donaldson & Borm 2006]. The increased use in recent years of NP in various industrial and medical applications has also led to the concern about their safety. NP may find their way into the human body by different uptake or translocation routes upon inhalation, ingestion, dermal exposure or application and injection [Oberdörster et al 2005].

However, there is still a lack of consensus in the literature on NP toxicity due to varying testing strategies concerning the applied methods, materials and cell lines. Therefore, standardization in experimental set ups, such as choice of model (cell line, animal species) and exposure conditions (cell confluency, culture medium conditions for suspending cells, dosimetry) are necessary in order to get a common basis for effective comparisons between studies conducted by different groups [Oberdörster et al 2005]. All studies of the present thesis were performed in the well established and widely accepted rat AMΦ cell line NR8383 [Helmke et al 1989] as the shared basis for comparisons of cellular reactions to different types of particles.

The aim of this thesis was the investigation of the mechanisms and consequences of particle-MΦ-interactions. This was achieved by the evaluation of the cellular responses of AMΦ in relation to specific physico-chemical properties of the particles, i.e. particle size, surface area and shape, chemical composition and surface contamination with iron. Three independent studies were conducted in the framework of this thesis, using the NR8383 rat MΦ cell line. The particulate materials under investigations were TiO_2 [study 1], crystalline silica [study 2],

and hydroxyapatite [study 3], respectively. In the latter study, apart from NR8383 cells primary AMΦ obtained from rat lung by bronchoalveolar lavage were used. The well investigated crystalline silica sample DQ12 represented another common basis in all three studies, being the positive control. This sample has been demonstrated to induce oxidative stress and cytokine release from AMΦ *in vitro* [Albrecht et al 2007; Haberzettl et al 2008; van Berlo et al 2009] as well as to trigger pulmonary inflammation and oxidative stress *in vivo*, i.e. in the lungs of rats [Albrecht et al 2004; 2005] and mice [van Berlo et al 2010]. Furthermore, DQ12 has also been proven as a relevant material to investigate processes of phagocytosis [Albrecht et al 2007; Haberzettl et al 2007]. The chosen cellular endpoints were selected to address the pathways of particle uptake as well as the subsequent responses of the phagocytes in terms of oxidative stress induction and activation of pro-inflammatory responses on various cellular levels. Table 5.1 provides a combined overview of the major findings of the three studies.

Study 1 [chapter II] describes the comparative evaluation of uptake of TiO_2 particles in the fine size mode versus those in the ultrafine, i.e. nanosize range, by AMΦ and their subsequent distinct cellular reactions to these particles in comparison to DQ12. TiO_2 particles were chosen for various reasons. On the one hand, TiO_2 represents a material for which exposure is relevant in view of its wide use in a current and anticipated future applications (e.g. as pigment, filler, food colorant). On the other hand, TiO_2 particles are highly insoluble in biological systems and hence different types of these materials in terms of size represent an ideal model to address the effect of particle size and surface area on biological responses [Oberdörster et al 2005]. The two different samples of TiO_2 used in present study were thoroughly characterized by elemental- and thermogravometric analysis as well as transmission electron microscopy. Particle aggregation and agglomeration tendency in assay-specific suspensions were investigated with dynamic- and dark field light scattering microscopy. Distinct cellular endpoints were investigated, i.e. cellular toxicity, ROS generation, intracellular calcium release, NF-κB activation, cytokine release and mRNA expression, to represent a panel of markers of oxidative and pro-inflammatory responses. Additionally, the particle type-specific routes of active uptake mechanisms in AMΦ were evaluated by applying specific inhibitors to caveolae and clathrin-mediated endocytosis, actin-dependent macropinocytosis and classical phagocytosis.

The results of the study revealed the existence of marked differences in particle size distributions and agglomeration sizes for each, ufTiO_2 and fTiO_2, when suspended in culture medium. The behaviour of the samples in suspension provided an explanation for the

observed size-specific uptake mechanisms by the AMΦ. The enhanced reactivity of $ufTiO_2$ when compared to the $fTiO_2$ was reflected by its ability to trigger a typical pro-inflammatory response characterized by NF-κB activation, TNF-α secretion, as well as iNOS mRNA up-regulation. The $ufTiO_2$ sample, in contrast to $fTiO_2$, induces the oxidative stress marker HO-1 as well as enhanced ROS generation measured in the supernatants of the AMΦ. Interestingly however, $ufTiO_2$ did not lead to the production of IL-1β, unlike DQ12, whereas DQ12 failed to induce iNOS mRNA expression. As such, further investigations are required, on the one hand, to determine the precise impact of both materials on the induction of proIL-1β and its subsequent activation via the inflammasome pathway as well as on the other hand, on the signal transduction pathways that cause activation of the iNOS gene in AMΦ. Interestingly, in this regard, it could be observed that all three materials (i.e. $ufTiO_2$, $fTiO_2$ and DQ12) were taken up by the phagocytes and increased intracellular ROS generation, whereas no difference in enhancing of $[Ca^{2+}]_i$ was found between both TiO_2. This suggests that these responses may be due to the particle uptake itself, irrespective of the physico-chemical properties of the materials. The overall evaluation of this study demonstrates that the extent and pattern of cellular responses of AMΦ upon interaction with particles is determined by the composition of the material (DQ12 versus TiO_2) as well as by the size and/or the surface area of the material ($fTiO_2$ versus $ufTiO_2$) as depicted in Table 5.1.

In **study 2** [chapter III] iron impregnated quartz particles (0.67 and 6.7 % wt), as well as two control quartzes were investigated. Again, the responses of the AMΦ cells to the different materials were investigated in relation to a thorough investigation of their physico-chemical properties. All samples used in the study showed a remarkable Fenton activity in cell-free measurements. Especially the particles which were impregnated with high iron content showed the highest ability in HO· generation, followed by the low iron loaded sample. In contrast to these observations in a cell free system, the reactivity of iron loaded quartz particles *in vitro* was significantly reduced compared to the original quartz sample. This suggests that intracellular defence mechanisms anticipate radical effects, and that iron thereby causes an inhibition of quartz-mediated activation of MΦ. The original quartz sample displayed inflammatory activity by triggering TNF-α secretion as well as cytotoxic capacity, which were completely abolished in iron loaded quartzes. Another major observation was that the original quartz sample still exhibits much lower inflammatory responses by AMΦ when compared to the DQ12 sample which was used as positive control. These differences could be explained by the presence of traces of aluminium found on the purchased quartz. In previous studies it has been shown that aluminium compounds, which may be naturally

occurring on quartz samples reduce the toxic potential of this material [Duffin et al 2001; Albrecht et al 2004]. The present study also shows that trace amounts of iron may impact on the toxic and inflammatory potency of crystalline silica

It is nowadays generally accepted that the hazard of crystalline quartz dusts is a variable entity. In 1997, the International Agency for Research on Cancer has highlighted that this mineral dust is not uniformly carcinogenic across all industries where there is quartz exposure [IARC 1997]. This variable quartz hazard is considered to be due to natural interactions of particle surfaces with for instance aluminium ions, e.g. present in kaolinites and bentonites, or variable iron content, hence leading to altered health effects of quartz [Donaldson & Borm 1998; Fubini 1998]. In this regard, it was previously shown that quartz samples collected from different workplaces have contrasting inflammogenic potency [Clouter et al 2001; Fubini et al 2004]. The results from study 2 indicate that such differences may result from specific interactions between AMΦ and contamination on the quartz particle surface. As such, it will be interesting to investigate whether iron and/or aluminium can affect specific mechanisms of particle uptake and/or associated MΦ responses as described for quartz in study 1 [chapter II].

In **study 3** [chapter IV], the biocompatibility of five hydroxyapatite (HA) materials of different size and morphology was investigated. The materials used in this study were, along with D12, the following: nano-needle shaped, -rod-like, -plate-like, fine-dull needle-shaped and a hydroxyapatite-protein-composite (HPC). Two types of cytotoxicity tests as well as inflammatory and oxidative endpoints were performed in NR8383 cells. Specific experiments were also performed in primary AMΦ obtained from rat lungs by bronchoalveolar lavage. The fine-sized structure and the HPC showed a partial tendency in the activation of NR8383 cells by enhanced cytotoxicity and release of TNF-α, unlike to the nano-sized samples. In contrast, no effect on cytotoxicity and HO· generation was determined in primary AMΦ, which are considered being more relevant to physiological conditions. These contrasting observations of HA effects in the primary cells versus cell line may be explained by the modified characteristics of NR8383 cells: responses to particles may depend on the immortalization and differentiation status of the cells as well as on differences in antioxidant defence mechanisms. The results of the current study are confirmed by similar studies on primary human monocyte-MΦ [Motskin et al 2009] and the murine MΦ-like RAW264.7 cell line [Scheel et al 2009]. In detail, Motskin et al. treated human monocyte-MΦ with HA particles exhibiting a surface area in the range of the HA particles used in study 3. These HA particles merely varied in the mode of synthesis and processing, which can lead to different physico-

chemical properties. Since MΦ are able to recognize size and shape of their targets, the quantitative and qualitative particle uptake is very dependent on particles' morphology, thus being crucial for the subsequent cellular responses [Champion & Mitragotri 2009; Doshi & Mitragotri 2010]. Overall, the obtained findings in study 3 support a good biocompatibility of the various pure HA particles as well as for the HPC, since the results of the primary AMΦ are estimated to be more relevant in the physiologic context. Furthermore, this study demonstrates that not all materials in the nano-size range are toxic *per se*. The nano-sized HA appears to be biocompatible and suitable for industrial approaches for instance for cosmetic and medical applications.

Table 5.1 Summary of the key parameters in NR8383 cells of study 1, 2 and 3.

Study	Material	Cytotoxicity	Inflammation		Oxidative Stress	
		(LDH, WST-1)	TNF-α (ELISA)	IL-1β (ELISA)	ROS (EPR)	HO-1 (RT-PCR)
1, 2, 3	DQ12	+++	+++	++	++	++
1	$fTiO_2$	–	–	–	–	–
	$ufTiO_2$	+++	++	–	++	++
2	Qz	+	+	n.d.	n.d.	–
	Qz + Fe	+/–	+/–			–
3	HPC	–	++		+	
	HA-NP	–	+		–	
	HA-NR	–	+	n.d.	–	n.d.
	HA-NN	–	+/–		–	
	HA-FN	+	+/–		+	

n.d. - not done

In conclusion, the combined findings of the studies described in this thesis demonstrate that cellular responses of MΦ to particles are driven by specific physico-chemical properties of particles. $fTiO_2$ particles are considered as inert and harmless to humans, whereas $ufTiO_2$ particles have been shown to cause inflammation and morphological damage in experimental studies *in vivo* [Witschi & Last 1996; Oberdörster et al 2005] and *in vitro* [study 1 of this thesis]. However, in the case of nano-HA particles the "ultrafine hypothesis" [paragraph 1.2.3] appeared not to hold true [study 3 of this thesis]. Moreover, in the casethe fine-sized DQ12, minor surface modifications with iron, that are known to increase the reactivity of quartz particles in cell free assays [Fubini 1998], were found to behave contrary when evaluated *in vitro* [study 2 of this thesis].

In this sense, one must be aware that particle toxicology comprises more than "more particle surface area equals more toxicity", and that increased chemical reactivity does not necessarily imply increased toxicity. Overall, further mechanistic studies are urgently required on cellular mechanisms whereby the detailed analysis of physico-chemical properties (i.e. particle size and distribution, agglomeration behaviour, chemical composition and surface contamination) is a prerequisite. Such observations provide important benefits for the hazard and risk assessment of fine and ultrafine particles as well as for smart engineering of novel NP for potential medical-preventive or therapeutic applications.

5.2 REFERENCES

Albrecht C, Höhr D, Haberzettl P, Becker A, Borm PJ, Schins RP. Surface-dependent quartz uptake by macrophages: potential role in pulmonary inflammation and lung clearance. Inhal Toxicol 2007, 19 Suppl 1:39-48.

Albrecht C, Knaapen AM, Becker A, Höhr D, Haberzettl P, van Schooten FJ, Borm PJ, Schins RP. The crucial role of particle surface reactivity in respirable quartz-induced reactive oxygen/nitrogen species formation and APE/Ref-1 induction in rat lung. Respir Res 2005, 6:129.

Albrecht C, Schins RP, Höhr D, Becker A, Shi T, Knaapen AM, Borm PJ. Inflammatory time course after quartz instillation: role of tumor necrosis factor-alpha and particle surface. Am J Respir Cell Mol Biol 2004, 31(3):292-301.

Castranova V, Vallyathan V. Silicosis and coal workers' pneumoconiosis. Environ Health Perspect 2000, 108 Suppl 4:675-84.

Champion JA, Mitragotri S. Shape induced inhibition of phagocytosis of polymer particles. Pharm Res 2009, 26(1):244-9.

Clouter A, Brown D, Höhr D, Borm P, Donaldson K. Inflammatory effects of respirable quartz collected in workplaces versus standard DQ12 quartz: particle surface correlates. Toxicol Sci 2001, 63(1):90-8.

Donaldson K, Borm PJ. The quartz hazard: a variable entity. Ann Occup Hyg 1998, 42(5):287-94.

Donaldson K, Borm PJA. Particle Toxicology. CRC Press/Taylor and Francis Group 2006, Boca Raton USA.

Doshi N, Mitragotri S. Macrophages recognize size and shape of their targets. PLoS One 2010, 5(4):e10051.

Duffin R, Gilmour PS, Schins RP, Clouter A, Guy K, Brown DM, MacNee W, Borm PJ, Donaldson K, Stone V. Aluminium lactate treatment of DQ12 quartz inhibits its ability to cause inflammation, chemokine expression, and nuclear factor-kappaB activation. Toxicol Appl Pharmacol 2001, 176(1):10-7.

Fubini B. Surface chemistry and quartz hazard. Ann Occup Hyg 1998, 42(8):521-30.

Fubini B, Fenoglio I, Ceschino R, Ghiazza M, Martra G, Tomatis M, Borm P, Schins R, Bruch J. Relationship between the state of the surface of four commercial quartz flours and their biological activity in vitro and in vivo. Int J Hyg Environ Health 2004, 207(2):89-104.

Haberzettl P, Duffin R, Kramer U, Höhr D, Schins RP, Borm PJ, Albrecht C. Actin plays a crucial role in the phagocytosis and biological response to respirable quartz particles in macrophages. Arch Toxicol 2007, 81(7):459-70.

Haberzettl P, Schins RP, Höhr D, Wilhelmi V, Borm PJ, Albrecht C. Impact of the FcgammaII-receptor on quartz uptake and inflammatory response by alveolar macrophages. Am J Physiol Lung Cell Mol Physiol 2008, 294(6):L1137-48.

Helmke RJ, German VF, Mangos JA. A continuous alveolar macrophage cell line: comparisons with freshly derived alveolar macrophages. In Vitro Cell Dev Biol 1989, 25(1):44-8.

IARC. Silica, Some Silicates, Coal Dust and Para-Aramid Fibrils. IARC Monogr Eval Carcinog Risks Hum 1997, 68:1-475.

Motskin M, Wright DM, Muller K, Kyle N, Gard TG, Porter AE, Skepper JN. Hydroxyapatite nano and microparticles: correlation of particle properties with cytotoxicity and biostability. Biomaterials 2009, 30(19):3307-17.

Oberdörster G, Oberdörster E, Oberdörster J. Nanotoxicology: an emerging discipline evolving from studies of ultrafine particles. Environ Health Perspect 2005, 113(7):823-39.

Rao KM. Molecular mechanisms regulating iNOS expression in various cell types. J Toxicol Environ Health B Crit Rev 2000, 3(1):27-58.

Scheel J, Weimans S, Thiemann A, Heisler E, Hermann M. Exposure of the murine RAW 264.7 macrophage cell line to hydroxyapatite dispersions of various composition and morphology: assessment of cytotoxicity, activation and stress response. Toxicol In Vitro 2009, 23(3):531-8.

Schins RP, Knaapen AM. Genotoxicity of poorly soluble particles. Inhal Toxicol 2007, 19 Suppl 1:189-98.

Schins RPF, Hei TK. Genotoxic effects of particles. *In:* Particle Toxicology - Donaldson K & Borm PJA, CRC Press/Taylor and Francis Group 2006, Boca Raton USA.

van Berlo D, Haberzettl P, Gerloff K, Li H, Scherbart AM, Albrecht C, Schins RP. Investigation of the cytotoxic and proinflammatory effects of cement dusts in rat alveolar macrophages. Chem Res Toxicol 2009, 22(9):1548-58.

van Berlo D, Knaapen AM, van Schooten FJ, Schins RP, Albrecht C. NF-kappaB dependent and independent mechanisms of quartz-induced proinflammatory activation of lung epithelial cells. Part Fibre Toxicol 2010, 7:13.

Witschi H, Last JA. Toxic Responses of the Respiratory System. *In:* Casarett & Doull's Toxicology - The Basic Science of Poisons - Klaassen CD, McGraw-Hill Professional 1996.

Zhang Z, Shen HM, Zhang QF, Ong CN. Involvement of oxidative stress in crystalline silica-induced cytotoxicity and genotoxicity in rat alveolar macrophages. Environ Res 2000, 82(3):245-52.

5.3 ABSTRACT

Macrophages (MΦ), effector cells of the innate immune system, are very important in the phagocytosis and elimination of pathological invaders such as microorganisms and particles. The process of internalization can be associated with MΦ activation resulting in the release of inflammatory mediators like cytokines, chemokines and reactive oxygen species (ROS). An uncontrolled persistent inflammatory response in particle-exposed lungs is discussed as a risk factor for the development of chronic obstructive pulmonary disease, fibrosis and cancer. Within the lung, alveolar macrophages (AMΦ) representing key target cells for interaction with inhaled particles. However, the precise mechanisms of particle uptake and associated generation of inflammatory mediators by these cells are still poorly understood. Therefore, mechanistic studies are urgently required, especially for engineered nanoparticles, as their potential to cause adverse health effects is increasingly debated. The aim of this thesis is to unravel the interactions between particles and AMΦ in relation to the physico-chemical properties of these compounds.

To this extent, three independent studies were performed.

In **study 1** the molecular mechanisms of interactions of fine versus ultrafine TiO_2 with AMΦ (NR8383 cells) were investigated in comparison to fine-sized quartz (DQ12). The results showed that particle-specific physico-chemical properties determine the pattern as well as the extent of induction of oxidative stress and inflammatory responses. Analysis of uptake, with the use of specific inhibitors, revealed differences in uptake mechanisms for the three particle types. In contrast, intracellular ROS and calcium influx occurred to a similar extent with all particle types and thus unlikely provide an explanation for the observed differential uptake and pro-inflammatory responses.

Study 2 focused on the cytotoxic and inflammatory responses in quartz-treated NR8383 cells in relation to particle-surface associated iron. The findings indicate that low levels of surface bound and potentially bioavailable iron may reduce quartz related adverse health effects.

In **study 3** the biocompatibility of a panel of five hydroxyapatite materials of different size and morphology was investigated in NR8383 cells as well as in primary AMΦ. The findings support a good biocompatibility of all the tested materials unlike DQ12, the positive control.

Overall, these results demonstrate that the interaction with-, and activation of-, MΦ by particles strongly depends on various physico-chemical properties, such as particle size and distribution, agglomeration behaviour, chemical composition and surface contamination. Current observations are of special importance for hazard and risk assessment of inhaled particles as well as for smart engineering of novel nanoparticles for therapeutic applications.

5.4 ZUSAMMENFASSUNG

Makrophagen (MΦ), die Effektorzellen des angeborenen Immunsystems, sind von großer Bedeutung bei der Phagozytose und Eliminierung von Pathogenen, wie Mikroorganismen und Partikeln. Die Internalisierung kann mit der Aktivierung der MΦ einhergehen, welche in der Ausschüttung inflammatorischer Mediatoren, wie Zytokinen, Chemokinen und reaktiver Sauerstoffspezies (ROS - engl. reactive oxygen species) resultiert. Eine unkontrolliert andauernde Entzündungsreaktion in partikelexponierten Lungen wird als Risikofaktor für die Entwicklung der chronisch obstruktiven Lungenerkrankung, von Fibrose und Krebs diskutiert. In der Lunge sind es die Alveolarmakrophagen (AMΦ), welche hauptsächlich mit inhalierten Partikeln interagieren. Die genauen Mechanismen der Partikelaufnahme, sowie die damit verbundene Generierung und Ausschüttung von inflammatorischen Mediatoren sind bis dato nur unzureichend geklärt. Daher sind mechanistische Untersuchungen dringend erforderlich, vor allem für die vermehrt eingesetzten industriell hergestellten Nanopartikel, deren gesundheitsschädliches Potential immer intensiver diskutiert wird. Das Ziel dieser Arbeit ist die genaue Untersuchung der Interaktionen zwischen Partikel und AMΦ im Verhältnis zu physiko-chemischen Partikeleigenschaften.
Drei verschiedene Studien wurden hierzu durchgeführt:
In **Studie I** wurden die molekularen Mechanismen der Interkation von feinem und ultrafeinem TiO_2 mit AMΦ (NR8383 Zellen) im Vergleich zu feinem Quarz (DQ12) untersucht. Die Ergebnisse zeigen, dass partikelspezifische physiko-chemische Eigenschaften für die qualitative und quantitative Ausprägung von oxidativem Stress und Entzündungsreaktionen entscheidend sind. Untersuchungen der Partikelaufnahme, unter Verwendung spezifischer Inhibitoren, zeigten unterschiedliche Mechanismen für die jeweiligen Partikel. Dem entgegengesetzt traten intrazellulläre ROS Bildung und Kalzium Einstrom für alle drei Partikel in gleichem Maße auf.
Studie II setzte den Schwerpunkt auf zytotoxische und inflammatorische Reaktionen Quarz-behandelter NR8383 Zellen. Die Partikeloberfläche des Quarzes war mit Eisen in unterschiedlichen Konzentrationen versehen. Die Ergebnisse zeigen, dass bereits geringe Mengen an oberflächengebundenem und potentiell bioverfügbarem Eisen, Quarz-induzierte gesundheitsschädliche Effekte reduzieren können.
In **Studie III** wurde die Biokompatibilität von fünf Hydroxyapatiten verschiedener Größe und Morphologie in NR8383 Zellen und in primären AMΦ untersucht. Die Ergebnisse unterstützen eine gute Biokompatibilität aller getesteten Materialien, mit Ausnahme von DQ12, welches als Positivkontrolle mitgeführt wurde.

Insgesamt zeigen die Ergebnisse, dass Interaktion mit- und Aktivierung von- MΦ, durch Partikel, stark von den physiko-chemischen Eigenschaften der Partikel abhängig, wie Partikelgröße, Größenverteilung, Agglomerationsverhalten, chemische Zusammensetzung und Oberflächenkontaminierungen.
Diese aktuellen Beobachtungen sind von großer Relevanz für Gefahr- und Risikobewertungen von inhalierbaren Partikel, sowie für mögliche gezielte Anwendungen neuer Nanopartikel in medizinisch-therapeutischen Ansätzen.

5.5 LIST OF ABBREVIATIONS

7-AAD	7-amino-actinomycin D
$[Ca^{2+}]_i$	intracellular calcium concentration
AP-1	activator protein 1
AMΦ	alveolar macrophages
a.u.	arbitrary units
BAL	broncho-alveolar lavage
BET	Brunauer-Emmett-Teller method
BSI	British Standards Institution
CB	carbon black
CCP	clathrin-coated pit
Chl	chlorpromazine
CR	complement receptor
CytD	cytochalasin D
DC	dendritic cells
DCFH-DA	2',7'-dichlorodihydrofluorecein diacetate
DF-LSM	dark field light scattering microscopy
DHR	dihydrorhodamine
DLS	dynamic light scattering
DMPO	5,5-dimethyl-1-pyrroline-N-oxide
DMSO	dimethyl sulfoxide
DPI	diphenyleneiodonium chloride
DQ12	Dörentruper quartz
EA	elemental analysis
EPA	Environmental Protection Agency
ELISA	enzyme-linked immunoabsorbent assay
ELS	electrophoretic light scattering
eNOS	epithelial nitric oxide synthase
ENP	engineered nanoparticle
EPR	electron paramagnetic resonance
ESEM	environmental scanning electron microscopy
FACS	fluorescence-activated cell sorter
FcγII-R	fragment crystallizable of immunoglobulin G II receptor
FCS	fetal calf serum
FSC	forward scatter
GM-CSF	granulocyte-macrophage-colony stimulating factor
G-CSF	granulocyte-colony stimulating factor
HA-FN	hydroxyapatite-fine, dull needles
HA-NN	hydroxyapatite-nano, needles
HA-NP	hydroxyapatite-nano, plate-like
HA-NR	hydroxyapatite-nano, rods
HBSS	Hank's balanced salt solution
HO-1	heme oxygenase 1
HPC	hydroxyapatite-protein-composit
ICP	inductively coupled plasma

IFN-γ	interferon gamma
Ig	immunoglobulin
IκB	inhibitor of kappa-light-chain-enhancer of activated B cells
IL-1β	interleukin 1 beta
iNOS	inducible nitric oxide synthase
IR	infrared light
ITAM	immunoreceptor tyrosine-based activation motif
ITIM	immunoreceptor tyrosine-based inhibition motif
LDH	lactate dehydrogenase
LPS	lipopolysaccharides
MARCO	macrophage receptor with collagenous structure
MCP-1/3	monocyte chemoattractant protein 1/3
M-CSF	macrophage-colony stimulating factor
MGG	May-Grünwald-Giemsa
MIP-1	macrophage inflammatory protein 1
MMP	matrix metalloproteinases
MPS	mononuclear phagocyte system
MPO	myeloperoxidase
MR	mannose receptor
NADPH	nicotineamide adenine dinucleotid phosphat
NF-κB	nuclear factor kappa-light-chain-enhancer of activated B cells
nNOS	neuronal nitric oxide synthase
NO	nitric oxide
NOX	NADPH-oxidase enzymes
NP	nanoparticles
PBS	phosphate buffered saline
PDI	polydispersity index
PKC	protein kinase C
PLCγ-1	phospholipase C gamma 1
PM	particulate matter
PMA	phorbol-12-myristate 13-acetate
PMN	polymorphonuclear leukocytes
Qz	fibrogenic quartz
RANTES	regulated on activation, normal T-cell expressed and secreted
RNS	reactive nitrogen species
ROS	reactive oxygen species
SEM	scanning electron microscopy
SEM	standard error mean
SR-A	scavenger receptor class A
SSA	specific surface area
SSC	sideward scatter
TEM	transmission electron microscopy
TGA	thermogravimetric analysis
TIMP	tissue inhibitors of metalloproteinases
TNF-α	tumour necrosis factor alpha
TiO2	titanium dioxide

UV-Vis DR	ultraviolet-visible spectral region diffuse reflectance
WST-1	water-soluble tetrazolium salt 1
XRD	X-ray diffraction
XRF	X-ray fluorescence
XO	xanthine oxidase
ZnO	zinc oxide

5.6 LIST OF PUBLICATIONS

Albrecht C, Scherbart AM, van Berlo D, Braunbarth CM, Schins RPF, Scheel J
Evaluation of cytotoxic effects and oxidative stress with hydroxyapatite dispersions of different physicochemical properties in rat NR8383 cells and primary macrophages.
Toxicol In Vitro, 2009 Apr;23(3):520-30

van Berlo D, Haberzettl P, Gerloff K, Li H, Scherbart AM, Albrecht C, Schins RPF
Investigation of the cytotoxic and proinflammatory effects of cement dusts in rat alveolar macrophages.
Chem Res Toxicol, 2009 Sep;22(9):1548-58

Wessels A, van Berlo D, Boots AW, Gerloff K, Scherbart AM, Cassee FR, Gerlofs-Nijland ME, Van Schooten FJ, Albrecht C, Schins RPF
Oxidative stress and DNA damage responses in rat and mouse lung to inhaled carbon nanoparticles.
Nanotoxicology, 2010 Jun [Epub ahead of print]

van Berlo D*, Wessels A*, Boots AW, Wilhelmi V, Scherbart AM, Gerloff K, van Schooten FJ, Albrecht C, Schins RP
Neutrophil-derived ROS contribute to oxidative DNA damage induction by quartz particles.
Free Radic Biol Med, 2010 Dec;49(11):1685-93 * equal contributions

Ghiazza M*, Scherbart AM*, Fenoglio I, Grendene F, Turci F, Martra G, Albrecht C, Schins RPF, Fubini B
Surface-bound iron inhibits quartz-induced cytotoxic and inflammatory responses in alveolar macrophages.
Chem Res Toxicol, 2011 Jan;24(1):99-110. * equal contributions

Scherbart AM, Langer J, Bushmelev A, van Berlo D, Haberzettl P, van Schooten FJ, Schmidt AM, Rose CR, Schins RPF, Albrecht C
Contrasting macrophage activation by fine and ultrafine titanium dioxide particles is associated with different uptake mechanisms
Part Fibre Toxicol, submitted

van Berlo D, Albrecht C, Wessels A, Wilhelmi V, Scherbart AM, Gerloff K, Hellack B, Huaux F, Boots A, Schins RPF
Role of phagocyte-derived reactive oxygen species (ROS) in fibrosis induced by respirable quartz.
J Leukoc Biol, submitted

Scherbart AM, Sacha B, Kerschbaum HH
Corticosterone suppresses LPS-induced nitric oxide as well as urea release in BV-2 microglial cells.
Brain Res Bull, manuscript in preparation

DANKE AN . . .

Prof. Dr. Christine R. Rose für meine Betreuung an der Mathematisch-Naturwissenschaftlichen Fakultät der Heinrich-Heine-Universität Düsseldorf und für die erfolgreiche Kooperation in Studie 1 dieser Doktorarbeit.

Prof. Dr. Charlotte Esser für die Übernahme des Amtes der Zweitgutachterin und für ihre leitende Arbeit im Graduiertenkolleg 1427, im Rahmen dessen ich die Möglichkeit hatte, am Postgraduiertenstudium zur „Fachtoxikologin DGPT" teilzunehmen.

Dr. Catrin Albrecht, dass sie mir dieses interessante Thema zur Bearbeitung gegeben hat und für meine Betreuung am IUF, welche am Ende zu Einsätzen der besonderen Art führte.
Dr. Roel P.F. Schins, Leiter der Partikelgruppe am IUF, für seine enthusiastische Art und seine kreativen Ideen.
Danke euch beiden für diese persönliche und angenehme Atmosphäre, sowohl am Arbeitsplatz als auch drüber hinaus.

Prof. Dr. Stefanie Ritz-Timme, meiner Mentorin, die ich durch das Selma-Meyer-Mentoring Programm der HHU kennenlernen durfte, für ihre mentale Unterstützung durch motivierende Gespräche in stets sehr freundlicher Atmosphäre.

Meinen Partikelkollegen Damiën van Berlo, Anton Wessels, Verena Wilhelmi, Kirsten Gerloff, Bryan Hellack, Agnes W. Boots, Maja Rohling and Julia Kolling.
Die Zusammenarbeit mit euch war ein Vergnügen. Ihr seid tolle Kollegen!

Christel Weishaupt, Kirstin Ledermann und Gabriele Wick für die technische Assistenz und die stetige Aufrechterhaltung der Labore.

Bryan Hellack für seine aufmunternde Unterstützung und für die Kaffee-Zeiten.
Agnes Czapla für die soziale Unterstützung durch lange Telefonate, gerade in der Zeit des „Einigelns" während des Schreibens - „Auf mich!" ☺
Thorsten Bocks vor allem für die technische Unterstützung. Gerade als ich mit dem Schreiben beginnen wollte, funktionierte mein Laptop nicht mehr. Ohne seinen Notfall-Laptop wäre das Schreiben dieser Arbeit in der kurzen Zeit nicht möglich gewesen.

Meinen Eltern Renata und Diethard Scherbart und meiner Schwester Eva-Maria, dass sie immer für mich da sind!

EIDESTATTLICHE ERKLÄRUNG

Ich versichere, dass ich die vorliegende Arbeit selbständig verfasst und keine anderen als die angegebenen Quellen und Hilfsmittel verwendet habe.

Ferner versichere ich, dass ich weder an der Heinrich-Heine-Universität Düsseldorf noch an einer anderen Universität versucht habe, diese Doktorarbeit einzureichen.

Ebenso habe ich bisher keine erfolglosen Promotionsversuche unternommen.

_____ Düsseldorf, den 18. Oktober 2010

Agnes M. Scherbart